SOLID ACID CATALYST DERIVED FROM SPENT COFFEE GROUND FOR BIODIESEL PRODUCTION VIA ESTERIFICATION OF OLEIC ACID AND METHANOL

LAW ZHI PIN

A project report submitted in partial fulfilment of the requirements for the award of Bachelor of Engineering (Honours) Chemical Engineering

Lee Kong Chian Faculty of Engineering and Science
Universiti Tunku Abdul Rahman

April 2023

DECLARATION

I hereby declare that this project report is based on my original work except for citations and quotations which have been duly acknowledged. I also declare that it has not been previously and concurrently submitted for any other degree or award at UTAR or other institutions.

Signature :

Name : LAW ZHI PIN

ID No. : 18UEB01324

Date : 24 APRIL 2023

APPROVAL FOR SUBMISSION

I certify that this project report entitled **"SOLID ACID CATALYST DERIVED FROM SPENT COFFEE GROUND FOR BIODIESEL PRODUCTION VIA INTERESTERIFICATION PROCESS"** was prepared by **LAW ZHI PIN** has met the required standard for submission in partial fulfilment of the requirements for the award of Bachelor of Engineering (Honours) Chemical Engineering at Universiti Tunku Abdul Rahman.

Approved by,

Signature   :   *steven*

Supervisor   :   Dr. Steven Lim

Date   :   24.4.2023

The copyright of this report belongs to the author under the terms of the copyright Act 1987 as qualified by Intellectual Property Policy of Universiti Tunku Abdul Rahman. Due acknowledgement shall always be made of the use of any material contained in, or derived from, this report.

ACKNOWLEDGEMENTS

This research project would not have been completed without many individuals' participation, guidance and support. First, I would like to express my appreciation to my research supervisor, Dr. Steven Lim, who shared meaningful advice and feedback throughout the research. I was honored to carry out my final year project under his supervision.

Moreover, I am blessed to have a learning and research platform for my final year project. I would like to thank Universiti Tunku Abdul Rahman (UTAR), especially all the Assistant Laboratory Managers from the Department of Laboratory Management and Safety Administration (DLMSA) at Lee Kong Chian Faculty of Engineering and Science (LKC FES), who provided technical support when necessary.

In addition, a special thanks to the postgraduate students, Ms. Wong Wan Ying and Mr. Chai Kian Hoong, for their precious advice and assistance in operating the instruments. Besides, I will never forget the support and encouragement from all the coursemates, especially those working on the research on synthesizing catalysts from biomass. Last but not least, my deepest gratitude to my parents and siblings, who gave me non-stop help and showed consistent trust in my hard work.

ABSTRACT

The transesterification process catalysed by a homogeneous basic catalyst is the most common reaction used for biodiesel production. The major concerns of such catalysts are the difficulties in separating the catalyst after reaction, sensitivity to the free fatty acids and moisture contents in the feedstock. In contrast, a solid acid catalyst can ease the downstream separation and is less likely to be influenced by the free fatty acid in the feedstocks. In this work, biomass waste was used to derive the solid acid catalysts subjected to the transesterification process to lower the cost for biodiesel production. This study aimed to evaluate the possibility of spent coffee grounds being converted into effective carbon precursors and acidic catalysts for biodiesel production. The biomass waste was treated via direct sulfonation with concentrated sulfuric acid at different temperatures ranging from 80 ℃ to 240 ℃. Various catalyst characterisations, including Scanning Electron Microscopy Equipped with Energy Dispersive X-ray, X-ray Diffraction, Fourier Transform Infrared Spectroscopy, surface analysis (BET and BJH methods) and acid density, were carried out to examine the impact of sulfonation temperatures on the catalytic performance. The catalyst with optimum properties was used in the transesterification process at 80 ℃ and rotational speed of 500 rpm for 7 hours to study the effect of catalyst loading and methanol-to-oleic acid molar ratio on biodiesel yield. The catalyst loading was manipulated from 4 to 20 wt.%, whereas the molar ratio was changed from 4:1 to 20:1. It was found that the acid density and catalytic performance improved with increasing sulfonation temperature until the optimum 200 ℃. The catalytic properties of the sample dropped beyond the optimum temperature. Moreover, the optimum catalyst loading and methanol-to-oleic acid were 12 wt.% and 16:1, respectively. The biodiesel yield of 99.67 % was achieved from the transesterification process catalysed by 12 wt.% of the catalyst sulfonated at 200 ℃ and 16:1 of methanol-to-oleic acid molar ratio. The results of present work proved the potential of spent coffee grounds to be converted into useful heterogeneous acid catalysts for the transesterification process to produce biodiesel in a relatively environmentally benign way.

TABLE OF CONTENTS

LIST OF TABLES

LIST OF FIGURES

LIST OF SYMBOLS / ABBREVIATIONS

AV	acid value, g KOH/g
C	concentration, mmol/mL or mol/L
DF	dilution factor
m	mass, g
MW	molar weight, g/mol
V	volume of solution, mL or L
CaO	calcium oxide
CH_3OK	potassium methoxide
CH_3ONa	sodium methoxide
CO	carbon monoxide gas
CO_2	carbon dioxide gas
NO_x	nitrogen oxides gases
HCl	hydrochloric acid
H_2SO_4	sulfuric acid
KOH	potassium hydroxide
$NaCl$	sodium chloride
$NaOH$	sodium hydroxide
N_2	nitrogen gas
$-SO_3H$	sulfonic group
$ZnCl_2$	zinc chloride
AC	activated carbon
BET	Branauer-Emmett-Teller
BJH	Barrett-Joyner-Halenda
CAC	solely carbonised carbon
CSCG	carbonised spent coffee ground
DAMG	diacetinmonoglyceride
EDX	Energy Dispersive X-ray
EIA	Energy Information Administration
EPA	Environmental Protection Agency
FAAE	fatty acid alkyl ester

FAEE	fatty acid ethyl ester
FAME	fatty acid methyl ester
FFA	free fatty acid
FID	Flame-Ionization Detector
FTIR	Fourier Transform Infrared Spectroscopy
GC	Gas Chromatography
IEA	International Energy Agency
IR	infrared radiation
ktoe	kilo tonnes of oil equivalent
MADG	monoacetindiglyceride
MeOH	methanol
MOAMR	methanol-to-oleic acid molar ratio
OA	oleic acid
OECD	Economic Co-operation and Development
RE	renewable energy
SCAC	sulfonated and carbonised carbon
SCF	supercritical fluid
SCG	spent coffee ground
SCSCG	sulfonated and carbonise spent coffee ground
SEM	Scanning Electron Microscopy
TGA	Thermogravimetric Analysis
UN	United Nations
WCO	waste cooking oil
XRD	X-ray Diffractometer

LIST OF APPENDICES

CHAPTER 1

INTRODUCTION

1.1   Global Energy Demand and Consumption

Energy is so essential for all living organisms, especially humans, to survive as it is one of the keys driving all the processes that occur across the entire universe. Transportation, electricity generation, industrial and residential are the main sectors that consume energy. The factors affecting how the world uses energy include policy, technology and consumer preferences which vary over time depending on locally available resources and public support. It was stated by Exxon Mobil (2021) that the global energy demand may increase up to 15 % in 2050 versus 2019 due to the growing population and rising prosperity. According to the press release by International Energy Agency, IEA (2021), global electricity demand growth was almost 5 % in 2021 and 4 % in 2022 after a 1 % decrement in 2020 due to the Covid-19 pandemic. Besides Energy Information Administration, EIA projected that there will be an increment of 50 % in global energy demand between 2020 and 2050 (Adler, 2021). The graph in Figure 1.1 clearly illustrates the predicted energy consumption of the countries in the Organisation for Economic Co-operation and Development (OECD) and non-OECD reported by the U.S. EIA (2021).
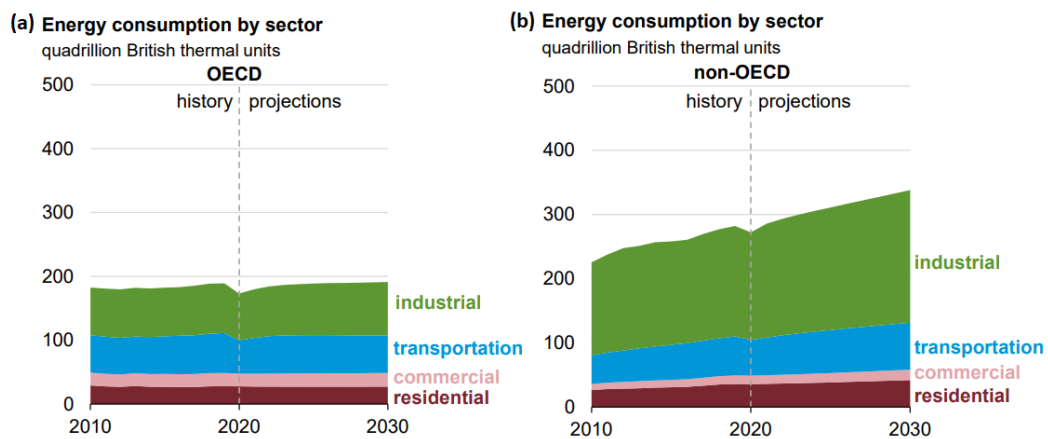
Figure 1.1: Projected Energy Consumption by Sectors in (a) OECD and (b) non-OECD (U.S. EIA, 2021).

Many reasons are driving the consumption of energy in our daily life. For instance, urbanization, better accessibility to electricity and rising income. Moreover, the rising population and quality of life also contribute to electricity usage growth (EIA, 2019). United Nations, UN (n.d.) reported that it was expected that the world's population in 2050 will reach 9.7 billion and could peak at around 11 billion in 2100. This significant population growth indicates that the usage of energy and energy resources will be one of the global major crises. In the Statistical Review of World Energy Report 2021, BP revealed fuel consumption by categories, as illustrated in Figure 1.2. It was clearly shown that more than 80 % of the energy consumed comes from fossil fuels.
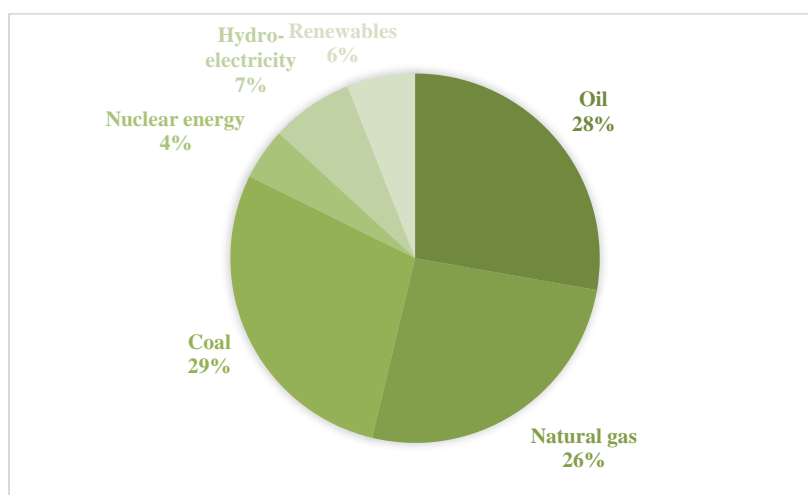
Figure 1.2: Global Energy Consumption in 2020 (BP, 2021).

Malaysia is a developing country whereby the energy supply and consumption are very coupled with economic growth since energy is one of the main pillars that drive economic growth. Table 1.1 shows Malaysia's increasing trend in total primary energy supply from 1999 to 2018. Since energy will become more viable, it was projected that the energy demand in Malaysia would continue to rise. The total primary energy supply in 2019 was reported as 98,960 ktoe, 2.8 % higher than in 2018. The biggest share of 42 % came from natural gas, followed by crude oil and petroleum products at 33 % as well as coal and coke at 21 %, while renewable energy took the smallest energy at 4 % (Lim, 2021).

Table 1.1: Total Primary Energy Supply by Fuel Type from 1999 to 2018 (Energy Commission, 2021).

Year	Primary Energy Supply (ktoe)							
	Crude Oil, Petroleum Products and others	**Natural Gas**	**Coal and Coke**	**Hydropower**	**Biodiesel**	**Biomass**	**Biogas**	**Solar**
1999	19450	21476	1940	1668	0	0	0	0
2000	20242	26370	2486	1612	0	0	0	0
2001	21673	25649	2970	1687	0	0	0	0
2002	22124	26101	3642	1329	0	0	0	0
2003	23936	27275	5316	1056	0	0	0	0
2004	25253	29145	7109	1329	0	0	0	0
2005	24096	33913	6889	1313	0	0	0	0
2006	23240	34917	7299	1567	0	0	0	0
2007	25381	36639	8848	1522	0	0	0	0
2008	24996	39289	9782	1964	0	0	0	0
2009	26482	35851	10623	1627	0	0	0	0
2010	25008	35447	14777	1577	0	0	0	0
2011	26903	35740	14772	1850	24	0	0	0
2012	29502	38647	15882	2150	115	183	4	11
2013	32474	39973	15067	2688	188	297	6	38
2014	33422	40113	15357	3038	300	181	12	63
2015	29165	41852	17406	3582	389	189	18	75
2016	31327	41257	18744	4501	389	198	21	90
2017	29379	41201	20771	6240	379	194	41	93
2018	29429	40939	22280	6230	436	241	147	172

Renewable energy (RE) will become more viable due to the economic and population growth in the world. RE not only reduces the negative environmental impact of non-renewable energy but also diversifies the energy supply, thus reducing dependence on fossil fuels. In terms of power generation, solar, wind, biogas, and geothermal are the most common renewable power technologies (U.S. EPA, n.d.). These energy sources are naturally and constantly replenished, avoiding the problem of depletion. In contrast, non-renewable energy, for example, fossil fuels, form in the Earth's crust by taking millions of years, and they will eventually run out. Although their relative affordability and easy accessibility, carbon dioxide emission into the atmosphere during fossil fuel combustion contributes to the greenhouse effect and global warming. Furthermore, coal combustion or natural gas emits sulfur dioxide gas which contributes to the formation of acid rain (BBC, n.d.). Therefore, RE is a promising alternative to replace non-renewable energy for environmental preservation as well as energy security.

1.2   Biodiesel

Biodiesel is one of the renewable energy resources commercially accepted as a substitution for non-renewable energy resources. Biodiesel refers to a mono-alkyl ester, which is the product of conversion involving vegetable oil, animal fat or waste oil (Kashyap et al., 2019). According to Saka & Kusdiana (2000), biodiesel and paraffinic diesel fuel compounds are similar in terms of molecular structure, thus resulting in a higher chance of biodiesel meeting the demands that diesel engine makes of their fuel. In other words, when diesel fuel is replaced with biodiesel, no or fewer engine modifications are needed to maintain the engine performance. It can be used in 100 % pure (B100) or blended with petroleum diesel, such as B20, which is a blend with 80% diesel fuel and 20 % biodiesel.

In contrast with diesel fuel, biodiesel comes with some advantageous characteristics, including non-toxic, biodegradable, oxygenated nature and lesser sulfur emission during combustion (Kumar and Raheman, 2022). The feedstocks for biodiesel production, for example, palm oil trees and soybeans, absorb CO_2 when they grow. As stated by U.S EIA (2020), biodiesel was

claimed to be carbon-neutral as the absorption of CO_2 offsets the CO_2 that forms during the production and combustion of biodiesel.

McCarthy, Rasul and Moazzem (2011) found that both biodiesel A and B emitted less carbon monoxide, CO compared to diesel, given that biodiesel A was a blend of tallow and canola oil (80: 20), whereas biodiesel B was a mixture of chicken tallow with waste cooking oil (70: 30). The reduced emission of CO was attributed to the higher oxygen content in biodiesel, giving rise to complete combustion with less CO formation. Regarding NO_x emission, Figure 1.3 shows that biodiesel A obtained a decreasing trend while biodiesel B showed an increasing trend with the blend ratio. Jääskeläinen and Majewski (2021) added that highly unsaturated fuels such as soybean and rapeseed oil gave higher NO_x emissions. Meanwhile, the animal fats which are more saturated produced lower NO_x. The reason was due to the combustion of sufficiently oxygenated biodiesel, which resulted in higher temperatures, favouring the production of NOx.
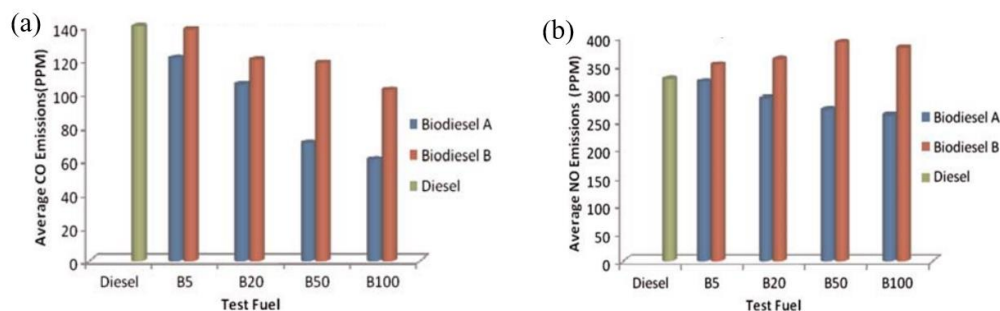
Figure 1.3: Emission of (a) CO and (b) NO_x of Diesel and Biodiesel A and B with Different Blend Ratios (McCarthy, Rasul and Moazzem, 2011).

In the past 30 years, the number of cars worldwide increased dramatically, leading to the steady growth of the transportation sector. Eurostate (2020) reported that road transportation became the largest sector in oil consumption, with a share of 47.56 %. Meanwhile, water and air transportation accounted for 9.12 % and 4.55 %, respectively. Among various types of resources, diesel oil dominated transportation with a share of 66.46 %, followed by motor gasoline with 23.91 %, as shown in Figure 1.4. It is more desirable to substitute fossil-taken petrochemical diesel with renewable biodiesel

considering the depletion of fossil resources and environmental limitations (Maleki, Ashraf Talesh and Mansouri, 2022).
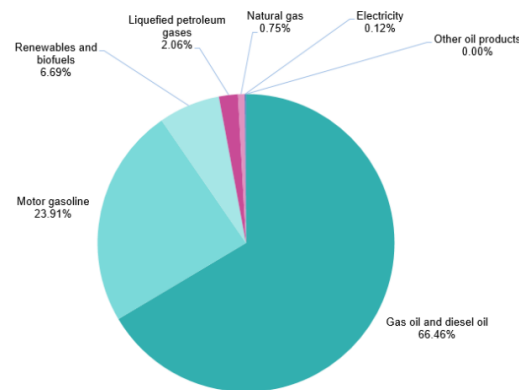
Figure 1.4: Types of Fuels Used in Road Transportation (Eurostate, 2020).

1.3 Problem Statement

Biodiesel is a great alternative to replace non-renewable diesel oil to reduce RE dependency while minimizing pollutants emissions. Biodiesel is widely investigated in the industry and research fields for energy security. Nevertheless, the high production cost of biodiesel is a major problem that needs to be solved. Figure 1.5 compares the production cost of gasoline and ethanol as well as diesel and biodiesel. The production cost of biodiesel includes the cost of the processing plant, catalyst and feedstocks.
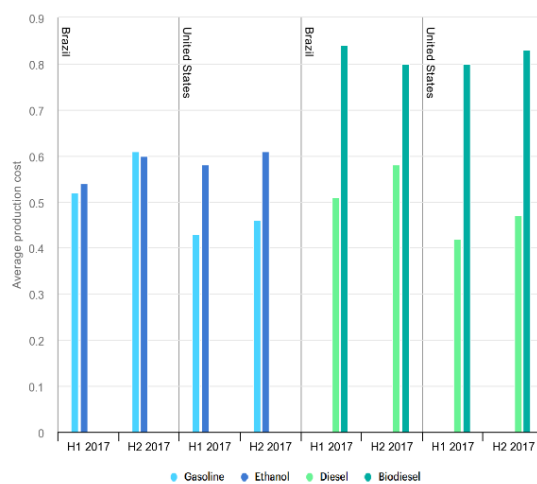
Figure 1.5: Comparison of Production Cost of Biofuel and Transport Fuel in 2017 (IEA, 2017).

Biodiesel is typically produced via a transesterification process that involves oils and methanol with the aid of a catalyst. The production cost may be reduced by using the appropriate catalyst. Utilizing heterogeneous catalysts could simplify the separation for removing the catalysts from the reaction products. The triglycerides used for biodiesel production generally comprise a high free fatty acids (FFAs) composition. Despite its high catalytic performance, the heterogeneous alkaline catalyst will react with the FFAs and lead to saponification that inhibits the product separation as well as deactivates the catalysts (Rizwanul Fattah et al., 2020). Therefore, a solid acid catalyst that is insensitive to the FFAs content becomes a good choice for biodiesel production. Carbon-based acid catalyst derived from biomass is relatively environmentally friendly and low-cost compared with the other catalysts.

It is essential to determine the appropriateness of the biomass to be modified as the carbon support of the catalyst used in biodiesel production. Hence, the study of different sulfonation conditions and different conditions of biodiesel production should be conducted to synthesise an effective catalyst for the optimum biodiesel yield.

1.4 Aim and Objectives

The aim of this research was to synthesise a potential catalyst derived from biomass waste to produce biodiesel and investigate the influence of different pretreatment parameters on the synthesised catalyst. The goals of the study are:

i. To fabricate and characterise the solid acid catalysts derived from spent coffee grounds using sulfuric acid, H_2SO_4, via direct sulfonation.

ii. To determine the conversion and biodiesel yield obtained via catalytic esterification of oleic acid with methanol as an acyl acceptor.

iii. To study the impact of sulfonation temperature, methanol-to-oleic acid molar ratio and catalyst loading on biodiesel production.

1.5 Scope and Limitations of the Study

This study covers the synthesising method of solid acid catalysts derived from biomass. Determining the appropriate biomass to synthesise the catalyst for

optimum biodiesel production is necessary. While preparing the biomass-supported catalyst, the sulfonation process is one of the keys to altering the catalytic performance. The synthesised catalyst will then produce biodiesel via the esterification process. The operating parameters of biodiesel production are manipulated to achieve the optimum biodiesel yield.

This study uses spent coffee grounds to derive the catalysts via a direct sulfonation process with concentrated sulfuric acid. Different sulfonation temperatures are used while preparing the catalyst. The catalyst is characterised to study its physicochemical properties, including structure and porosity. Moreover, the acid value is examined to determine the catalytic performance in biodiesel production.

The catalyst prepared under optimum sulfonation temperature is then employed in the esterification reaction for biodiesel production. Methanol (MeOH) and oleic acid are used as the reactants to synthesis methyl oleate (main product) and water (by-product). The impacts of the molar ratio of two reactants and catalyst loading are observed using gas chromatography and titration to identify the biodiesel yield and free fatty acids conversion.

However, several limitations must be noted for further improvement in future studies. Regarding catalyst preparation, this project only covers the sulfonating temperature without studying the concentration of sulphuric acid. Furthermore, the molar ratio of MeOH to oleic acid and amount of catalysts are investigated regarding biodiesel production. Meanwhile, other operating parameters such as temperature and reaction time are only studied through literature review instead of experimental work.

1.6   Contribution of the Study

Transesterification catalysed by solid acid catalyst overcomes the limitations of homogeneous alkaline catalysts. The derivation of solid acid catalysts from biomass waste reduces the solid waste in the environment and lowers the production cost. Since drinking coffee is a common habit for most people recently, the spent coffee ground becomes a promising biomass waste to synthesise solid acid catalysts. Then, the biodiesel yield and conversion can be optimised using the synthesised catalyst with optimum catalytic performance. Thus, the outcome of this study may determine the potential of spent coffee

grounds to be converted into effective solid acid catalysts which can be used in transesterification to produce biodiesel.

1.7   Outline of the Report

The present report consists of five chapters. Chapter 1 briefly describes the background, problem statement, aims and limitations of the research project. Chapter 2 discusses the literature review of biodiesel production, including the reaction mechanisms, types of feedstocks and catalysts. Besides, the characterisation methods of both catalysts and biodiesel are also included. Next, Chapter 3 highlights the research methodology and planning of the experiment, which comprises two main parts: synthesising solid acid catalyst and biodiesel production. Furthermore, Chapter 4 demonstrates the results obtained as well as their corresponding interpretation and discussion. Last but not least, Chapter 5 concludes the research project and lists some possible suggestions for improvement in future studies.

CHAPTER 2

LITERATURE REVIEW

2.1 Reactions for Biodiesel Production

Direct utilization of vegetable oil in the diesel engine is not workable due to the high viscosity and low volatility of vegetable oils. These properties resulted in poor atomization of the fuel and led to the deposit and coking in the engine (Lin et al., 2011). Different refinement attempts were carried out, for instance, pyrolysis, blending and micro emulsification, to approximate the properties of conventional diesel and make vegetable oils a quality fuel. Table 2.1 shows the strengths and weaknesses of several technologies used to produce biodiesel.

Table 2.1: Advantages and Disadvantages of Different Technologies for Biodiesel Production (Lin et al., 2011).

Technologies	Advantages	Disadvantages
Dilution or micro-emulsification	- Simple process	High viscosity
		Low volatility
		Low stability
Pyrolysis	- Simple process - Less pollution	High temperature (500 ℃ - 800 ℃)
		High-cost equipment
		Low purity
Transesterification	- Similar properties to diesel - High conversion efficiency - Low cost - Suitable for production on an industrial scale	Required feedstock with low content of free fatty acid and water
		Possible pollution due to the neutralisation of washing the products
		Side reactions
		Difficult to separate products

Pyrolysis, also known as thermal cracking, decomposes the organic matter with a catalyst in the absence of oxygen. Despite the high cetane number and low viscosity fuel, the pyrolysis of vegetable oils resulted in unacceptable ash contents and carbon residues. According to Brahma et al. (2022), dilution blending mixed vegetable, animal or waste oil with petrochemical diesel ranged from 10 to 40 %. However, this method was not workable when oil with higher viscosity and a more unsaturated carbon chain was used. On the other hand, a microemulsion refers to a colloidal equilibrium dispersion of fluid microstructures with a commonly 1 to 150 nm size range. In contrast, transesterification is the most common and popular technology used to produce biodiesel usable in internal combustion engines.

2.1.1   Transesterification

Transesterification is the conventional biodiesel production that involves the conversion of triglycerides using alcohol and produces the by-product, glycerol. The alkyl group of fatty acid and the methyl group of methanol will exchange to produce the fatty acid alkyl ester (FAAE) and glycerol. The triglycerides will first be converted into diglycerides, subsequently into monoglycerides (Hoang, Bensaid and Saracco, 2013). Figure 2.1 demonstrates the transesterification of triglycerides with methanol, which produced fatty acid methyl ester (FAME) and glycerol. Methanol and ethanol are two conventional alcohols used in biodiesel production due to their low cost and high availability. Nevertheless, the major drawback of the process is the generation of low-purity by-products which requires further separation from the biodiesel product. The market saturation and impossibility of disposal of crude glycerol will eventually lead to profit loss (Simões et al., 2020).
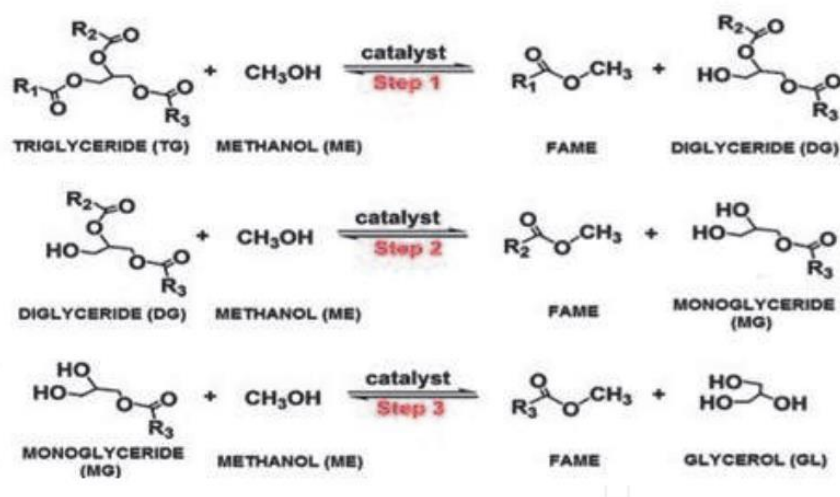
Figure 2.1: Steps Involved in Transesterification of Triglycerides with
Methanol (Edeh, n.d.).

2.1.2   Interesterification

Interesterification is a novel alternative to transesterification where triacetin is produced as the by-product instead of glycerol due to the replacement of alcohol with a short-chain alkyl ester. Triacetin is used in other industries for plasticizers, gelatinizing agents, explosives or additives. Other than its higher market value, it was found that triacetin can be utilized as a fuel additive when added into the formulation of biodiesel because of its mutual solubility to biodiesel. Therefore, further separation after the reaction is not necessary. Moreover, based on the study of Dhawan, Barton and Yadav (2021), the biodiesel still fulfils the quality requirement set by ASTM D6451 and EN14214 even with up to 10 wt.% of triacetin. The chemical interesterification reaction is still insufficiently investigated, especially with the aid of heterogeneous catalysts, despite having many benefits. As stated in the work of Kampars et al. (2020), the polarity of the mixture was lowered due to the substitution of methanol with methyl acetate during the interesterification. It consequently led to the partial or complete insolubility of catalysts in the reaction mixture.

Compared to conventional transesterification, the alcohol group of one ester exchanges with another ester to form the FAAE during the interesterification. Figure 2.2 demonstrates the three consecutive reversible steps involved in the complex reaction. According to Casas, Ramos and Pérez (2011), a monoacetindiglyceride (MADG) molecule and FAME are produced

when triglyceride reacts with methyl acetate (MA). The MADG molecule then converts into diacetinmonoglyceride (DAMG) using the same reaction path, followed by the final conversion of DAMG to triacetin and produces FAME. During interesterification, carboxylate esters are used as the acyl acceptor, for example, methyl acetate (MA), ethyl acetate and isopropyl acetate.
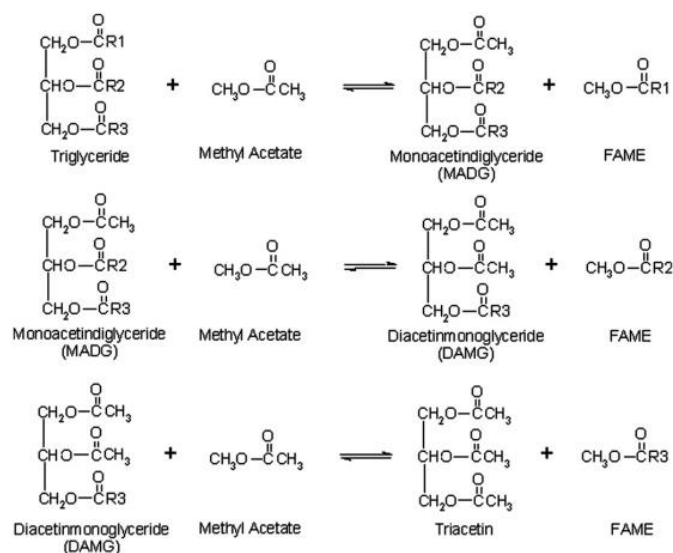
Figure 2.2: Interesterification of Triglycerides with Methyl Acetate (Casas, Ramos and Pérez, 2011).

2.1.3 Esterification

The feedstock oil used in the process will significantly affect biodiesel production. Therefore, oleic acid is usually chosen as the model oil in studying biodiesel becaused of its excellent physical and chemical properties, such as high density, kinematic viscosity and heating value (Moradi, Saidi and Najafabadi, 2021). In addition, oleic acid is the main component in the feedstock oil from different generations which is discussed in Section 2.2. According to Singh et al. (2020), oleic acid's composition ranged from 36 to 44 %, slightly lower than the palmitic acid (39 to 48 %) in palm oil. Table 2.2 shows the composition of fatty acids in various feedstocks.

Table 2.2: Composition of Fatty Acids in Various Feedstocks.

Feedstocks	Composition (%)				Reference
	Oleic C18:1	Palmitic C16:0	Stearic C18:0	Linoleic C18:2	
First Generation					
Palm Oil	36 – 44	39 – 48	3 – 6	9 – 12	
Soybean Oil	20 – 30	6 – 10	5 – 11	50 – 60	
Sunflower Oil	15 – 40	5 – 8	2 – 6	30 – 70	(Singh et al., 2020)
Second Generation					
Jatropha Oil	34.3 – 44.7	13.6 – 15.1	7.1 – 7.4	31.4 – 43.2	
Karanja Oil	44.5 – 71.3	-	2.4 – 8.9	10.8 – 18.3	
Waste Chicken Fat	2.45 – 48.5	19.8 – 35.4	4.5 – 8.3	15.0 – 35.4	
Duck Tallow	59.4	17	4	19.6	
Mutton Fat	40.7	27	24.1	2	(Kirubakaran and Arul Mozhi Selvan, 2018)
Beef Tallow	29.9	25.3	34.7	0.75	
Pork Lard	38.1	28.1	11.6	18.8	

Esterification is a chemical reaction similar to transesterification, where alcohol is used to convert the lipids to form FAAE. The esterification process produces water as the by-product using FFA, as shown in Figure 2.3. In contrast, the by-product of transesterification using triglycerides is glycerol, as illustrated in Figure 2.1 (Mandari and Devarai, 2021). The deviation in by-product is attributed to the difference in the structure of fatty acids and triglycerides. Fatty acids consist of a carboxylic functional group connecting to long-chain hydrocarbons, while triglyceride is formed by three fatty acids chemically bonded to a glycerol molecule.

$$R\text{-COOH} \quad + \quad R'\text{-OH} \quad \rightleftharpoons \quad R\text{-COO-}R' \quad + \quad H_2O$$

Fatty acid   Alcohol   Ester (biodiesel)   Water
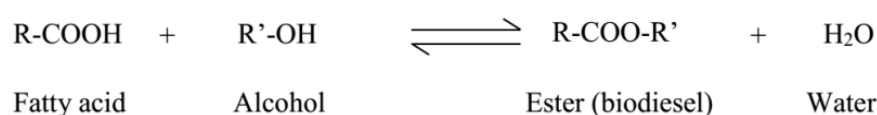
Figure 2.3: Esterification of Oleic Acid and Methanol (Banchero and Gozzelino, 2018).

2.2   Feedstocks for Biodiesel Production

Biodiesel is normally classified into different generations based on its origin, for instance, the first, second and third generations. In addition, there is also fundamental research studying the fourth generation biodiesel drawn from human-made biological tools (Singh et al., 2020).

Edible feedstocks, such as corn, palm, rapeseed, and soybean, were used as the sources of the first generation biodiesel. The large consumption of edible oil led to the food-versus-fuel debate, which caused the rising of food prices as most of the food products are used in fuel production. According to Khan et al. (2022), the price of biodiesel might increase by 1.5 to 2.0 times compared to petrochemical diesel due to the consumption of virgin edible oil as the feedstock cost contributed 70 to 95% of the biodiesel price. Moreover, land and water competition are also obstacles to using edible oil as the feedstock for first-generation biodiesel.

In contrast, the second generation of biodiesel, which uses non-edible oil as the feedstock, can eliminate the food-versus-fuel crisis. For instance, Jatropha oil, Karanja oil and Neem oil. This generation of biodiesel requires less land for farming, is more eco-friendly and incurs lower production costs. Most

importantly, the feedstock can be cultivated on non-arable land (Singh et al., 2020). Nevertheless, some of the waste oil contains high FFA content that will significantly affect biodiesel production, and the amount of alcohol and alkyl acetate required also will increase.

Recently, new promising sources of non-edible oil for third-generation biodiesel production have been found, which are microalgae and waste oil. It was stated in the study of Mani Rathnam and Madras (2019) that the yield of oils from microalgae was around 5000 to 100,000 L/ha·year. The algae can grow in degraded land with wastewater instead of freshwater, requiring much CO_2 consumption for growth. Similar to the second generation of biodiesel, using microalgae as the feedstock also avoids the competition of farmland and reduces the influence food supply chain. However, the third generation of biodiesel is not yet available on a commercial scale.

2.3   Conventional Catalysts Used in Biodiesel Production

The biodiesel production, either transesterification or esterification, is usually carried out with a catalyst to improve the synthesis process. The catalysts are critical in improving the rate of reaction, thereby enhacing the product yield. The catalyst used can be homogeneous or heterogeneous as well as acidic or alkaline, as illustrated in Figure 2.4. The factors that need to be considered while selecting the appropriate catalyst include the content of FFAs and water in the feedstock. The selection of a catalyst is crucial to achieving the optimum catalytic performance and biodiesel yield with minimum operating cost.
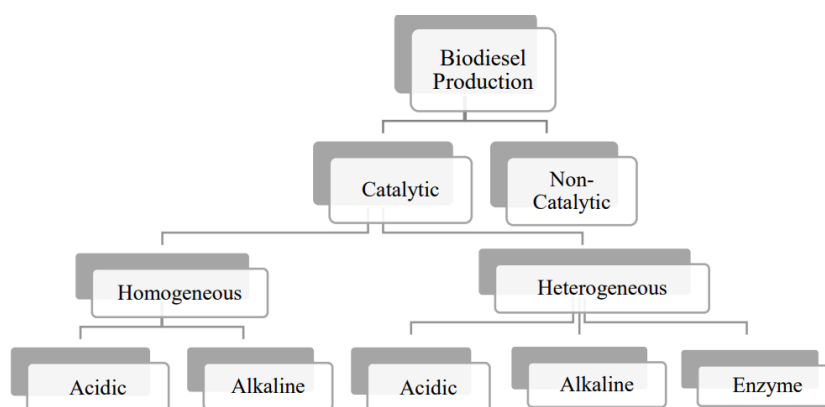
Figure 2.4: Types of Catalysts Used for Biodiesel Production.

2.3.1 Homogeneous Catalysts

A homogeneous catalyst refers to a catalyst that is in the same phase as the reactant mixture. In this case, the homogeneous catalyst is in the liquid phase and miscible with the mixture of triglycerides or fatty acids and alcohol for transesterification or esterification. Currently, the homogeneous catalyst is the most conventional catalyst used to produce FAME due to its high solubility and lower cost (Kirubakaran and Arul Mozhi Selvan, 2018). However, the homogeneous catalyst is not reusable and requires a further process for catalyst separation and product purification. Besides, it is not recommended when biodiesel production involves feedstocks with high water and FFA content as an acidic catalyst may cause reactor corrosion. In contrast, an alkaline catalyst may lead to saponification that reduces the yield of the final product (Mansir et al., 2017).

Homogeneous base catalyst is widely used in industrial and commercial biodiesel production. It is mainly due to its ability to achieve high conversion under mild conditions and in a minimal time. Table 2.3 shows several experiments of homogeneous base-catalysed transesterification. This type of catalyst includes metal-based hydroxides, metal-based oxides and carbonates, for example, NaOH, KOH, CH_3ONa and CH_3OK. The reaction rate with an alkaline catalyst is 4000 times higher than that with an acid catalyst (Rizwanul Fattah et al., 2020). However, it was reported that the composition of FFA and water in the feedstock oil should not exceed 0.06 wt.% and 0.5 wt.%, respectively, to avoid a negative impact on the biodiesel product when the basic catalyst is used (Lin and Ma, 2020).

Table 2.3:   Transesterification with Homogeneous Catalyst.

Catalyst	Alcohol (A)	Feedstock Oil (B)	Reaction Conditions				FAME Yield (%)	Reference
			T (°C)	Time (h)	A:B Molar Ratio	Catalyst		
Homogeneous Basic Catalyst								
Ionic liquid choline hydroxide	Methanol	Sunflower oil	65	0.5	10:1	2 wt.%	95	(Lima et al., 2022)
NaOH	Methanol	*Riscinus communis* seeds oil	65	3	9:1	5% w/w	98.99	(Martínez et al., 2018)
NaOH	Methanol	*Jatropha* seed oil	-	9	16:1	1.2 wt.%	99.99	(Claudette Romero-Ibarra et al., n.d.)
NaOH	Methanol	Waste cooking oil	50	-	6:1	0.7 %	93.474	(Contreras Andrade et al., 2014)
Homogeneous Acid Catalyst								
H_2SO_4	Methanol	Dry microalgae	50	1	8:1	3.361% w/w	89.583	(Chamola et al., 2019)
Glacial Acetic acid	Methanol	Palm kernel oil	60	0.5	15:1	15mL	98 (Conversion)	(Ejeromedoghene, 2021)

Besides alkaline catalysts, there is also acidic catalyst in homogeneous phase such as sulfuric acid and hydrochloric acid. The homogeneous acid catalysts are insensitive to the FFA content of feedstocks, meaning that in the presence of acid catalysts, the biodiesel can be produced from low-cost lipid feedstocks that normally consist of high FFA levels. Moreover, the acidic catalysts, for example, Lewis acid, can catalyse both esterification and transesterification processes simultaneously, as reported in the work of Shahidul Islam, Robin Hart and Casadonte (2022). In contrast, an additional step is required to convert the FFA to methyl esters when a base catalyst is used. Therefore, in terms of economic, the acid-catalysed production, which is a one-step process, is more favourable compared to the alkaline-catalysed process. Nevertheless, the difficulties in catalyst removal still limit the commercialization of homogeneous acid catalysts.

2.3.2   Heterogeneous Catalysts

On the other hand, the heterogeneous catalyst is now preferable as it can eliminate some drawbacks of using the homogeneous catalyst. As Rizwanul Fattah et al. (2020) mentioned, separating the catalyst from the products can be easily done as the heterogenous catalyst is at a different phase from the reaction mixture. In addition, the catalyst is reusable without intensive washing and thus significantly reduces wastewater generation. The eliminations of product and catalyst recovery lower the production cost while enhancing the efficiency and profitability of biodiesel production (Hoang, Bensaid and Saracco, 2013).

Similar to the homogeneous basic catalyst, the heterogeneous basic catalysts will lead to reactor corrosion or soap formation if the feedstock with high water and FFA contents is involved in the process. Moreover, the conversion is relatively lower when a heterogeneous catalyst is used. It may be attributed to the partial leaching of active sites, leading to catalyst deactivation and product contamination (Mandari and Devarai, 2021). Heterogeneous catalysis also requires elevated operating conditions, as shown in Table 2.4.

Table 2.4: Transesterification/Interesterification with Heterogeneous Catalysts.

Catalyst	Alcohol (A)	Feedstock oil (B)	Reaction Conditions				FAME Yield (%)	Reference
			T (°C)	Time (h)	A:B Molar Ratio	Catalyst		
Heterogeneous Basic Catalysts								
Na$_2$ZrO$_3$	Methanol	*Ricinus communis* oil	65	4	37:1	5 wt.%	99.99	(Martínez et al., 2018)
Na-CaO/MgO	Methanol	Canola oil	65	6	12:1	5 wt.% of oil	95.4	(Murguía-Ortiz et al., 2021)
MgO-KOH	Methanol	Mutton fat	65	20 min	22:1	4 wt.%	> 98% conversion	(Mutreja, Singh and Ali, 2011)
Heterogeneous Acid Catalysts								
AlCl$_3$	Methanol	*Lesquerella fendleri* oil	25	40 min	6:1	5 wt.%	95.5	(Shahidul Islam, Robin Hart and Casadonte, 2022)
SO$_3$H-Graphene Oxide@TiO$_2$	Methanol	Palm fatty acid distillate	70	40 min	9:1	3 wt.%	96.73	(Soltani et al., 2021)
Sulfonated carbon microspheres	Methanol	Waste frying oil	140	4	16:1	0.6 g	92.2	(Wang et al., 2021)

It is known that various heterogeneous base catalysts have been applied for biodiesel production since they are environmentally benign, non-corrosive and can be designed for high catalytic activity. According to Mansir et al. (2017), both Bronsted-type and Lewis-type solid acid catalysts possessed the merits of heterogeneous alkaline catalysts and mineral acids. Bronsted-type catalysts refer to materials that contain sulfonic acid, whereas mixed sulphated oxides are defined as Lewis-type catalysts. Same as the homogeneous acid catalyst, it can catalyse both esterification and transesterification reactions simultaneously. It also can be used with high moisture and FFA-containing feedstocks without soap formation. However, solid acid-catalysed biodiesel production has not been widely investigated due to its relatively low reaction rate and the possibility of leaching. Table 2.4 demonstrates the biodiesel production catalysed by the heterogeneous acid catalyst.

2.3.3   Enzymatic Catalyst

Enzyme catalyst is a promising alternative to overcome the limitations of chemical catalyst for biodiesel production, such as saponification, by-product separation and product purification. According to Guo, Sun and Liu (2020), enzymes can perform catalytic activity even in the presence of high moisture and FFA contents. Additionally, the enzyme-catalysed process is more energy efficient and eco-friendly. As stated in Rizwanul Fattah et al. (2020) work, extracellular and intracellular lipases are the two common enzymes catalysing biodiesel production. The enzymes that are recovered from the microorganism broth and purified are known as extracellular lipases, while intracellular lipases remain in the cell-producing wall or within the cell. Despite its environmental friendliness, using enzymatic catalysts for biodiesel production is still limited due to their high cost, low yield and longer reaction time. Table 2.5 presents the operating conditions and results of enzyme-catalysed biodiesel production.

2.3.4   Non-Catalytic Supercritical Process

Supercritical transesterification is defined as a non-catalytic biodiesel production at a pressure and temperature over the critical point of the reactants mixture. The physical state of a pure substance is controlled by pressure and temperature. Above the critical point between the gas and liquid phases, the

supercritical fluid (SCF) will be formed, and its density will vary depending on the temperature and pressure (Mani Rathnam and Madras, 2019). According to Ngamprasertsith and Sawangkeaw (n.d.), the density of SCF is high, like a liquid, but the molecules possess high kinetic energy, like the gas molecules. This characteristic improves the reactivity of the SCF in a chemical process. The non-catalytic biodiesel production can be conducted under supercritical conditions, as shown in Table 2.6.

The oil and alcohol are well dissolved and form a single phase for reaction under supercritical conditions due to the high molecular level miscibility of the two reactants. This is attributed to the reducing dielectric constant of polar components with the increasing temperature, thus improving reactant solubility (Singh, Singh and Sharma, 2022). In addition, more feedstocks can be used as the supercritical process is insensitive to moisture and FFA content. As listed in Table 2.6, the process generally requires higher temperature and pressure to achieve the critical point of mixtures and thus resulting in high power consumption and operating cost. Moreover, the high operating condition may degrade the FAAE formed or induce the reaction between the by-products and other components in the reaction medium. Consequently, the conversion and product yield are reduced.

Table 2.5: Enzyme-Catalysed Transesterification/Interesterification for Biodiesel Production.

| Catalyst | Alcohol (A) | Feedstock (B) | Reaction Conditions | | | | FAME Yield (%) | Reference |
			T (°C)	Time (h)	A:B Molar Ratio	Catalyst		
Commercial lipase	Ethanol	Acid waste oil	35	24	1.5:1	4 wt.%	68.4	(Cruz et al., 2018)
Candida antarctica lipase A	Methanol	Frying palm oil	30	22	7:1	5.5 Wt.%	94.6	(Guo, Sun and Liu, 2020)

Table 2.6: Supercritical Non-Catalytic Transesterification.

| Alcohol (A) | Feedstock (B) | Reaction Conditions | | | | FAME yield (%) | References |
		T (°C)	P (MPa)	Time (min)	A:B Molar Ratio		
Ethanol	Mahua oil	425	30	10	50:1	99% (conversion)	(Lamba, Modak and Madras, 2017)
Methanol	Jojoba oil	287	12.3	23	30:1	95.67	(Singh, Singh and Sharma, 2022)
Ethanol	Leather tanning waste	374.6	-	47.4	40.02:1	98.91	(Yuliana et al., 2020)

2.4   Synthesis of Carbon-based Solid Catalyst Derived from Biomass

Carbon-based catalysts are attractive in acid-catalysed biodiesel production due to their thermal stability, high acid density and ease of preparation. Following Naji and Tye (2022), the catalyst's structure, morphology and characteristics will determine its performance as a support. Activated carbon (AC) has been successfully used as a catalyst or catalyst support owing to its amorphous phase. The non-crystalline structure allows modification to improve the internal pore structure, porosity, surface reactivity and surface chemistry features. The carbon materials can be activated to obtain the desired AC structure due to their properties, such as high porosity with a wide range of pore-size distribution and large specific surface area (Wong et al., 2022).

Biomass is a carbon precursor that is widely investigated due to its high sustainability and availability. Based on the study of Chen et al. (2020), the diversity and inherently porous structure of carbonaceous materials derived from biomass led to a broader research space for its applications. Meanwhile, its elemental composition allows the biomass to be further processed for more active sites to act as catalysts. The low inorganic and ash content, high carbon content as well as high strength to retain the physicochemical features render the wastes as productive precursors for AC fabrication (Naji and Tye, 2022). Apart from reducing the production cost, using biomass as the catalyst support is an encouraging method to resolve the solid waste disposal issue in the world. It was disclosed that agricultural wastes such as rice straw, corn straw and sugarcane bagasse were generated annually up to 731, 204 and 181 million tons, respectively (Zhou and Wang, 2020). Most of the biomass wastes are directly disposed of in a landfill or incinerated in the open, which eventually increases greenhouse gas emissions and deteriorates the air quality. Therefore, biomass has been intensively investigated to convert it into value-added products for different applications.

Table 2.7:   Biodiesel Production Catalysed by Biomass Derived Catalyst.

Catalyst	Alcohol / Alkyl Acetate (A)	Feedstock (B)	Reaction Conditions				FAME Yield (%)	Reference
			T (°C)	Time (min)	A:B Molar Ratio	Catalyst		
Olive cake	Methanol	Waste vegetable oil	65	60	35:1	10 wt.%	57	(Sandouqa, Al-Hamamre and Asfar, 2019)
Sugar cane bagasse	Methanol	Waste cooking oil	60	15	18:1	15 wt.%	89.19	(Nazir et al., 2021)
Cacao shell	Methanol	Oleic acid	45	6 (h)	7:1	5% w/w	79	(Bureros et al., 2019)
Potato peel	Methanol	Oleic acid	80	2.5	12:1	5 wt.%	97.2 (Conversion)	(Hussein et al., 2021)
Powdered bamboo	Methanol	Oleic acid	65	8	8:1	10 wt.%	97.98 (Conversion)	(Zhang et al., 2021)

The biomass with high calcium content can be directly transformed into a solid base catalyst for biodiesel production, for example, shells, bones, peels and leaves. Calcium oxide, CaO derived from waste chicken eggshells, was used as a solid catalyst and produced 98.62 % biodiesel yield in the work of Zhou and Wang (2020). In the study of Miladinović et al. (2022), a hazelnut shell was used to synthesise a heterogeneous catalyst and successfully resulted in a biodiesel yield of 98 %. On the other hand, the solid acid catalyst can be synthesised by subjecting it to pyrolysis followed by sulfonation or sulfation process. The soft aggregated aromatic polymer with unique pore structures and hydrophobic in nature will be formed during pyrolysis. Meanwhile, the functional group will be attached to the surface of sulfonated or sulfated biomass, contributing to its catalytic activity (Agapay et al., 2021). Table 2.7 shows the biodiesel production catalysed by a solid catalyst derived from biomass.

Coffee is one of the highest consuming beverages in the world. According to the Coffee Market Report released by International Coffee Organization (2021), global coffee consumption steadily grew for the last 10 years before the covid-19 pandemic outbreak, as shown in Figure 2.5. It was estimated to increase by 1.9 % from 164.13 million bags of coffee in 2019/20 to 167.26 million bags in 2020/21. As reported by Agapay et al. (2021), more than 65 % w/w of green coffee beans were used for coffee brewing, and a significant amount of spent coffee grounds (SCGs) were generated. The SCGs are used as soil conditioners or fertilizers, but the leaching of caffeine and polyphenols can be detrimental to the environment.
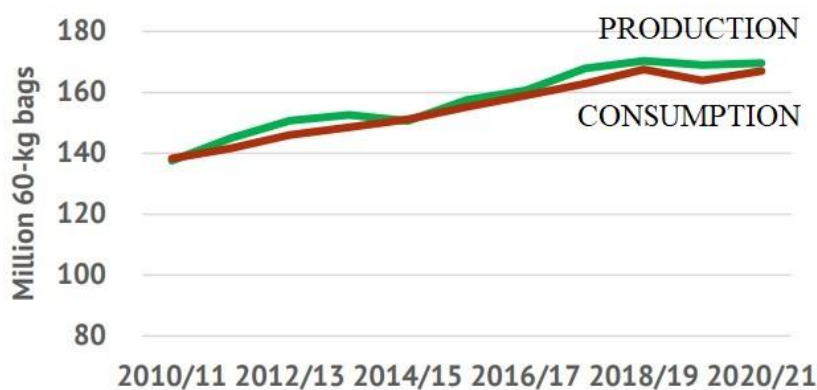
Figure 2.5: Production and Consumption of Coffee from 2010 to 2020 (International Coffee Organization, 2021).

SCG wastes have been broadly investigated for further utilization or recycling instead of disposal at the landfill to relieve the environmental issues. The SCG is a potential biodiesel feedstock due to its high lipid content of 10 to 16 wt.% of dry mass. In the experiment of Supang et al. (2022), the highest fatty acid ethyl ester (FAEE) obtained from the interesterification of oil extracted from SCGs with ethyl acetate was 91.80 wt.%. Besides, the lignocellulosic material constitutes up to 50 % of dry SCGs and can produce bioethanol and bio-composites by fermentation and using a polypropylene matrix, respectively (Tian et al., 2021). SCGs also be activated to form AC and used as adsorbents for contaminant removal from water, such asline yellow dye (Pagalan et al., 2020) and tetracycline (Dai et al., 2019).

Like other AC, it was believed that activated carbon derived from SCGs could be further sulfonated to form the solid acid catalyst for biodiesel production. However, limited research uses SCGs as carbon precursors for catalysed esterification or transesterification. In Ngaosuwan, Goodwin and Prasertdham (2016) work, the SCG was carbonised with $ZnCl_2$ as the activation agent and subsequently treated with concentrated sulfuric acid for sulfonation. The transesterification of caprylic acid with methanol was carried out with 5 wt.% catalyst loading and resulted in a conversion of 71.5 %. The solid acid catalyst was also prepared without activation, only carbonisation and direct sulfonation using concentrated sulfuric acid (Agapay et al., 2021). The conversion of 90 % was achieved via the transesterification of oleic acid using methanol and 10 wt.% of catalyst.

2.4.1   Activation and Carbonisation

The carbon precursor can be converted into AC in two different ways, either through direct activation or a two-stage process that including carbonisation followed by activation. Figure 2.6 demonstrates the series of steps in preparing an AC. The washing and drying steps before activation remove the impurities and free moisture, respectively. Then, the material is ground and sieved to serve as the carbon precursors for AC fabrication.
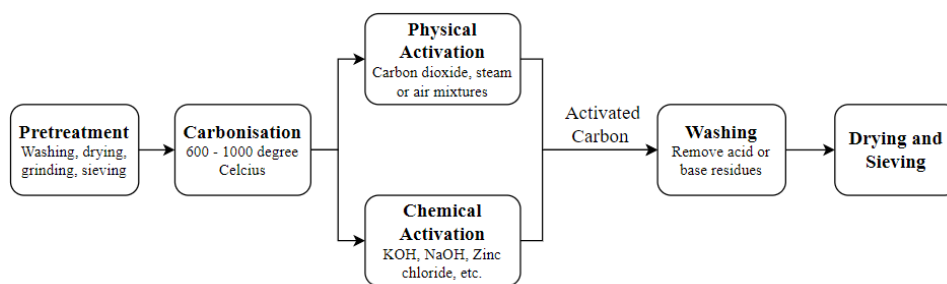
Figure 2.6: Synthesis of Activated Carbon from Biomass (Naji and Tye, 2022).

Carbonisation transforms the carbon precursor into a carbon-rich material by eliminating the volatile non-carbon components. Normally, the material is subjected to pyrolysis at 600 to 1000 °C in the absence of oxygen with gases like N_2 or argon. The less stable bonds broke during the carbonisation, releasing the volatile portion of the precursor material and forming a carbonaceous residue with a rudimentary porous structure. However, the adsorption capacity is low as part of the volatile components released in the pyrolysis re-polymerise and condense on the surface, thus filling or blocking the pores (Pallarés, González-Cencerrado and Arauzo, 2018). Hence, the subsequent activation stage is vital to eliminate the deposits and increase the porosity and adsorption capacity.

In activation, the microporous structure can be improved when the disorganised carbon is removed. Meanwhile, the degradation of walls between the pores leads to pore enlargement (Naji and Tye, 2022). Physical activation is a chemical-free process as the material is activated in atmospheric oxidising gases, for example, steam, CO_2, N_2 and air mixtures with an elevated temperature at around 800 to 1100 °C. In contrast, chemical activation involves impregnating carbonised material in oxidising and highly dehydrated chemicals. During chemical activation, the precursor is thermally decomposed due to the reaction between activating chemical and carbonaceous material, which reduces the evolution of volatile matter and inhibits the shrinkage of the particle (Ngaosuwan, Goodwin and Prasertdham, 2016). Heidarinejad et al. (2020) reported that the tiny pores in the AC were developed due to the deep penetration of activation agents into the carbon surface, thereby increasing the surface area. The macropores, mesopores and micropores formed on the surface

of AC can be differentiated based on their sizes, which are larger than 25 nm, between 1 to 25 nm and smaller than 1 nm, respectively. Table 2.8 concludes the merits and demerits of physical and chemical activation.

Common chemical activating agents include KOH, NaOH, $CaCl_2$, $ZnCl_2$ and H_3PO_4. Among all activating agents, zinc chloride and phosphoric acid are widely used to activate lignocellulosic materials that mainly constitute cellulose, hemicellulose and lignin (Yakout and Sharaf El-Deen, 2016). However, H_3PO_4 is preferable to $ZnCl_2$ due to the environmental disadvantages associated with $ZnCl_2$. In the work of Zięzio et al. (2020), the spent coffee ground was impregnated in phosphoric acid solution with a specific concentration for 24 h before subjecting to rinsing and drying for further analysis. The resulting activated carbon developed a satisfactory porosity with a surface area and pore volume of 720.9 m^2/g and 0.334 cm^3/g, respectively.

Table 2.8:   Advantages and Disadvantages of Physical and Chemical Activation (Heidarinejad et al., 2020).

	Advantages	**Disadvantages**
Physical Activation	- Inexpensive - Chemical-free	- Long activation time - Low adsorption capacity - High energy consumption
Chemical Activation	- Short activation time - Lower temperature - High carbon efficiency - Structure with high porosity	- Repeated and long washing step - Toxic wastewater generation

2.4.2   Sulfonation

Sulfonation is defined as a process for introducing the sulfonic groups, $-SO_3H$, to functionalise the carbonised biomass and modify its surface for enhanced catalytic activity. The aromatic polycyclic carbon rings are formed due to the dissociation of -C-O-C bonds during carbonisation at high temperatures. As illustrated in Figure 2.7, the $-SO_3H$ groups are then introduced into the carbon rings and covalently bound to the carbon base when aromatic carbon rings are oxidised during sulfonation (Fonseca et al., 2022).

Carbon sources, including lignin, biochar, AC and biomass are normally sulfonated via direct sulfonation with H_3SO_4, H_2SO_4, 4-aminobenzenesulfonic acid or a blend of H_2SO_4 with nitric acid, HNO_3 (Zailan et al., 2021). It was reported that $-SO_3H$ groups are the only active sites when homogeneous H_3SO_4 is used. As opposed to it, there are three different functional groups, which are -COOH, -OH and $-SO_3H$, that serve as the active sites in the sulfonated carbon-based acid catalyst. According to Fonseca et al. (2022), the hydrophilic -COOH and -OH groups could incorporate water on the catalyst surface and improve the accessibility of reactants to the sulfonic group. Consequently, the catalytic activity and reaction rate will increase even for materials with a small surface area.
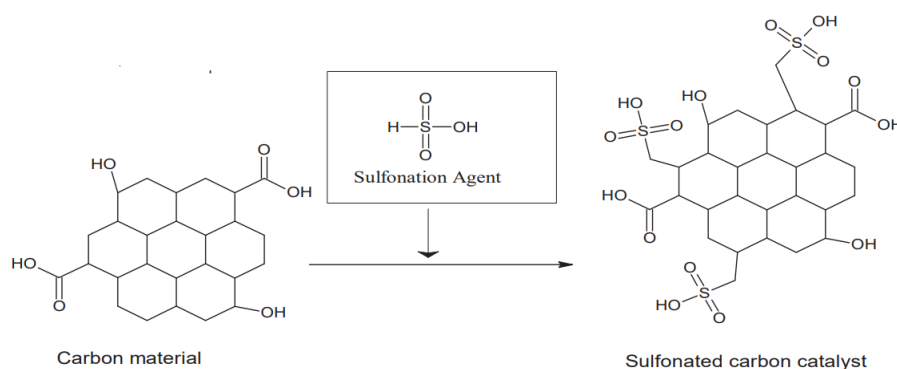
Figure 2.7: Direct Sulfonation Scheme to Synthesis Carbon Acid Catalyst (Zailan et al., 2021).

In the case of using SCG to produce a solid acid catalyst, Ngaosuwan, Goodwin and Prasertdham (2016) conducted the sulfonation with concentrated sulfuric acid and a carbon-to-acid ratio of 1 g to 20 mL. The highest conversion was obtained using the catalyst, which was sulfonated under 200 °C for 4 h. In the study of Agapay et al. (2021), the highest acid density of 4.22 mmol H^+/g was achieved by sulfonating the SCG carbonised catalyst at a temperature of 100 °C for 1 h, resulting in the conversion of more than 90%.

2.5   Characterisation of Synthesised Catalyst

Various analytical techniques can be used for the characterisation of the synthesised biomass-derived catalysts prior to application in biodiesel

production. The catalysts' structure, morphology, surface area and acid density can be studied using the analytical techniques listed in Table 2.9 to analyse its catalytic performance.

Table 2.9: Analytic Techniques for Catalyst Characterisation (Kirubakaran and Arul Mozhi Selvan, 2018).

Analytic Technique	Characterisation
SEM	Identification of surface structure and morphology
XRD	Identification of crystalline phases
FTIR	Analysis of functional groups attached to the sample
TGA	Determination of thermal transition of the sample
BET	Identification of specific surface area, pore distribution and volume of the sample

2.5.1   Acid Density

Apart from the strong sulfonic groups, there are weak acid groups, for instance, carboxylic and phenolic groups, contributing to the catalytic activity of the solid catalyst. Therefore, the total acid density is claimed as the main characteristic of a sulfonated catalyst (Fonseca et al., 2022). The performance and textural properties of the synthesised solid acid catalysts are influenced by the temperature and time for both carbonisation and sulfonation. Table 2.10 presents the acid density of the sulfonated catalysts synthesised under different carbonisation and sulfonation conditions. Based on the table, it can be observed that the most common sulfonating agent is concentrated sulfuric acid. The carbonisation of catalysts was conducted at a temperature ranging from 350 ℃ to 600 ℃ for 1 h to 4 h to achieve good acid density, whereas sulfonation was carried out at a temperature of 100 ℃ to 200 ℃ for 1 h to 6 h.

2.5.2   Scanning Electron Microscopy Equipped with Energy Dispersive X-ray (SEM-EDX)

Scanning electron microscopy (SEM) is an analytical tool that provides high-resolution images of the specimen, while energy dispersive x-ray analyser (EDX) identifies the elements and provides compositional information quantitatively

(Lucideon, n.d.). Figure 2.8 presents the X-ray generation process when the sample is analysed using SEM-EDX.

When the electron beam hits (primary e⁻ beam) the specimen, some of the energy will be transferred to the atoms in the specimen. The electron of the atoms will "jump" to the higher energy shell by using the energy and create a vacancy in the inner lower-energy shell. The negatively-charged electrons from higher-energy shells tend to be attracted to the positively-charge holes. Once the electron from a higher energy shell occupies the hole, the energy difference will be released as X-ray radiation, as illustrated in Figure 2.8. The energy possessed by the X-ray is varied for each element depending on the atomic number; thus, it can be used to identify the elements that exist in the sample (AZO Material, 2018).
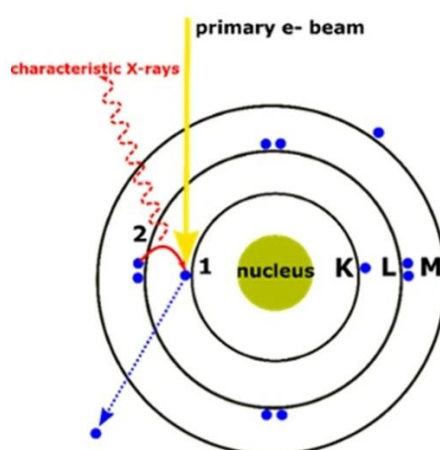
Figure 2.8: The Generation of Characteristic X-rays (AZO Material, 2018).

Ngaosuwan, Goodwin and Prasertdham (2016) carried out SEM on the samples of activated SCG without sulfonation and with sulfonation at different temperatures to examine the surface morphology of the synthesised catalyst. As demonstrated in Figure 2.9, the crystallinity of the activated catalyst that was sulfonated at 180 ℃ (SCAC-180) was more significant than the solely activated SCG (CAC). On the other hand, EDX analysis was conducted by Agapay et al. (2021) to identify the elemental composition on the surface of the sulfonated activated carbon derived from the spent coffee ground. Table 2.11 clearly shows that the composition of sulfur significantly increased after sulfonation.

Table 2.10: Carbonization and Sulfonation Conditions to Synthesis Solid Acid Catalysts.

Catalysts	Carbonisation		Sulfonation			Acid density (mmol/g)	Reference
	T (°C)	Time (h)	Agents	T (°C)	Time (h)		
Olive cake	400	1	98% conc. H_2SO_4	150	1	4.24	(Sandouqa, Al-Hamamre and Asfar, 2019)
Sugar cane bagasse	400	1	Conc. H_2SO_4	180	2	4.74	(Nazir et al., 2021)
Cacao shell	350	1	Conc. H_2SO_4	120	6	4.56	(Bureros et al., 2019)
Oil palm empty fruit bunch	600	3	Conc. H_2SO_4	100	6	9.00	(Wong et al., 2020)
Spent coffee grounds	600	4	Conc. H_2SO_4	200	4	-	Ngaosuwan, Goodwin and Prasertdham (2016)
Spent coffee grounds	400	2	Conc. H_2SO_4	100	1	4.22	Agapay et al. (2021)
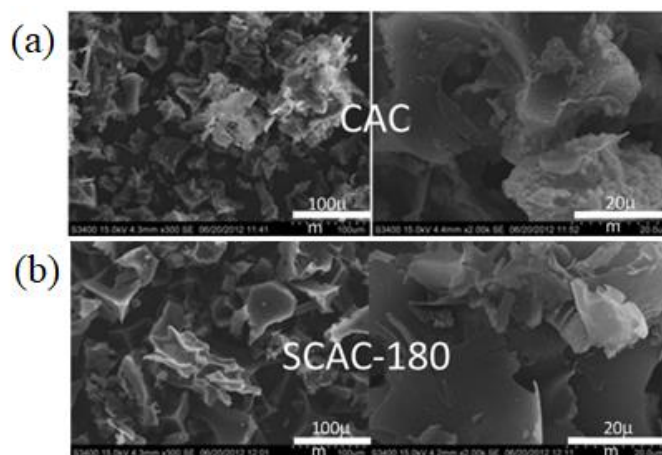
Figure 2.9: SEM Images of (a) Solely Activated SCG and (b) Activated SCG with Sulfonation at 180 °C (Ngaosuwan, Goodwin and Prasertdham, 2016).

Table 2.11: Elemental Composition from EDX Analysis (Agapay et al., 2021).

Catalyst	Relative elemental composition (% mol/mol)			
	C	O	N	S
SCG	70.97	23.08	5.91	0.03
Carbonised SCG (400 °C for 2 h)	88.32	3.87	7.30	0.51
Carbonised (400 °C for 2 h) and sulfonated (100 °C for 1 h) SCG	70.17	22.86	4.02	2.95

2.5.3 X-ray Diffractometer (XRD)

In X-ray diffraction analysis, an incident X-ray beam is irradiated on the sample and diffracted into various directions with electromagnetic radiation ranging from 0.01 to 0.7 nm. The bulk crystal structure and chemical phase composition are then characterised using the angles and intensities of the diffracted beams. In crystalline materials, the arrangement of atoms is in a regular three-dimensional pattern known as crystal structure. In contrast, the atoms in amorphous materials are in a regular periodic manner with short-range order (Dumbre and Choudhary, 2020). Figure 2.10 illustrates the XRD patterns of carbonised SCG without sulfonation (CAC) and with sulfonation (SCAC) at a temperature of 140, 160, 180 and 200 °C.
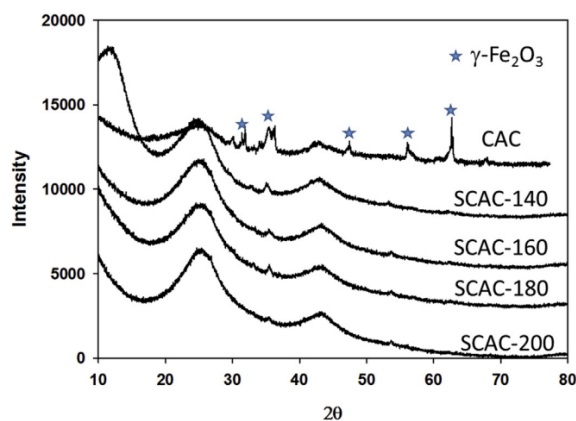
Figure 2.10:   XRD Patterns of CAC and SCAC Sulfonated at Temperature of 140, 160, 180 and 200 °C (Ngaosuwan, Goodwin and Prasertdham, 2016).

The weak and broad diffraction peaks at 2θ of 10 to 30° represented the amorphous carbon with a C(002) plane. Meanwhile, another peak at 2θ of 30 to 50° indicated the definitive C(101) plane in the graphene structure. It was claimed that there were more graphene sheet structures in SCAC that were sulfonated compared to CAC. Besides, the presence of peaks of crystalline γ-Fe_2O_3 was attributed to the iron impurities from the stainless steel tube used for carbonisation. Nevertheless, the impurities were removed in the sulfonation process based on the obviously reduced peak in the XRD of SCAC, as shown in Figure 2.10.

2.5.4   Fourier Transform Infrared Spectroscopy (FTIR)

Vibrational spectroscopy, known as FTIR, identifies the sample's molecular structure based on infrared radiation (IR) absorption by molecular vibrations. During IR irradiation, the functional groups in the sample absorb some radiation while some radiation is transmitted. The output of detectors is then converted into an interpretable spectrum that can be used to identify the functional groups on the sample, given that different chemical structures result in different spectral "fingerprints". The locations and intensities of IR radiation transmittance identify the type of functional groups that exist in the sample. In the study by Agapay et al. (2021), the functional groups in catalyst samples were identified using FTIR analysis, as shown in Figure 2.11, given that C400(2) referred to the

catalyst that was carbonised at 400 °C for 2 h while S50(1), S100(1), S150(1) represented the carbonised catalyst that was sulfonated at 50, 100 and 150 °C, respectively for 1 h. Table 2.12 summarises the functional groups attached to the catalyst samples using FTIR.
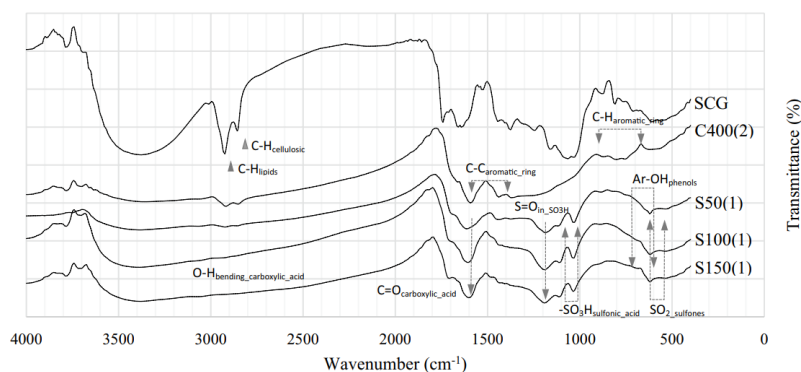
Figure 2.11:   FTIR Spectra of SCG, Carbonised SCG and Sulfonated SCG (Agapay et al., 2021).

Table 2.12: Functional Groups in Raw SCG, Carbonised SCG (C400(2)) and Sulfonated SCG (S50(1), S100(1) and S150(1)).

Functional groups	Wavelength (cm^{-1})	Catalysts
C-H bonds of aliphatic carbon structure from cellulosic component and lipid	2850 and 2920	Raw SCG
C-H bonds in aromatic rings	657 to 900	Carbonised SCG and sulfonated SCG
C-C bonds in aromatic rings	1400 to 1500	
	1585 to 1600	
SO_2 in sulfones	545 to 610	Sulfonated SCG
Ar-OH in phenols	600 to 720	
$-SO_3H$ in sulfonic acid	1040 to 1100	
S=O stretching in $-SO_3H$	1150 to 1245	
S=O stretching in sulfonate	1335 to 1372	
O-H bending in the carboxylic acid	1395 to 1440	
OH stretching	2400 to 3400	
C=O stretching in the carboxylic acid	1690 to 1710	

2.5.5   Thermogravimetric Analysis (TGA)

In TGA analysis, the weight of the sample is measured outside the furnace while the temperature of the furnace with the sample inside is gradually increased. The loss of volatile components during the thermal event is indicated by the mass loss recorded in TGA (PhotoMetrics, n.d.). The evaluation of the thermal stability of the catalyst is essential to avoid using the temperature that may decompose the sulfonic groups, and it can be determined with TGA analysis.

Figure 2.12 illustrates the thermal stability of solid sulfonated acid derived from SCG, which fits the result of Chellappan et al. (2018), where the biomass lost mass at around 400 °C. At high temperatures, releasing the sulfonic group forms volatile species, which changes the mass loss profile and catalyst degradation. Hence, a temperature lower than 400 °C is suitable for biodiesel production to preserve the catalytic performance while preventing the degradation of the catalyst.
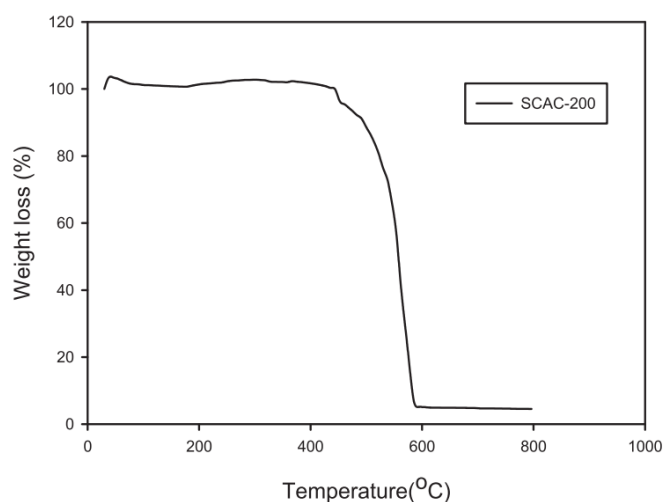
Figure 2.12:   Thermal Stability of Sulfonated SCG Catalyst using TGA Analysis (Ngaosuwan, Goodwin and Prasertdham, 2016).

2.5.6   Surface Analysis

Brunauer-Emmett-Teller (BET) is a technique analysing the surface of a solid material according to the adsorption of gas molecules on the surface (Dumbre and Choudhary, 2020). Meanwhile, Barrett-Joyner-Halenda (BJH) technique is well-known as a method to evaluate the pore area and specific pore volume via the adsorption and desorption of nitrogen. A probing gas that is chemically inert

with material surfaces is usually used as the adsorbate to quantify the specific surface area. In most cases, nitrogen is used as the adsorbate, and its boiling point of around 77K is often set as the analysis temperature. The synthesised catalysts can be analysed in terms of specific surface area, pore volume and distribution based on the amount of nitrogen gas corresponding to a monomolecular layer on the solid surface that is formed via physical adsorption.

Based on the study of Fu et al. (2019), the optimum calcination temperature of the catalysts was determined using BET isotherm plots, as shown in Figure 2.13. The commercial Ni-based catalyst (CNC) calcinated at 600 °C (CNC600) resulted in more gas adsorbed as new pores formed on the solid surface. Nevertheless, the amount of adsorbed gas molecules was reduced with further rising calcination temperature. The isotherm curve was similar to the type IV isotherm according to the classification of International Union of Pure and Applied Chemistry (IUPAC) shown in Appendix B, signifying that the synthesised catalysts were mesoporous materials. It was confirmed by the pore size distribution obtained from BJH adsorption, as illustrated in Figure 2.14. It showed that the pore size ranged from 5 nm to 50 nm, which fell in the range of mesopores.
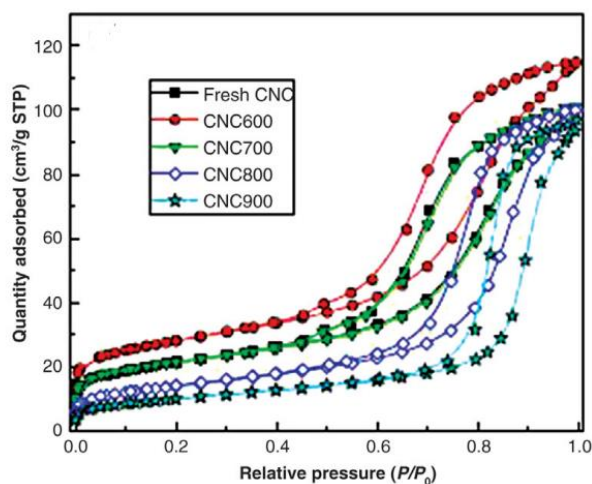
Figure 2.13:   Nitrogen Adsorption-Desorption Isothermal Curves (Fu et al., 2019).
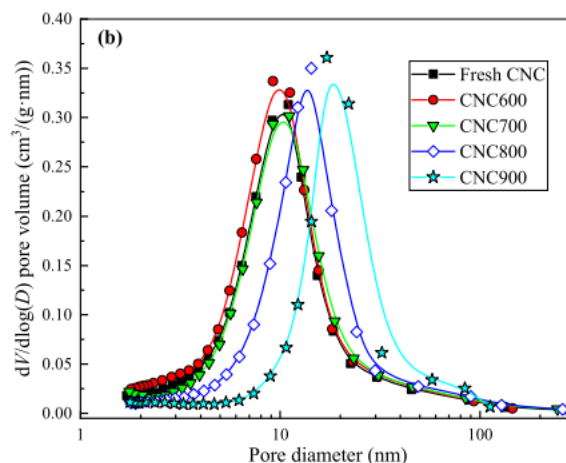
Figure 2.14:   Pore Size Distribution of Synthesised Catalysts (Fu et al., 2019).

2.6   Characterisation of Feedstocks and Product

The first and second-generation biodiesel are generally produced from edible and non-edible oils, respectively. The most abundant FFAs in both oils are usually palmitic, stearic, and oleic acids. Oleic acid (C18:1) is widely used for biodiesel production due to its properties, such as high heating value, density, kinematic viscosity, cetane index, pour and cloud point. It is suitable to use solid acid catalysts when the feedstock with high FFA content is used to produce biodiesel. Therefore, the chemical composition, especially the FFA content of oleic acid, has to be identified prior to biodiesel production.

2.6.1   Acid Value

Acid value is used to identify the FFA content in a sample. By titrating the oil with KOH, the acid value can be determined and is expressed as the amount of KOH required (mg) to neutralise 1 g of oil. For the study of biodiesel production, it is used to measure the FFA content in the feedstock oil before the reaction and the biodiesel formed after the reaction. Then, the conversion of FFA can be determined by finding the difference in FFA to investigate the performance of biodiesel production. For instance, the acid value of waste vegetable oil was reduced from 3.67 mg KOH/g to 0.22 mg KOH/g, indicating the FFA conversion of 94% in the work of Sandouqa, Al-Hamamre and Asfar (2019).

2.6.2   Gas Chromatography (GC)

GC is often used to quantitatively analyse a sample due to its high sensitivity, accuracy and separation ability. During GC analysis, the chemical components are separated, followed by detecting their presence and the amount present in the sample. Flame-ionization detector (FID) is one of the most commonly used detectors with GC to detect the organic compounds in the sample. After the column, carbon ions are generated as the sample is subjected to combustion in a hot, hydrogen-air flame. The higher number of ions indicates a higher number of carbons in the sample. Thus, the amount of carbon can be determined by measuring the current generated from the ions (JoVE Science Education Database, 2022).

GC-FID is usually used to identify the fatty acid composition in the feedstock and the final product in biodiesel production. In most of the studies, the analysis result of the final product using GC-FID was further calculated to find out the biodiesel yield or conversion. In the study of Mostafa Marzouk et al. (2021), GC-FID was utilised to analyse both feedstock and the final product. It was reported that the WCO contained 43.52 % of oleic acid, followed by 36.58 % of linoleic acid, 11.14 % of palmitic acid and 3.86 % of stearic acid. Meanwhile, the biodiesel conversion was up to 99.89 % under optimum operating conditions.

In the study of Nguyen et al. (2018), a GC-FID with a capillary column was used to analyse the final product. Nitrogen at a 29 mL/min flow rate was used as the carrier gas. The temperature of the injector and detector were 220 °C and 250 °C, respectively. The temperature of the column was increased by 4 °C/min from the initial temperature of 140 °C to 240 °C and maintained for 15 minutes. Under optimum operating conditions, the biodiesel yield of 96.97 % was determined using GC-FID analysis.

2.7   Parameter Studies

Parameter studies are vital to optimise the catalytic performance of the synthesised catalyst. The attachment of functional groups to the precursor is influenced by the sulfonation temperature. Besides, the catalytic performance is also influenced by the operating conditions of the esterification process, such as methanol-to-oleic acid molar ratio and catalyst loading.

2.7.1 Effect of Sulfonation Temperature

As tabulated in Table 2.10, the sulfonation of the catalyst is generally conducted at a temperature ranging from 100 °C to 200 °C for 1 h to 6 h. The effect of sulfonation temperature was studied by Xiao and Hill (2020), and the result was demonstrated in Figure 2.15. The acidity of -SO₃H groups increased from 80 °C to 100 °C and decreased at temperatures 100 °C onwards. This result agreed with the experiment of Wong et al. (2020), where the total acid density increased when the sulfonation temperature increased from 75 °C to 100 °C and significantly dropped when the temperature was higher than 100 °C. The low acidity was attributed to the low sulfonation rate, as the low temperature was insufficient to support the reaction of sulfonating reagent and the AC
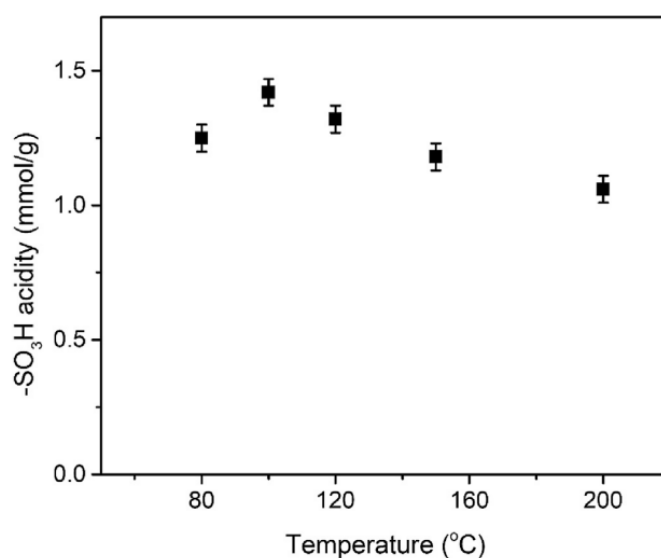
Figure 2.15:   Effect of Sulfonation Temperature on the Acidity of the Synthesised Catalyst (Xiao and Hill, 2020).

However, the acidity of strong acid groups drops when too high temperature is used for sulfonation. It was found that the amount of -SO₃H groups attached to the catalyst surface is significantly reduced due to the domination of side reactions such as oxidation, hydrolysis, condensation and dehydration at high temperatures. In addition to the surface morphology, the porous structure of carbon support may also destroy under high sulfonation temperatures, resulting in bad catalytic performance. In contrast to strong -SO₃H

acid groups, Ngaosuwan, Goodwin and Prasertdham (2016) revealed that the density of weak acid sites increased with rising sulfonation temperature. Since weak acid sites also contribute to the catalytic activities, the balance of strong and weak acid sites must be considered when selecting the sulfonation temperature.

2.7.2 Effect of Molar Ratio of Methanol to Oleic Acid

Methanol is a common acyl acceptor in the esterification or transesterification reactions for FAME production. As one of the factors affecting the reaction performance, the molar ratio of two reactants plays a key role in optimising the FAME yield. Methanol is generally added in excess to promote the reaction, as esterification is reversible. In the work of Zhang et al. (2021), the conversion yield of FFA increased rapidly as the molar ratio increased from 4:1 to 8:1, as shown in Figure 2.16. However, a downward trend is observed beyond the molar ratio of 8 due to the reduction in collision frequency of reactant particles in the large volume of reactant mixture. A similar trend was obtained by Senoymak Tarakcı and Ilgen (2018), where the oleic acid conversion increased with the methanol-to-oleic acid molar ratio of 1:1 to 9:1 and remained constant when it is further increased to 12:1.
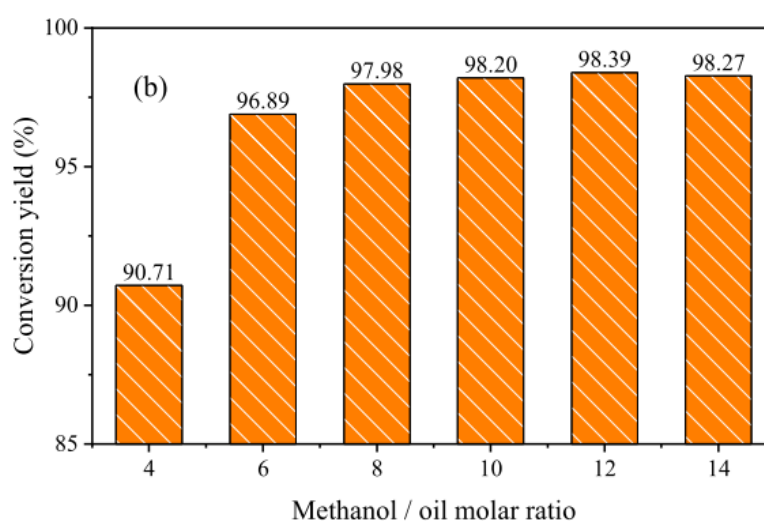
Figure 2.16:   Impact of Methanol-to-Oleic Acid Molar Ratio on Free Fatty Acid Conversion (Zhang et al., 2021).

2.7.3   Effect of Catalyst Loading

Catalysts speed up the reaction by providing an alternative pathway with lower activation energy to synthesise the final products. Nazir et al. (2021) conducted experiments to look into the influence of catalyst loading on the biodiesel yield by using 5, 10, 15 and 20 wt.% of catalyst based on the weight of feedstock given that other parameters were fixed constant. The biodiesel yield increased significantly from 49.46 % to 88.7 % when the catalyst loading was up to 15 wt.%, as shown in Figure 2.17. Nevertheless, the effect of further increase of catalyst loading was not pronounced.
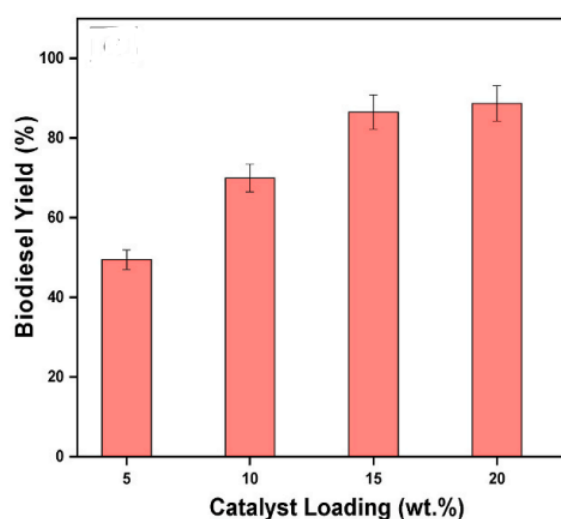
Figure 2.17:   Impact of Catalyst Loading on the Biodiesel Yield (Nazir et al., 2021).

The result obtained by Wong et al. (2020) supported that the yield of FAME initially increased with increasing catalyst loading and decreased beyond the optimum point. The maximum yield of 50.5 % was achieved with a 10 wt.% catalyst, which dropped to 42.7 % with a 12 wt.% catalyst. It was due to the formation of a more viscous mixture when an excessive heterogeneous catalyst was added. Despite more available acidic sites, the poor dispersion of the catalyst hindered the mass transfer of reactants, resulting in a low reaction rate.

CHAPTER 3

METHODOLOGY AND WORK PLAN

3.1 List of Material and Equipment

Various chemicals and materials were prepared before the experiment was conducted. The production, characterisation and evaluation of synthesised catalysts and biodiesel also required some apparatus and equipment. In this study, the materials, chemicals, apparatus and equipment involved were listed in sections 3.1.1 and 3.1.2.

3.1.1 Materials and Chemicals

The waste of coffee brewing, spent coffee ground (SCG) was used as the biomass waste to fabricate the solid acid catalyst in this experiment. The SCG was collected from a small coffee shop, Big Three Coffee, located at Jenjarom, Selangor, Malaysia. Table 3.1 lists the chemicals with their respective brand and purity used in this study.

Table 3.1: Chemicals Required for the Experiment.

Chemicals	Brand	Purity	Purpose
Ortho-Phosphoric Acid	Merck	85 %	Activation agent for biomass wastes
Sulfuric Acid	Merck	95 % - 97 %	Direct sulfonation of AC derived from biomass waste
Oleic Acid	Sigma-Aldrich	90 %	Reactant for interesterification process
Methanol	Merck	≥ 99.8 %	Reactant for interesterification process
Sodium Hydroxide, NaOH pellets	Merck	≥ 99.0 %	Titrant for measurement of acid density

Table 3.1: Chemicals Required for the Experiment (Cont.)

Chemicals	Brand	Purity	Purpose
Hydrochloric acid, HCl	Fisher Chemical	37 %	Blank titration to identify the acid density of the catalyst
Phenolphthalein	R & M Chemicals	1 g/L	Indicator of pH or colour change during titration
2-Propanol	Merck	$\geq$ 99.8 %	Solvent of oleic acid and biodiesel for measurement of acid values
Potassium Hydroxide, KOH pellets	Merck	$\geq$ 99.0 %	Titrant for measurement of acid value
Methyl Oleate	Sigma-Aldrich	$\geq$ 99.9 %	Preparation of calibration curve for GC
n-Hexane	Merck	$\geq$ 99.8 %	Solvent of biodiesel for GC analysis
Methyl Heptadecanoate	Sigma-Aldrich	4 g/L	Internal standard used in GC

3.1.2   Apparatus and Equipment

Various apparatus and equipment were utilised to carry out the experiment. All the instruments involved in preparing solid acid catalysts and biodiesel production, as well as characterising reactants, catalysts and final products, are listed in Table 3.2.

Table 3.2: Apparatus and Equipment Used in the Experiment.

Apparatus/Equipment	Specification	Purpose
Oven	Memmert	Drying of biomass waste and synthesised catalyst
Sieve	300 μm- and 600 μm-mesh size	Sieving of biomass waste
Programmable furnace	Wise Therm FP-03	Carbonisation of biomass waste
Heating mantle	Mtops	Maintain the desired temperature during interesterification
Scanning Electron Microscope Equipped with Energy Dispersive X-ray (SEM-EDX)	Hitachi S-3400N	Analysis of surface morphology and chemical elements in the synthesised solid acid catalyst
X-ray Diffractometer (XRD)	Shidmazu XRD-6000	Identification of crystalline phase, size and shape of the synthesised solid acid catalyst
Fourier Transform Infrared Spectrometer (FTIR)	Nicolet IS10	Identification of functional groups attached to the synthesised solid acid catalyst
Thermogravimetric Analyzer (TGA)	Perkin Elmer STA8000	Analysis of thermal decomposition of the synthesised catalyst
Gas Chromatograph (GC)	Perkin Elmer Claurus 500	Determination of the composition of methyl oleate in the biodiesel product
Surface Analyzer	Micromeritics 3Flex	Identification of specific surface, pore distribution and pore volume of the synthesised catalyst

3.2   Overall Experiment Methodology and Flowchart

The overall flow of this research study is displayed in Figure 3.1. The experiment was conducted step by step, as shown in the flowchart. Some steps were repeated, if necessary, to achieve the ultimate goals of fabricating the solid acid catalyst from biomass waste and producing biodiesel via esterification.

Pretreatment of Spent Coffee Grounds
- Drying
- Further grinding
- Sieving

Synthesis of Solid Acid Catalyst
- Chemical activation with H_3PO_4
- Carbonisation
- Direct sulfonation with sulfuric acid

Characterisation of Synthesised Catalyst
- Acid density
- Scanning Electron Microscopy Equipped with Energy Dispersive X-ray (SEM-EDX)
- X-ray Diffractometer (XRD)
- Fourier Transform Infrared Spectroscopy (FTIR)
- Thermogravimetric Analysis (TGA)
- Surface Area Analysis (BET)

Biodiesel Production
- Solid Acid-catalysed Esterification

Characterisation of Biodiesel
- Acid Value
- Gas Chromatography (GC)

Parameter Studies
- Effect of Sulfonation Temperature (80 ℃ - 200 ℃)
- Effect of Catalyst Loading (4 wt.% - 20 wt.%)
- Effect of Methanol to Oleic Acid Molar Ratio (4:1 - 20:1)

Figure 3.1: Overall Research Flowchart of This Study.

3.3 Experimental Procedures

3.3.1 Pretreatment of Biomass

The collected SCGs were washed using water to remove solid impurities before drying. The biomass wastes were dried in the oven overnight at 80 ℃ to remove the moisture. The dried SCGs were ground using a pestle and mortar, followed by a size reduction using a sieve with 600 μm mesh. The resulting sample was kept in sealed plastic bags before using for the following analysis and fabrication.

3.3.2 Activation and Carbonisation of Biomass

A mixture of SCGs and activation agent was prepared to activate biomass waste. In this study, 30 v/v% H_3PO_4 solution was used as the activation agent and mixed with SCGs with an SCG-to-H_3PO_4 mass ratio of 1:7. After 24-hour impregnation, the solid biomass was washed three times with distilled water, filtered and dried overnight at 80 ℃. Then, carbonisation was carried out at 500 ℃ for 4 h using a programmable furnace with a heating rate of 10 ℃/min. After carbonisation, the H_3PO_4-impregnated AC sample was further ground and sieved using a 300 μm-mesh sieve for size reduction. The carbonised spent coffee ground prepared was denoted as CSCG.

3.3.3 Sulfonation of Activated Carbon

The prepared CSCG was mixed with concentrated sulfuric acid with an AC-to-H_2SO_4 ratio of 1 g to 20 mL to introduce the functional group onto the carbon support. The mixture was heated at various temperatures with a constant stirring speed of 350 rpm for 2 h. After sulfonation, the mixture was diluted and filtered using the Buchner funnel, which was connected to the filtering flask and vacuum pump for vacuum filtration. Distilled water was used to wash the sample three times to remove the excess sulfuric acid before drying at 80 ℃ overnight in the oven. Table 3.3 shows the denotations of the catalysts prepared under different sulfonation temperatures.

Table 3.3: Catalyst Annotations with Different Sulfonation Temperatures.

Catalyst Sample	Sulfonation Temperature (°C)
SCSCG$_{80}$	80
SCSCG$_{120}$	120
SCSCG$_{160}$	160
SCSCG$_{200}$	200
SCSCG$_{240}$	240

3.3.4 Esterification for Biodiesel Production

In addition to characterisation, the catalytic performance of the synthesised solid acid catalyst from biomass waste was evaluated based on the FFA conversion and biodiesel yield. The catalyst synthesised at optimum sulfonation temperature was used in the esterification process, where oleic acid was used as the feedstock oil and reacted with methanol (MeOH). Since the mixture of reactants was less than 200 mL, a three-neck round bottom flask with a 500 mL capacity was used. Moreover, a water-cooled coil condenser was equipped to condense the evaporated MeOH, while a magnetic stirrer and heating mantle were used to perform uniform heating and well mixing in the reaction mixture.

With 20 mL of oleic acid, a mixture with a MeOH-to-oleic acid molar ratio of 12:1 was prepared in the flask. After adding 4 wt.% of catalyst, the mixture was heated to 80 °C and maintained for 7 h with a constant rotational speed of 500 rpm. Once the reaction was done, the mixture was transferred from the flask to a filter funnel for solid catalyst removal. The filtrate was then heated at 60 °C to evaporate the excess MeOH with a boiling point of 64.7 °C until the mass remained constant. This process was repeated with 8, 10, 12 and 14 wt.% of catalyst loading, given that the other operating parameters were constant. After that, the optimum catalyst loading was used to carry out esterification with a molar ratio of methanol to oleic acid of 4:1, 8:1, 16:1 and 20:1 to determine the optimum result.

3.4 Characterisation of Catalyst

Total acid density is used to evaluate the catalytic performance of the synthesised catalyst as it indicates the amount of strong and weak acid groups

attached to the samples. 0.1 g of SCSCG was uniformly mixed with 50 mL of a standardised 0.01M NaOH solution. The mixture was mixed for 30 minutes at room temperature and a rotational spped of 300 rpm using a magnetic stirrer, after which it was filtrated and titrated with 0.01M HCl standard solution. The phenolphthalein was added to indicate the endpoint of the titration, where the solution turned from pink (basic) to colourless (neutral).

Equation 3.1 demonstrated the chemical reaction of NaOH and HCl, where one mole of NaCl and one mole of water (H_2O) are formed when one mole of NaOH reacts with one mole of HCl. From the volume of HCl used to neutralise the NaOH solution, the acid density of the sample catalyst can be determined in terms of mmol NaOH/g using Equation 3.2.

$$NaOH + HCl \rightarrow NaOH + H_2O \qquad (3.1)$$
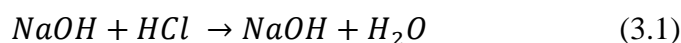
Total acid density (mmol/g) =
$$\{[NaOH]V_{NaOH} - [HCl]V_{HCl}\} \times \frac{1}{W_{CAT}} \qquad (3.2)$$

where

[HCl] & V_{HCl}	=	Concentration in M and volume in mL of acid used in titration
[NaOH] & V_{NaOH}	=	Concentration in M and volume in mL of basic solution used to mix with sample catalyst
W_{CAT}	=	Amount of sample subjected to the analysis in g

SEM Hitachi S-3400N equipped with EDX was utilised to examine the surface morphology of the synthesis catalysis. The dried catalyst samples adhered to the carbon tape during the analysis stage. Under the operating condition at 15 kV, the SEM images were captured with a magnification of 300X, 500X, 700X and 1000X. The elemental and chemical composition were determined accordingly by using the furnished EDX.

XRD was conducted to identify the crystalline phases, size and shape of the synthesised catalyst based on the diffraction peak using the model of Shidmazu XRD-6000. The test sample was pressed uniformly on a steel plate,

making a smooth surface for a more accurate analysis. Cu-Kα radiation was operated at 40 kV and 30 mA over a 2θ range of 10 to 80°.

The attachment of -SO₃H groups were examined via FTIR. Half a spatula of synthesised catalyst was placed on the sample holder and held at the fixed position using the pressure tower and compression tip. A transmittance spectrum was generated with the concept that different molecules can absorb different infrared light's energy. The molecular structure and amount of the sample were then identified based on the peak location and area, respectively.

TGA was conducted to identify the highest temperature the optimum sample catalyst can withstand before thermal decomposition. The initial and maximum temperatures for the analysis were specified at 30 °C and 1000°C, respectively, with a heating rate of 10 °C/min. Around 0.5 g of the sample catalyst was loaded into the sample pan above the balance. By taking advantage of gravity, the weight of the sample can be obtained accurately, and the weight changes were observed when the furnace temperature was increasing.

The specific surface area and pore distribution of the solid acid catalyst were identified using Micromeritics 3Flex surface analyzer which included the BET and BJH methods. The sample was first loaded into the cell and degassed prior to analysis. The temperature was first increased to 90 °C with a heating rate of 10 °C/min in 1 hour, followed by heating to 150 °C with a heating rate of 10 °C/min in 5 hours. Then, the sample was transferred from degassing chamber to the analysis chamber. The analysis was conducted at 77 K, the boiling point of the absorbate gas, N₂. The analysis was left overnight to obtain the isotherms and pore distribution plots.

3.5   Characterisation of Feedstock and Product

3.5.1   Acid Value

In this research study, the oleic acid as the feedstock oil reacted with MeOH for FAME production. 5 mL of 2-propanol was added to 1 g of oleic acid as the solvent in a conical flask, whereas 0.1 M KOH was used as the titrant. A phenolphthalein indicator was added to indicate the change in pH and colour. The endpoint was reached when the colour of the mixture changed from colourless to slightly pink. Solely 2-propanol was used as the analyte in the blank titration. The acid values were determined via titration and calculated

using Equation 3.5 to identify the FFA content in oleic acid. The same procedures were repeated using the final FAME product to determine the FFA content and the corresponding FFA conversion of the interesterification process by using Equation 3.6.

$$AV_{OC} = \frac{MW_{KOH} \times C_{KOH} \times (V_1 - V_0)}{m_{OC}} \tag{3.5}$$

$$FFA\ conversion\ (\%) = \frac{AV_{OC} - AV_{bd}}{AV_{OC}} \times 100\% \tag{3.6}$$

where

AV_{OC} = Acid value of oleic acid (g KOH/g)

AV_{bd} = Acid value of biodiesel formed (g KOH/g)

MW_{KOH} = Molar weight of KOH (g/mol)

C_{KOH} = Concentration of KOH, 0.1 M (0.1 mol/L)

V_1 = Volume of titrant used in sample titration (L)

V_0 = Volume of titrant used in blank titration (L)

m_{OC} = Mass of oleic acid (g)

3.5.2 Gas Chromatography (GC)

Additionally, GC was conducted to analyse the final FAME product. A fused silica capillary column with a dimension of 30 m x 0.53 mm x 0.5 μm was equipped in GC and used in this study to analyse FAME content in the sample quantitatively. Helium was the carrier gas to bring the vaporised sample flow along the capillary. Meanwhile, n-hexane and methyl heptadecanoate were used as the solvent of the sample and internal standard, respectively. Table 3.4 lists the setting values of different chromatographic conditions used for GC analysis.

Table 3.4: Chromatographic Conditions to Analyse the Biodiesel Sample.

Chromatographic conditions		Set Value
Inlet Temperature		200 °C
Oven	Initial Temperature	110 °C
	Heating	Up to 220 °C by 10 °C/min
Detector Temperature		220 °C
Flow Rate of Carrier Gas		3 mL/min

A standard calibration curve was prepared to identify the methyl oleate (MO) concentration in the product sample. Different methyl oleate concentrations were formed by diluting the pure methyl oleate with different volumes of n-hexane and a constant volume of internal standard. Subjecting those samples for GC analysis, a plot of methyl oleate-to-internal standard (MO/IS) ratio in terms of peak area versus concentration of methyl oleate was created. A line equation was derived and used to identify the composition of methyl oleate in the product of esterification.

The product samples were analysed similarly, where the samples were diluted using n-hexane and added with a constant volume of methyl heptadecanoate before GC analysis. After that, 1 μL of the test sample was injected, and a chromatogram was created. Once the product's concentration of methyl oleate was determined using the line equation derived from the calibration curve, Equation 3.7 was used to estimate the yield of methyl oleate from the interesterification process.

$$Yield \ (\%) = \frac{C_{MO} \times DF \times V_S}{V_{OC} \times D_{OC}} \times 100\% \qquad (3.7)$$

where

C_{MO} = Concentration of methyl oleate in g/L

V_S = Volume of the sample after evaporation in L

V_{OC} = Volume of oleic acid in mL

D_{OC} = Density of oleic acid in g/mL

DF = Dilution factor, which can be calculated using Equation 3.8 below:

$$DF = \frac{V_f}{V_i} \qquad (3.8)$$

where

V_f = Final volume after dilution in mL

V_i = Initial volume before dilution in mL

3.6   Reusability Study

The synthesised catalyst with optimum catalytic performance was used in the reusability study. The esterification processes were conducted at the optimum reaction conditions identified via parameter studies. The catalyst was filtered from the mixture when the reaction was completed and washed with water. The catalyst was then dried overnight at 80 °C in the oven. The dried catalyst was ground into powder and weighed before the next run. The weight of oleic acid required was back-calculated to achieve the desired catalyst loading, after which the volume of methanol needed was calculated accordingly to obtain a mixture with the optimum methanol-to-oleic acid molar ratio.

CHAPTER 4

RESULTS AND DISCUSSION

4.1 Effect of Sulfonation Temperature

Various methods were used to characterise the sample catalysts sulfonated at different temperatures to find out the catalyst with the optimum catalytic performance. Scanning Electron Microscopy (SEM), Energy Dispersive X-ray (EDX) Spectroscopy, Fourier Transform Infrared (FTIR) Spectroscopy, X-ray Diffraction (XRD) analysis and surface analyser were utilised to carry out the characterisation. The methods examined the structure, morphology, surface area and acid density of the catalysts in question and finally determined the optimum sulfonation temperature for the synthesis of solid acid catalyst derived from spent coffee grounds.

4.1.1 Scanning Electron Microscopy (SEM) & Surface Analysis

Scanning Electron Microscopy (SEM) captured high-resolution images to examine the surface morphology and structural properties of the raw spent coffee ground (SCG), H_3PO_4-activated SCG (CSCG) and H_2SO_4-sulfonated CSCG (SCSCG) at different temperature. Figure 4.1 demonstrates the SEM images taken under 1000X magnification, whereas the images under 300X, 500X and 700X were tabulated in Table B-1, B-2 and B-3 for comparison.

The raw SCG was naturally smooth and irregular, as illustrated in Figure 4.1 (a). Limited cracks or surface area were available for the deposition of sulfonic groups. On the contrary, it can be observed from Figure 4.1 (b) that the roughness of the catalyst surface increased significantly after undergoing chemical activation with H_3PO_4. According to Zięzio et al. (2020), the activation agent hindered the contraction of particles when it was introduced into the interior of the carbon precursors during the impregnation phase. The subsequent high-temperature carbonisation resulted in the removal of excessive activating agents and by-products, leading to a porous carbon structure with a well-developed surface. The increment in porosity was supported by the results obtained from the surface analyser, where the BET surface area (S_{BET}) of raw

SCG and CSCG were 0.3179 m^2/g and 80.23 m^2/g, respectively. The SEM images also clearly showed that the pores on the surface of sulfonated catalyst were more noticeable compared to the raw SCG and carbonised CSCG. The formation of occasional cracks and pores was caused by the side reactions, such as partial oxidation and condensation, during sulfonation with concentrated sulfuric acid (Ngaosuwan, Goodwin and Prasertdham, 2016). This was agreed with the significantly-increased BET surface area of 356.7 m^2/g.

Table 4.1: BET Surface Area, BJH Pore Volume and Pore Width of Different Sample Catalysts.

Sample Catalyst	BET Surface Area (m^2/g)	Pore Volume (m^3/g)	Average Pore Size (nm)
SCG	0.3179	0.03958	162.7
CSCG	80.23	0.00856	4.617
SCSCG$_{200}$	356.7	0.03233	3.397

Their porous characters were analysed based on the N$_2$ adsorption-desorption measurements, which resulted in the isotherms, as shown in Figure 4.2. Figure B-1 and Figure B-2 show the IUPAC classification of different isotherms and hysteresis loops, respectively. From Figure 4.2 (a), it can be seen that SCG demonstrated type II isotherm, indicating a macroporous or non-porous material. Type II isotherms demonstrated an upward convex at the lower relative pressure (P/P_O) due to the monolayer coverage of gas molecules. Then, the shape of the isotherm showed unrestricted adsorption as the relative pressure increased.

In contrast, the isotherms of the treated sample, SCSCG$_{200}$, were between type I and type IV isotherms, corresponding to the coexistence of both micro- and mesopores in porous solids (Hussein et al., 2021). The pronounced increase in adsorption at low relative pressure $(P/P_O < 0.1)$ was attributed to the adsorbent-adsorptive interactions in narrow micropores, usually demonstrated in type I isotherm. Meanwhile, the isotherms also showed the H4 hysteresis loop, which was often found in carbons with micro- and mesopores (Thommes et al., 2015).
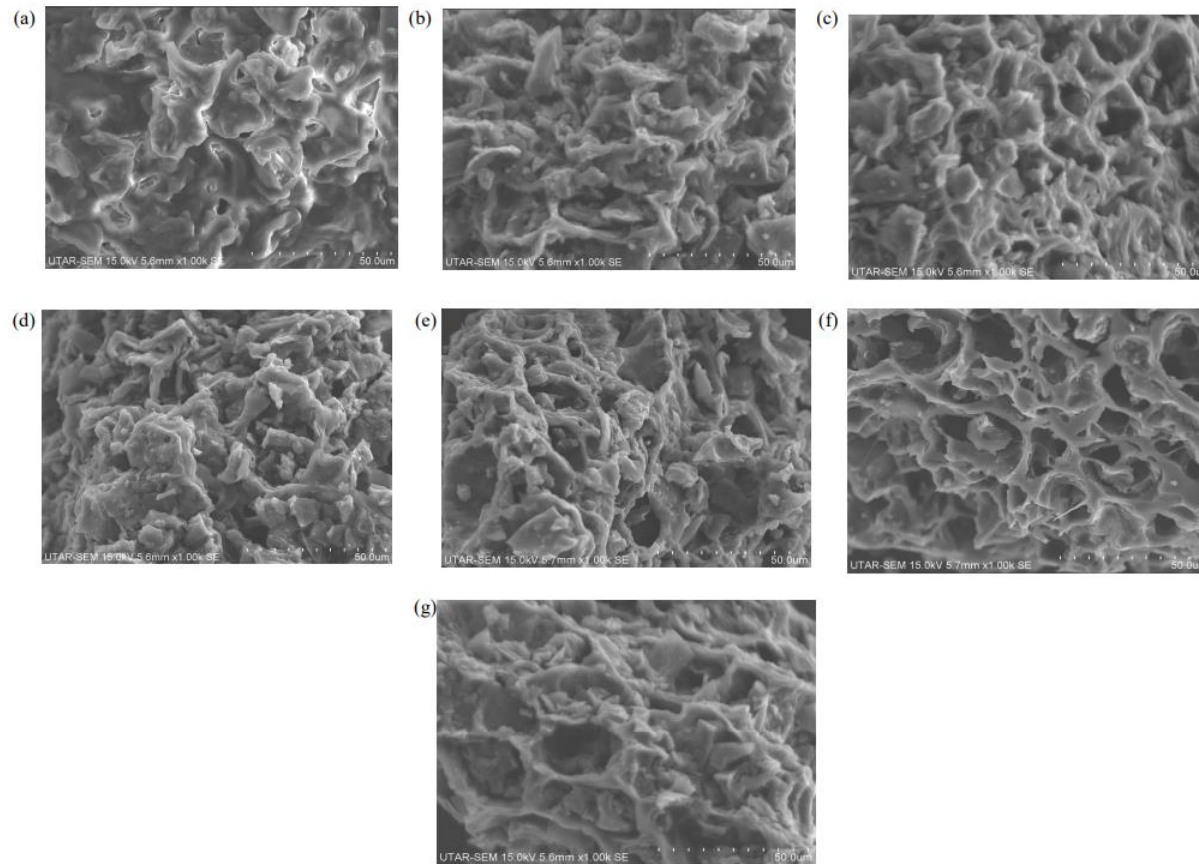
Figure 4.1: 1000X Magnification SEM Images of (a) SCG, (b) CSCG, (c) SCSCG$_{80}$, (d) SCSCG$_{120}$, (e) SCSCG$_{160}$ (f) SCSCG$_{200}$ and (g) SCSCG$_{240}$.

Besides, a significant drop in pore volume was noticed when SCG was carbonised into carbonaceous materials when macropores were converted into micropores after carbonisation. It agreed with the pore size analysis obtained from the BJH method, as shown in Figure 4.3. The BJH pore size distribution proved that SCG was macroporous material with 162.7 nm average pore size, whereas $SCSCG_{200}$ possessed an average pore sizes of 3.397 nm, attributing to its porous sturcture. Figure 4.3 (b) clearly shows that most of the pores were smaller than 2 nm, and thus it can be claimed that the pores of CSCG and $SCSCG_{200}$ were a combination of meso- and micropores. The further reduction in pore size (from CSCG to SCSCG) led to a higher pore volume and specific surface area, enhancing the samples' catalytic performance.

4.1.2   Energy Dispersive X-ray (EDX) & Acid Density

Energy Dispersive X-ray (EDX) analysis and titration to determine acid density were carried out for quantitative results. The distribution and composition of various elements, especially sulfur (S), on the catalyst surface were examined using EDX. Meanwhile, the total acidic sites comprised by the synthesised catalysts can be deduced via titration results, given that these active sites contributed to the acid density of the catalyst.

Table 4.2 shows the average composition of carbon (C), oxygen (O), sulfur (S) and phosphorus (P) on the surface of the samples. While impregnation in the activating agent increased the specific surface area, the direct carbonisation at 500 °C for 4 h converted the biomass to carbonaceous materials by removing the volatile non-carbon compounds. As shown in Table 4.2, the carbon composition of SCG increased after being carbonised, signifying that the non-carbon compounds were removed during the high-temperature pyrolysis. Zailan et al. (2021) reported that strong sulfonation induced the oxidation of aliphatic CH_3 or CH_2 to the carboxylic acid group, increasing the acid density of the sulfonated carbon catalyst. This explained the upward trend of the oxygen composition on the catalyst surface with increasing sulfonation temperature.
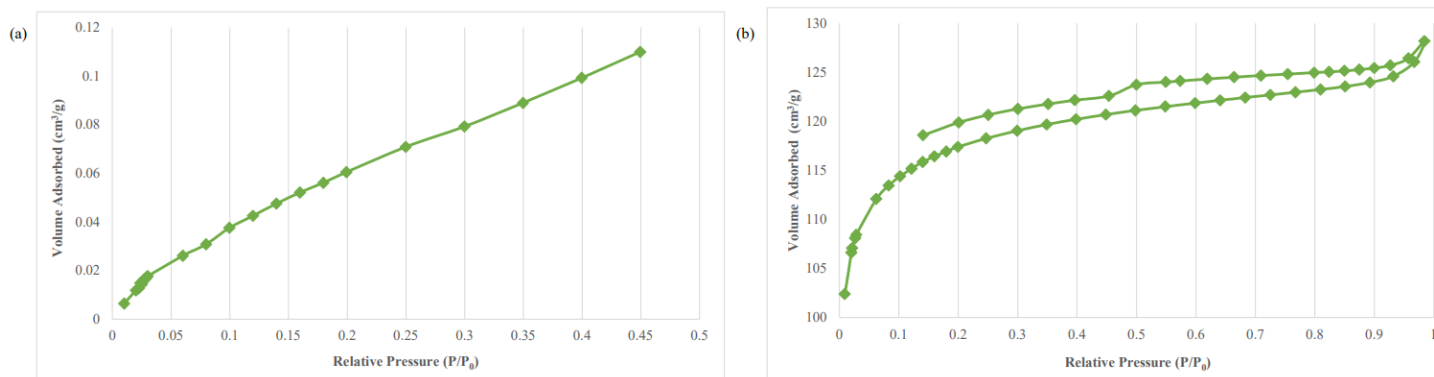
Figure 4.2: Isotherm Linear Plot of (a) SCG and (b) SCSCG$_{200}$.
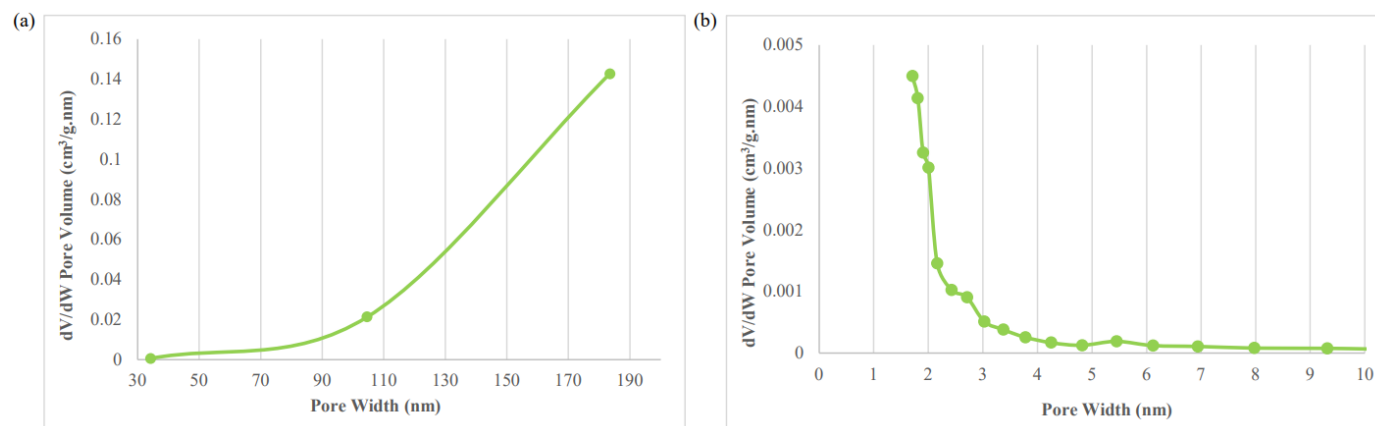
Figure 4.3: BJH Pore Size Distribution of (a) SCG and (b) SCSCG$_{200}$.

By assuming all S atoms represent sulfonic groups (-SO₃H), the density of -SO₃H was estimated using EDX analysis. It is shown that the sulfur composition on the surfaces of SCG and CSCG is negligible. In contrast, the amount of S increased significantly after sulfonation, indicating the effectiveness of direct sulfonation on the synthesised carbonaceous materials. At low temperatures, there is insufficient energy to support the attachment of sulfonic groups onto the surface of the catalysts. The composition of S increased with increasing sulfonation temperature until 200 °C and dropped at 240 °C. It was caused by the domination of side reactions, such as oxidation, hydrolysis, condensation and dehydration, which adversely reduced the adherence of sulfonic groups onto the catalyst surface. The results of acid density were consistent with that of EDX analysis, where the SCSCG sulfonated at 240 °C possessed the highest acid density, as shown in Figure 4.4.

Table 4.2:   Elemental Composition of Different Catalysts from EDX.

Sample	Elemental Composition (at%)			
	C	O	S	P
SCG	67.39	29.33	0.19	-
CSCG	84.54	8.84	0.18	1.09
SCSCG$_{80}$	85.50	9.90	1.06	0.49
SCSCG$_{120}$	83.09	9.66	1.45	0.31
SCSCG$_{160}$	84.09	10.94	1.75	0.23
SCSCG$_{200}$	82.88	12.04	1.91	0.15
SCSCG$_{240}$	82.35	13.59	1.75	0.19
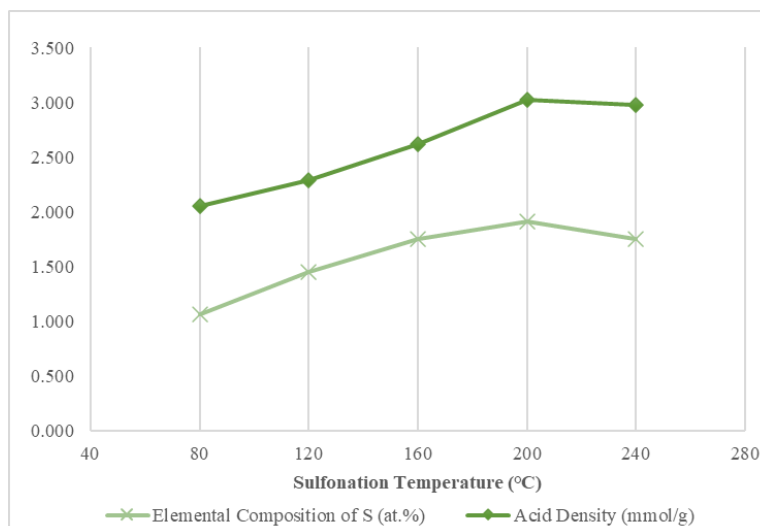
Figure 4.4: Effect of Sulfonation Temperature on Surface Elemental Composition of S and Acid Density.

4.1.3 X-ray Diffraction (XRD)

The results obtained from X-ray Diffraction (XRD) analysis, as illustrated in Figure 4.5, were used to determine the crystalline and amorphous nature of raw SCG and prepared catalysts. In the study of Sangsiri, Laosiripojana and Daorattanachai (2022), it was reported that the amorphous nature with polycyclic aromatic carbon sheets, which are randomly oriented, attributed to the broad peak at $2\theta = 10 - 30°$. On the other hand, the weak diffraction peak at $2\theta = 35 - 50°$ indicated the presence of graphite structure. Raw SCG exhibited the broad peak at $2\theta = 10 - 25°$, showing its amorphous nature with a C(002) plane before treatment. In contrast, the carbonised and sulfonated catalysts had peaks from $35 - 50°$, corresponding to the C(101) plane for a graphene structure. Additionally, a weak peak at $2\theta = 15 - 17°$, associated with the crystalline structure of cellulose, was detected in the raw SCG. Its absence in treated catalysts signified the changes in the carbon structure via carbonisation and sulfonation.
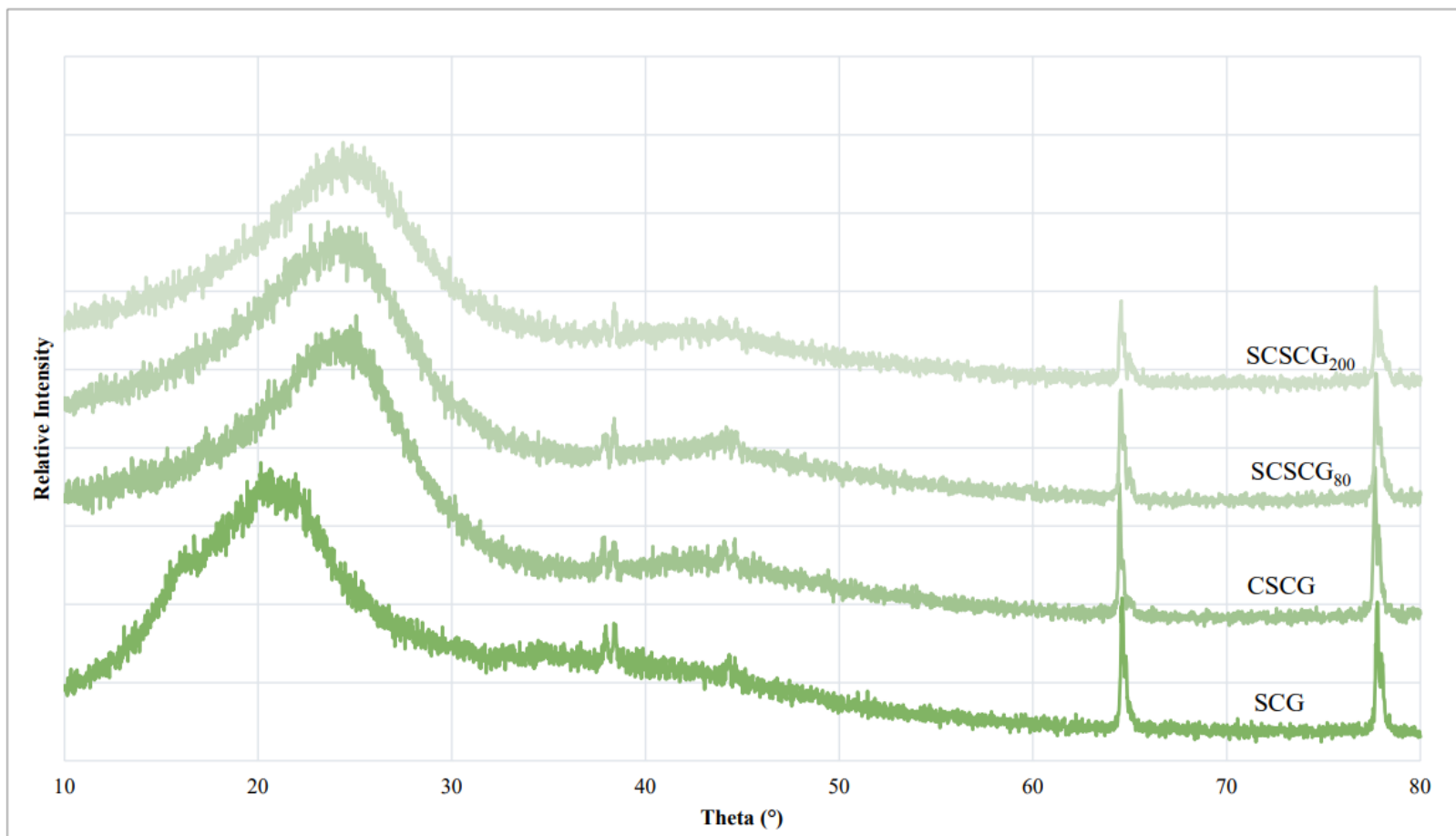
Figure 4.5: XRD Patterns of Raw SCG, CSCG, SCSCG80 and SCSCG200.

The background noise in the XRD pattern generally appears relatively large or small compared to the peak data of the samples. Therefore, the extremely sharp peaks at $2\theta = 64 - 65°$ and $77 - 78°$ were claimed as background noise which the sample holder, the amorphous state of the sample and poor calibration of the light may cause. From Figure 4.5, the intensity of the weak peak at $2\theta = 41 - 45°$ increased after carbonisation, indicating more graphite structure in CSCG compared to raw SCG. According to Nazir et al. (2021), the attachment of excess sulfonic groups on the catalyst surface increased the distortedness of the graphite structure, causing a reduction in peak intensity. This explained the reducing peak intensity when the sulfonation temperature increased from 80 °C (SCSCG$_{80}$) to 200 °C (SCSCG$_{200}$). The increment of the amorphous nature of carbon catalysts led to an improvement in their catalytic performance.

4.1.4 Fourier Transform-Infrared (FTIR) Spectroscopy

Fourier Transform-Infrared (FTIR) was used to determine the functional groups on the catalysts. The changes in functional groups after the raw SCG was carbonised and sulfonated at 80 °C and 200 °C were analysed based on the spectra shown in Figure 4.6.

The most apparent difference between the samples is the presence of a peak in the wavelength of 2800-3000 cm^{-1} due to the C-H bonds from aliphatic carbon in cellulosic components and lipids in spent coffee grounds (Agapay et al., 2021). Lin et al. (2022) reported that the treatment involved during the preparation of solid acid catalysts removed some cellulose and hemicellulose from the biomass materials. The weakened aliphatic C-H and O-H stretching ranged from 2400-3400 cm^{-1}, proving that carbonisation and sulfonation subjected to the SCSCG removed most of the aliphatic compounds from SCG. The peaks at 1500-1600 cm^{-1} indicated the formation of aromatic groups, which supported the presence of aromatic sheets after carbonisation. The aromatic sheets would facilitate the attachment of sulfonic groups onto the carbonised materials during direct sulfonation with concentrated H$_2$SO$_4$ (Bureros et al., 2019).
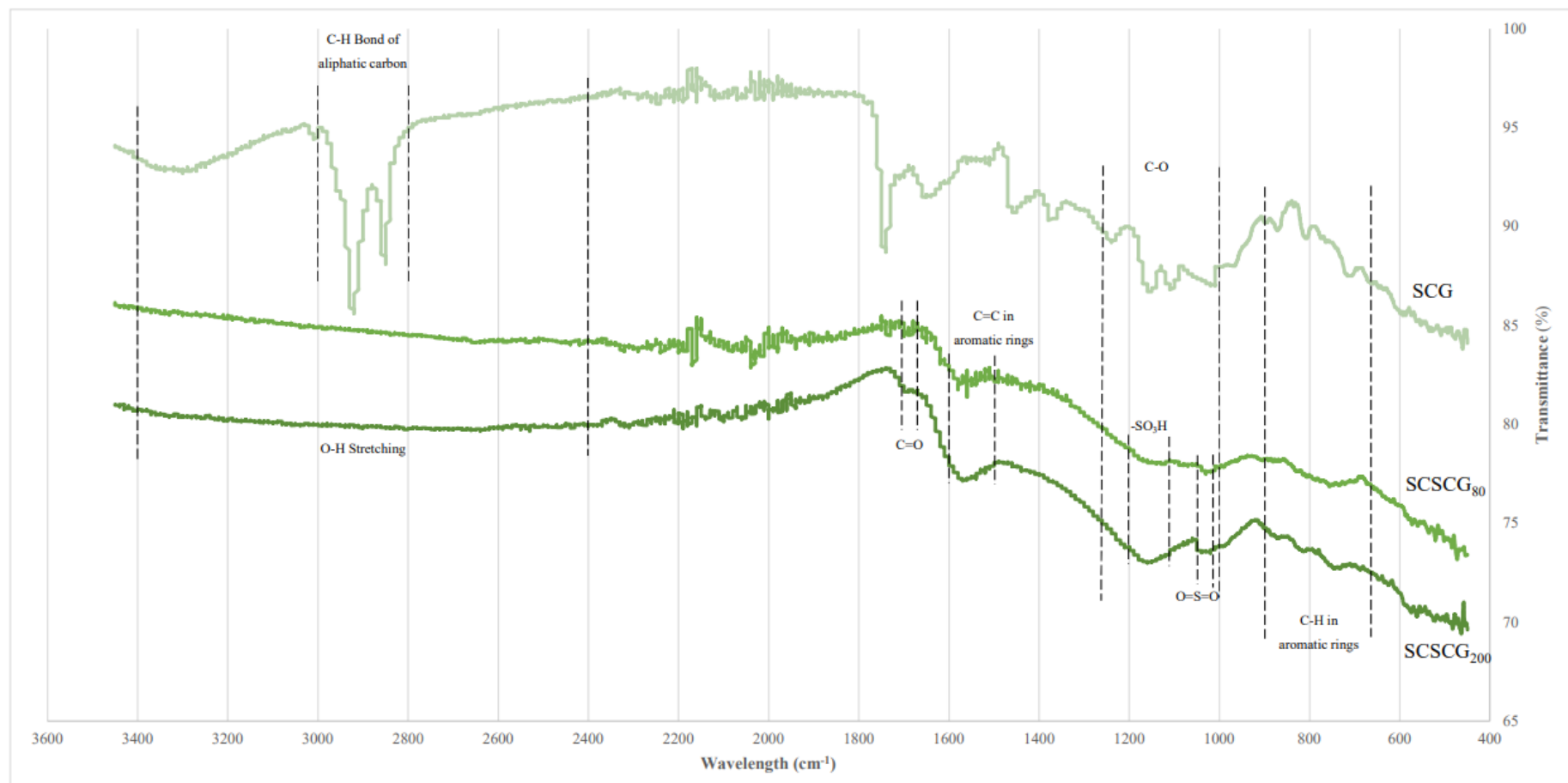
Figure 4.6: FTIR Spectra of SCG, SCSCG$_{80}$ and SCSCG$_{200}$.

While the peaks at wavelength 675-900 cm^{-1} referred to the C-H bonds stretching in the aromatic ring, the peaks at 1690-1710 cm^{-1} representing the C=O bonds in -COOH groups were only detected in SCSCG$_{200}$ (Zhang et al., 2023). This evidenced the presence of carboxylic groups in the synthesised acid catalysts, which contributed to the total acid density. The O=S=O and -SO$_3$H stretching were associated with the peaks at 1010-1040 cm^{-1} and 1100-1200 cm^{-1}, respectively. The slight intensifying in these peaks of SCSCG$_{80}$ and SCSCG$_{200}$ signified the increasing in acid density with increasing sulfonation temperature, consistent with the results obtained from EDX and titrimetric acid density test. According to Balasubramaniam et al. (2021), the multiple peaks in the wavelength 1000-1250 cm^{-1} referred to the C-O stretching and O-H deformation vibrations. They indicated the presence of esters, ethers, alcohols (primary, secondary or tertiary) and phenols. It is challenging to differentiate the presence of sulfonic groups in the same region. However, the presence of sulfonic groups on SCSCG$_{80}$ and SCSCG$_{200}$ was confirmed via acid-density titration.

4.1.5 Thermogravimetric Analysis (TGA)

Thermogravimetric Analysis (TGA) was conducted to identify the maximum temperature the sample catalysts can sustain. It is essential to determine the thermal decomposition temperature of the carbon material, especially the synthesised solid acid catalysts, to ensure its thermal stability when undergoing treatment or reaction. Figure 4.7 displays the TGA curves of SCG and SCSCG$_{200}$.

The curves clearly show that the sulfonated catalyst sample could withstand a higher temperature than the raw spent coffee ground. The small decline at low temperatures, which can be observed from both samples, was attributed to the drying or desorption of volatile compounds. For SCG, the single-stage decomposition occurred at 250 °C, displaying an obvious drop. On the contrary, the gradient of the downward curve increased at around 600 °C for SCSCG$_{200}$, indicating its thermal decomposition temperature. In other words, the thermal stability of the catalyst was improved compared to the raw material.
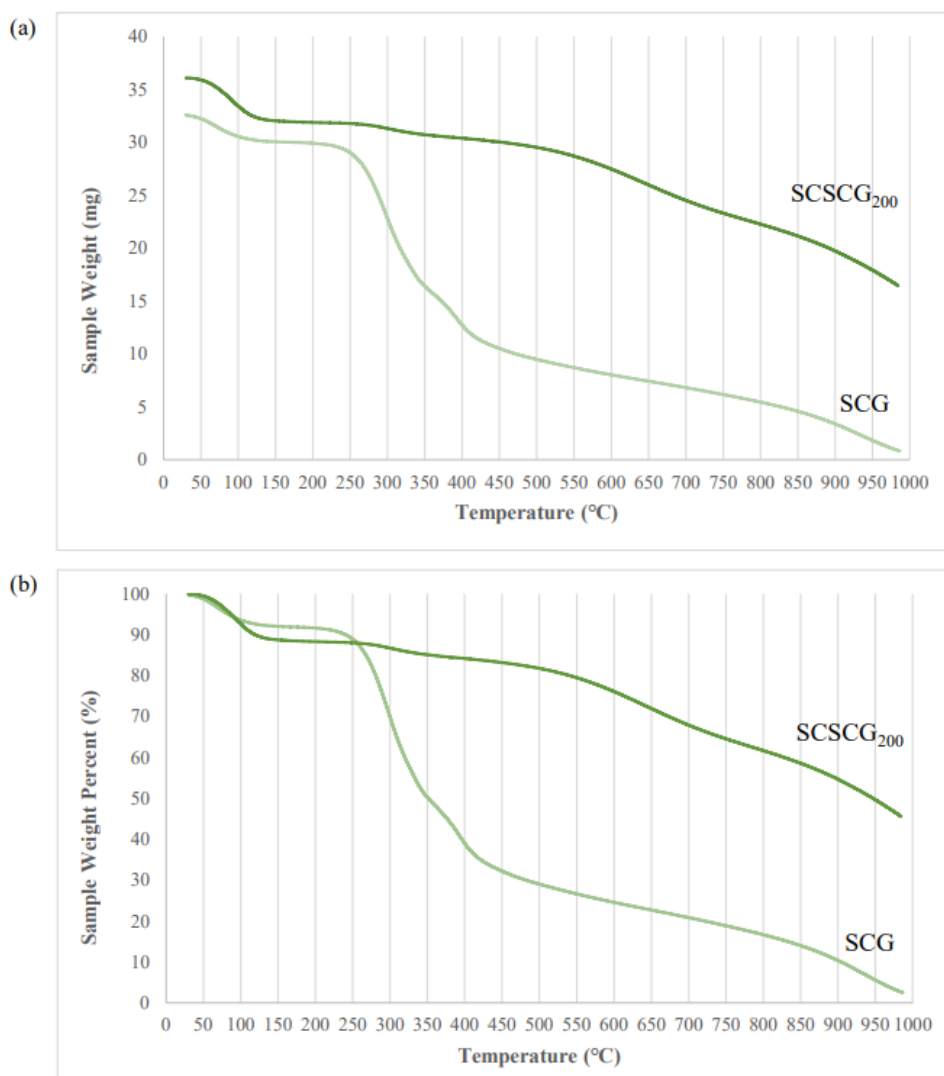
Figure 4.7: TGA Curves In Terms of (a) Sample Weight and (b) Weight
Percent.

4.1.6 Selection of Optimum Catalysts

Various characterisation methods were conducted to examine the physicochemical properties of the synthesised catalyst, such as surface area, surface morphology, porosity, functional groups, elemental composition, thermal stability and acid density. However, the catalytic performance in the reaction is the most crucial characteristic of a catalyst. Several esterification reactions were conducted using catalysts sulfonated at different temperatures while other reaction parameters were kept constant. Figure 4.8 shows the resulting biodiesel yields, which reflect the influence of sulfonation temperature on the catalyst performance. There was a noticeable peak of biodiesel yield at the sulfonation temperature of 200 °C, which clearly showed that the catalyst

sulfonated at 200 °C possessed the optimum catalytic properties for the esterification reaction to produce biodiesel. This was supported by the characterisation results, such as acid density and EDX, which were discussed in the previous sections.
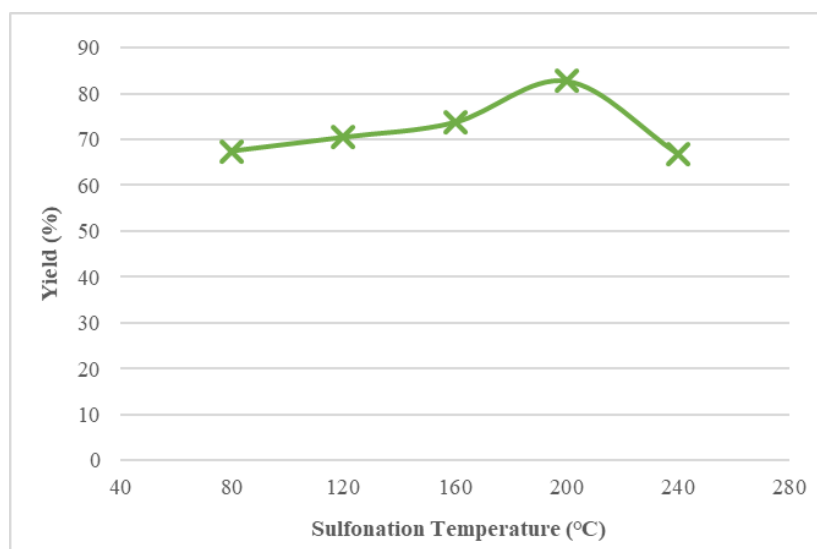
Figure 4.8: Effect of Sulfonation Temperature on Biodiesel Yield.

4.1.7   Activation with Zinc Chloride (ZnCl₂)

Zinc chloride is another common chemical that is used to activate cellulosic biomass. Therefore, this study also used it to activate the SCG via chemical activation. Similar methods were used to synthesise and determine its effectiveness as the activating agent for spent coffee grounds to produce heterogeneous acid catalysts for biodiesel production.

Figure 4.9 illustrates the SEM images of activated carbon after impregnation in $ZnCl_2$ solution for 24 h (a) and after sulfonation at 160 °C (b), with 1000X magnification. The figures show a porous structure formed after carbonisation, attributed to $ZnCl_2$ impregnation. Besides, after sulfonation, a substantial amount of cracks were formed on the activated carbon. The increment of S_{BET} from 697.6 m^2/g to 1192 m^2/g proved that the surface area of carbon was significantly increased via direct sulfonation in concentrated sulfuric acid (Appendix E).
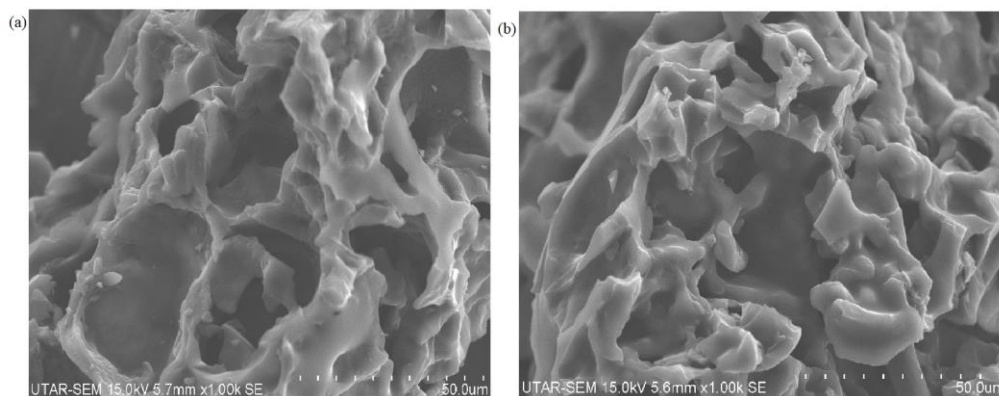
Figure 4.9: SEM Images of (a) ZnCl$_2$-Activated Carbon Derived from SCG and (b) the Corresponding Solid Acid Catalyst Sulfonated at 160 ℃.

Undeniably, the activation with ZnCl2 produced carbonaceous materials with high-surface-area microporous structure, which is one of the excellent characteristics for a catalyst to facilitate the facilitate. However, acid density or the composition of acid groups is another critical characteristic of a solid acid catalyst. FTIR analysis revealed that the average elemental composition of S is only 0.5350 at.%, which is much lower than the SCSCG synthesised using H$_3$PO$_4$ as the activating agent. The low percentage of S indicated the low attachment of sulfonic groups on the catalyst surface. The sulfonic groups are known to be the main active sites for catalytic activity. Therefore, the catalyst activated by ZnCl$_2$ was not applied in this study for acid-catalysed esterification to produce biodiesel due to the lack of active sites.

4.2   Esterification of Oleic Acid and Methanol

In section 4.1, the optimum catalyst was selected based on the results obtained from different characterisation methods and its catalytic performance. The solid acid catalyst sulfonated at 200 ℃ was chosen as the optimum catalyst in this study due to its high surface area, porosity, sulfur surface composition, and acid density. Most importantly, it resulted in a high biodiesel yield via the esterification process. The esterification process is affected by several parameters, including reaction temperature, duration, catalyst loading and the molar ratio of methanol to oleic acid. This study investigated and discussed the

effects of catalyst loading and methanol-to-oleic acid molar ratio (MOAMR) in sections 4.2.1 and 4.2.2, respectively.

4.2.1 Effect of Catalyst Loading

A catalyst is used in the reaction to facilitate the contact of reactants, increasing the conversion of reactants and product yield. Catalyst loadings ranging from 4 to 20 wt.% were used in the esterification process to determine the optimum amount of catalyst. The resulting biodiesel yield and FFA conversion were illustrated in Figure 4.10 and Figure 4.11, respectively.
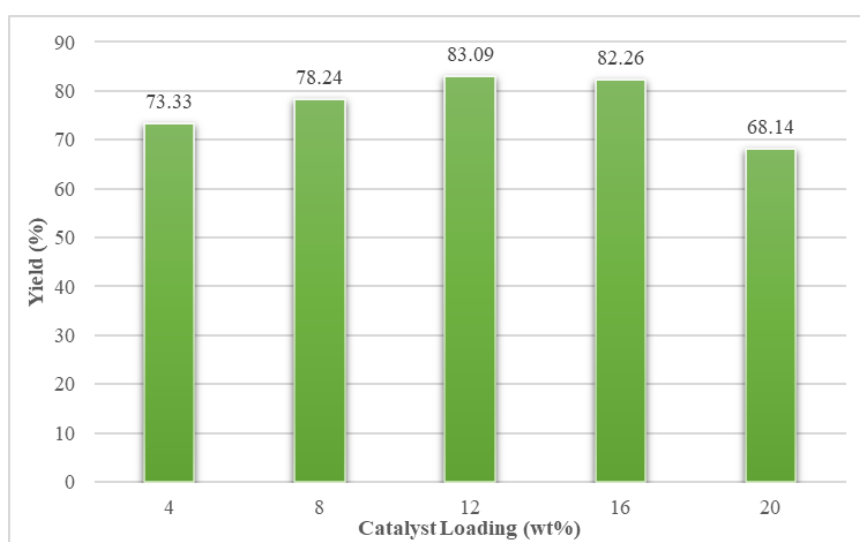
Figure 4.10:   Effect of Catalyst Loading on Biodiesel Yield.
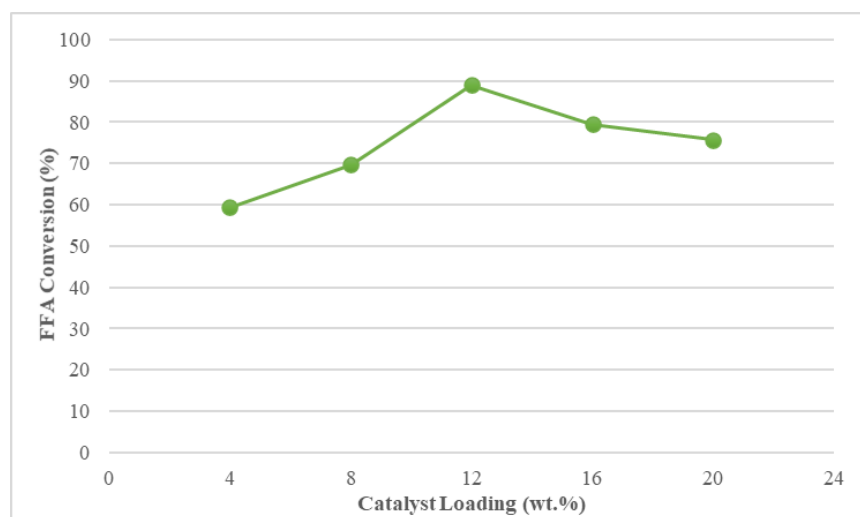
Figure 4.11:   Effect of Catalyst Loading on FFA Conversion.

From the figures, both yield and conversion demonstrated a similar trend with increasing catalyst loading. The catalyst, as the reactants' contact medium, contains the active sites which allow the conversion of reactants into products. More active sites were available for the reaction when more catalysts were added to the reactant mixture, resulting in higher yield and conversion. With 12 wt.% catalysts added, the conversion of 90% and yield of 83.09 %, respectively, were obtained. However, in this case, the yield dropped beyond the optimum point of 12 wt.%. It agreed with the results obtained by Soltani et al. (2021), where no further increment in biodiesel yield could be observed beyond the optimum catalyst loading. This was attributed to the increased viscosity of the reaction mixture due to the excess amount of catalyst, which restricted the mass transfer between the reactants and blocked the protonation of FFAs.

4.2.2   Effect of Methanol-to-Oleic Acid Molar Ratio

The methanol-to-oleic acid molar ratio is 1:1 based on the reaction stoichiometry. However, excessive alcohol is necessary to move the equilibrium to the product side, methyl oleate, according to Le Chatelier's Principle, since the esterification is a reversible reaction. Therefore, esterification processes were carried out using the methanol-to-oleic acid molar ratio (MOAMR) ranged from 4:1 to 20:1 in this study to investigate its impact on the biodiesel yield.

Figure 4.12 and Figure 4.13 show the obtained yield and conversion, which agreed with Le Chatelier's Principle before exceeding the optimum MOAMR. As the molar ratio increases, the methanol drives the reaction to the right side, resulting in a higher yield. The optimum result was achieved when 16:1 MOARM was used, where the biodiesel yield and FFA conversion were 96.6 % and 90.83 %, respectively. No further increment was observed when a higher molar ratio, 20:1, was used. The reduction in yield is caused by the lower frequency of effective collisions between the oleic acid molecules and the active groups since the oleic acid was diluted when a high volume of methanol was added. Moreover, it was reported that the catalytic performance would be inhibited due to the reaction between the sulfonic groups and excess methanol molecules (Zhang et al., 2021).

Figure 4.12:   Effect of MOAMR on Biodiesel Yield.
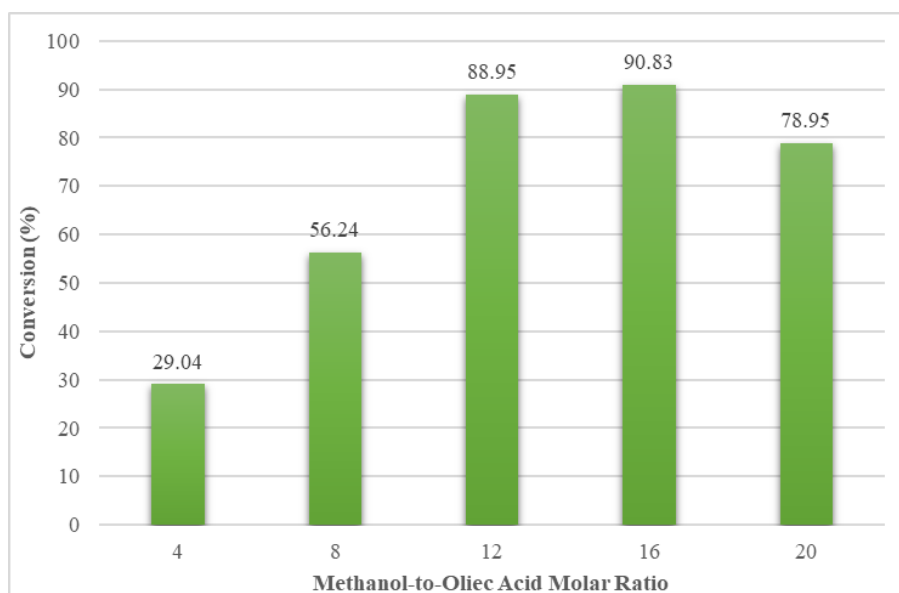
Figure 4.13:   Effect of MOAMR on FFA Conversion.

4.3   Reusability of the Synthesised Catalyst

It is essential to investigate the catalyst recovery and reusability to identify the usefulness of the synthesised catalyst in terms of economic and sustainability. The optimum catalyst loading and methanol-to-oleic acid molar ratio were identified via parameter studies, which are 12 wt.% and 16:1, respectively. Several esterification processes were carried out using the spent catalysts to examine the catalytic reusability of the synthesised catalyst at a sulfonation

temperature of 200 °C. Figure 4.14 demonstrates the biodiesel yield obtained from the esterification process at optimum reaction conditions. Figure 4.14 demonstrates the resulting biodiesel yield from different runs of the esterification process.
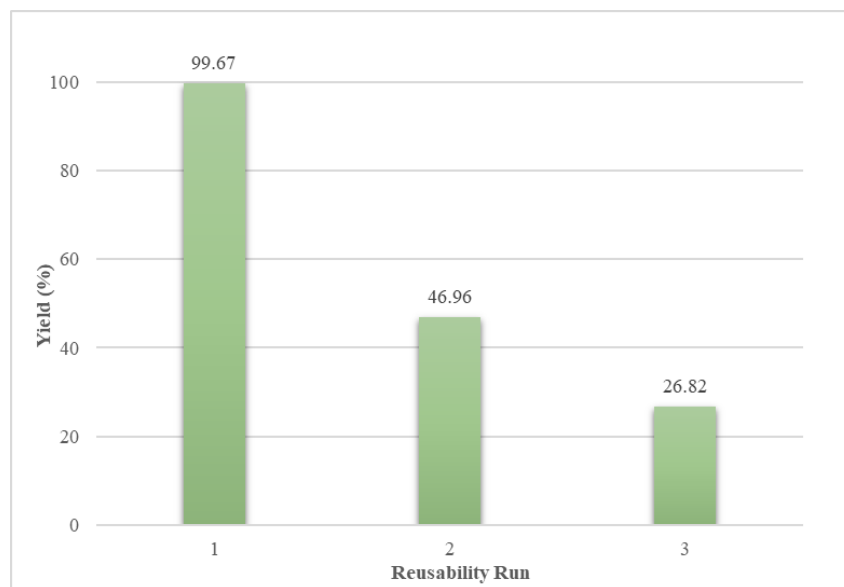
Figure 4.14:   Performance of Synthesised Catalyst in Reusability Study.

The excellent yield of 99.67 % from the first run proved that the optimum reaction conditions chosen via parameter studies were reasonable. However, the yield decreased dramatically to 46.96 % in the second run, followed by 26.82 % in the third run. The inevitable deactivation of the catalyst was attributed to the thermal degradation, fouling and leaching of active sites into the liquid phase (Miceli et al., 2021). On the other hand, instead of water, n-hexane and methanol were also used to wash the catalyst, resulting in a yield of only 33.83 % in the second run. While n-hexane was used to remove non-polar compounds, methanol removed the polar compounds. The low yield may be caused by the loss of sulfonic groups, which are polar components, when the catalyst was washed with methanol.

CHAPTER 5

CONCLUSIONS AND RECOMMENDATIONS

5.1 Conclusions

The present work's main focus was synthesising solid acid catalysts from spent coffee ground waste for biodiesel production via the esterification of oleic acid with methanol. The synthesised catalysts were characterised using various methods, including SEM-EDX, FTIR, XRD, TGA, surface analysis and acid density. SEM images showed that the synthesised catalysts possessed a rough surface and porous structure. The BET surface areas of raw spent coffee ground and synthesised catalyst were 0.3179 and 356.7 m2/g, respectively. The significant increment in the specific surface was consistent with the BJH pore distribution plots, which showed the conversion of macroporous biomass waste to meso- and microporous catalysts.

Moreover, the catalyst was shown to be in an amorphous structure via XRD analysis, contributing to its catalytic performance. While FTIR proved the presence of sulfonic groups after sulfonation, EDX examined the composition of sulfur quantitatively and demonstrated an upward trend with increasing sulfonation temperature until the optimum point. Based on the TGA curve, the maximum temperature of 600 ℃ that the synthesised catalyst can sustain before thermal decomposition was identified. The thermal stability of the carbon catalyst was improved by comparing it to the raw spent coffee grounds, which decomposed at 250 ℃. As a solid acid catalyst, the catalyst sulfonated at 200 ℃ possessed a sulfur elemental composition of 1.910 atomic percent and exhibited a high acid density of 3.025 mmol/g.

Several esterification processes were carried out by employing the catalyst with optimum catalytic performance to determine the effect of operating conditions on the biodiesel yield and FFA conversion. The optimum catalyst loading and methanol-to-oleic acid were identified from the experiment results, which were 12 wt.% and 16:1, respectively. With optimum catalyst loading and methanol-to-oleic acid molar ratio, an optimum yield of 99.67 % was achieved.

In addition, the catalyst can be reused twice before the yield drops to below 30 % in the third reusability cycle.

Overall, all the planned objectives were achieved. This study highlighted the synthesis of catalyst derived from low-cost biomass waste, which can be employed in biodiesel production. The results proved the potential of spent coffee grounds as an activated carbon and solid acid catalyst, assuring further exploration and application in other research areas.

5.2   Recommendations for Future Work

The experiment was successfully carried out according to the planned objectives and scopes. Nevertheless, several recommendations are made to improve the related research work in the future for a more comprehensive outcome.

i.   The other parameters during catalyst preparation, such as carbonisation temperature, carbonisation time, sulfonation time and sulfuric acid concentration, must be investigated to produce the optimum catalyst.

ii.   The other parameters of the esterification process, which are reaction temperature and time, must be investigated to obtain the optimum yield.

iii.   The synthesised catalyst must be subjected to characterisation, further treatment or an esterification process as soon as possible to avoid degradation and oxidation.

iv.   The produced biodiesel sample must be analysed as soon as possible to avoid degradation or contamination.

v.   The equipment used throughout the procedures must be consistent to reduce the discrepancies in the results obtained from every run.

vi.   Repetitive experimental run is desirable for the same parameter study to obtain higher reliability and accuracy results.

vii.   Mass production of sample is preferable if the reactor or equipment is available to eliminate the deviations between different batches, which reduces the accuracy of the results.

viii.   It is advisable to replace the oleic acid with other low-cost feedstocks, such as waste cooking oil or vegetable oils containing free fatty acids via transesterification reaction to produce biodiesel more economically.

REFERENCES

Adler, K., 2021. Global energy consumption to rise 50%, carbon emissions 25% by 2050: US EIA. *HIS Markit*, [online] 7 October Available at: <https://cleanenergynews.ihsmarkit.com/research-analysis/global-energy-consumption-to-rise-50-carbon-emissions-25-by-20.html> [Accessed 3 June 2022].

Agapay, R. C., Liu, H. C., Ju, Y. H., Go, A. W., Angkawijaya, A. E., Nguyen, P. L. T., Truong, C. T. and Quijote, K. L., 2021. Synthesis and Initial Evaluation of Solid Acid Catalyst Derived from Spent Coffee Grounds for the Esterification of Oleic Acid and Methanol. *Waste and Biomass Valorization*, 12(8), pp. 4387-4397.

Anisuzzaman, S. M., Joseph, C. G., Krishnaian, D., Bono, A., Suali, E., Abang, S. and Fail, L. M., 2016. Removal of chlorinated phenol from aqueous media by guava seed (Psidium guajava) tailored activated carbon. *Water Resources and Industry*, 16, pp. 29-36.

AZO Material, 2018. *How does EDX analysis with a scanning electron microscope (SEM) work?* [online] Available at: < https://www.azom.com/article.aspx?ArticleID=16256> [Accessed 15 July 2022].

Balasubramaniam, S., Ninomiya, S., Sasaki, M., Quitain, A., Kida, T. and Saldana, M. D. A., 2021. Carbon-based solid acid catalyst derived from *Undaria pinnatifida* and its application in esterification. *Algal Research*, 55.

Banchero, M. and Gozzelino. G., 2018. A simple pseudo-homogeneous reversible kinetic model for the esterification of different fatty acids with methanol in the presence of Amberlyst-15. *Energies*, 11, 1843.

BBC, n.d. *Generation of electricity*. [online] Available at: <https://www.bbc.co.uk/bitesize/guides/zbsdmp3/revision/3> [Accessed 5 June 2022].

BP, 2021. *Statistical Review of World Energy 2021*. 70th ed. [pdf] British: BP Plc. Available at: <https://www.bp.com/content/dam/bp/business-sites/en/global/corpclaorate/pdfs/energy-economics/statistical-review/bp-stats-review-2021-full-report.pdf> [Accessed 4 June 2022].

Brahma, S., Nath, B., Basumatary, B., Das, B., Saikia, P., Patir, K. and Basumatary, S., 2022. Biodiesel production from mixed oils: A sustainable approach towards industrial biofuel production. *Chemical Engineering Journal Advances*.

Bureros, G. M. A., Tanjay, A. A., Cuizon, D. E. S., Go, A. W., Cabatingan, L. K., Agapay, R. C. and Ju, Y. H., 2019. Cacao shell-derived solid acid catalyst for esterification of oleic acid with methanol. *Renewable Energy*, 138, pp. 489-501.

Casas, A., Ramos, M. J. and Perez, A., 2011. New trends in biodiesel production: Chemical interesterification of sunflower oil with methyl acetate. *Biomass and Bioenergy*, 35(5), pp. 1702-1709.

Chamola, R., Khan, M. F., Raj, A., Verma, M. and Jain, S., 2019. Response surface methodology based optimization of in situ transesterification of dry algae with methanol, H_2SO_4 and NaOH. *Fuel*, 239, pp. 511-520.

Chellappa, S., Nair, V., Sajith, V. and Aparna, K., 2018. Synthesis, optimization and characterization of biochar based catalyst from sawdust for simultaneous esterification and transesterification. *Chinese Journal of Chemical Engineering*, 26, pp. 2654-2663.

Chen, Q., Tan, X., Liu, Y., Liu, S., Li, M., Gu, Y., Zhang, P., Ye, S., Yang, Z. and Yang, Y., 2020. Biomass-Derived Porous Graphitic Carbon Materials for Energy and Environmental Applications. *Journal of Materials Chemistry A*.

Chuepeng, S. and Komintarachat, C., 2018. Interesterification optimization of waste cooking oil and ethyl acetate over homogeneous catalyst for biofuel production with engine validation. *Applied Energy*¸ 232, pp. 728-739.

Claudette Romero-Ibarra, I., Martínez Ponce Escuela, A., Elizabeth Mijangos Zúñiga, G. and Eridani Medina Munoz, M., 2022. Direct Transesterification: From Seeds to Biodiesel in One-Step Using Homogeneous and Heterogeneous Catalyst. *Advanced Biodiesel - Technological Advances, Challenges, and Sustainability Consideration*. IntechOpen. DOI: 10.5772/intechopen.108234.

Contreras Andrade, I., Parra Santiago, J., Ricardo Sodre, J., Sebastian Pathiyamattom, J. and Alberto Guerrero-Fajardo, C., 2014. Transesterification Reaction of Waste Cooking Oil and Chicken Fat by Homogeneous Catalysis. *Journal of Chemistry and Chemical Engineering*, 8, pp. 736-743.

Cruz, M., Cardinal Pinho, S., Mota, R., Fonseca Almeida, M. and Maia Dias, J., 2018. Enzymatic esterification of acid oil from soapstocks obtained in vegetable oil refining: Effect of enzyme concentration. *Renewable Energy*, 124, pp. 165-171.

Dai, Y., Zhang, K., Meng, X., Li, J., Guan, X., Sun, Q., Sun, Y., Wang, W., Lin, M., Liu, M., Yang, S., Chen, Y., Gao, F., Zhang, X. and Liu, Z., 2019. New use for spent coffee ground as an adsorbent for tetracycline removal in water. *Chemosphere*, 215, pp. 163-172.

Dhawan, M. S., Barton, S. C. and Yadav, G. D., 2021. Interesterification of triglycerides with methyl acetate for the co-production biodiesel and triacetin using hydrotalcite as a heterogeneous base catalyst. *Catalysis Today*, 375, pp. 101-111.

Dumbre, D. and Choudhary, V.R., 2020. Properties of functional solid catalysts and their characterization using various analytical techniques. In: *Advanced Functional Solid Catalysts for Biomass Valorization*. Elsevier.pp.77–88.

Edeh, I., n.d. Renewable Resource for the Potential Displacement of the Petroleum Diesel. In: V. Beschkov, ed. 2020. *Biorefinery Concepts, Energy and Products*. IntechOpen. DOI: 10.5772/intechopen.83180.

EIA, 2019. *EIA projects nearly 50% increase in world energy usage by 2050 led by growth in Asia*. [online] Available at: <https://www.eia.gov/todayinenergy/detail.php?id=41433#:~:text=Rising%20income%2C%20urbanization%2C%20and%20increased,to%20rising%20demand%20for%20energy.&text=The%20growth%20in%20end%2Duse,79%25%20between%202018%20and%202050.> [Accessed 4 June 2022].

Ejeromedoghene, O., 2021. Acid-catalyzed transesterification of Palm Kernel Oil (PKO) to biodiesel. In: *Materials Today: Proceedings*. Elsevier Ltd. pp. 1580-1583.

Energy Commission, 2020. *Malaysia Energy Statistics Handbook 2020*. [pdf] Malaysia: Energy Commission. Available at: < https://www.st.gov.my/en/contents/files/download/116/Malaysia_Energy_Statistics_Handbook_20201.pdf> [Accessed 4 June 2022].
Exxon Mobil, 2021. *Energy demand: Three drivers*. [online] Available at: <https://corporate.exxonmobil.com/Energy-and-innovation/Outlook-for-Energy/Energy-demand#Transportation> [Accessed 3 June 2022].

Eurostate, 2020. *Oil and petroleum products – a statistical overview*. [online] Available at: <https://ec.europa.eu/eurostat/statistics-explained/index.php?title=Oil_and_petroleum_products_-_a_statistical_overview#Final_consumption_of_petroleum_products_for_energy_use> [Accessed 13 June 2022].

Fonseca, J. M., Spessato, L., Cazetta, A. L., da Silva, C. and Almeida, V. C., 2022. Sulfonated carbon: synthesis, properties and production of biodiesel. *Chemical Engineering and Processing – Process Intensification*.

Fu, P., Zhang, A., Luo, S., Yi, W., Hu, S. and Zhang, Y., 2019. Catalytic Steam Reforming of Biomass-Derived Acetic Acid over Two Supported Ni Catalysts for Hydrogen-Rich Synges Production. *ACS Omega*, 4, pp. 13585-13593.

Guo, J., Sun, S. and Liu, J., 2020. Conversion of waste frying palm oil into biodiesel using free lipase A from Candida antarctica as a novel catalyst. *Fuel*, 267.

Heidarinejad, Z., Dehghani, M. H., Heidari, M. Javedan, G., Ali, I. and Sillanpaa, M., 2020. Methods for preparation and activation of activated carbon: a review. *Environmental Chemistry Letters*.

Hoang, D., Bensaid, S. and Saracco, G., 2013. Supercritical fluid technology in biodiesel production. *Green Process Synth*.

Hussein, M. F., Abo El Naga, A. O., El Saied, M., AbuBaker, M. M., Shaban, S. A. and El Kady, F. Y., 2021. Potato peel waste-derived carbon-based solid acid for the esterification of oleic acid to biodiesel. *Environmental Technology & Innovation*¸21.

IEA, 2021. *Global electricity demand is growing faster than renewables, driving strong increase in generation from fossil fuels*, [press release] 15 July 2021. Available at: <https://www.iea.org/news/global-electricity-demand-is-growing-faster-than-renewables-driving-strong-increase-in-generation-from-fossil-fuels> [Accessed 3 June 2022].

IEA, 2017. *Biofuel and fossil-based transport fuel production cost comparison, 2017*. [online] Available at: < https://www.iea.org/data-and-statistics/charts/biofuel-and-fossil-based-transport-fuel-production-cost-comparison-2017> [Accessed 5 July 2022].

International Coffee Organization, 2021. *Coffee Market Report - September 2021*. [pdf] International Coffee Organization. Available at: < http://www.ico.org/documents/cy2020-21/cmr-0921-e.pdf> [Accessed 9 July 2022].

Jääskeläinen, H. and Majewski, W. A., 2021. *Effects of Biodiesel on Emissions*. [online] Available at: < https://dieselnet.com/tech/fuel_biodiesel_emissions.php#nox> [Accessed 18 July 2022].

JoVE Science Education Database, 2022. *Gas Chromatography (GC) with Flame-Ionization Detection*. [online] Available at: < https://www.jove.com/v/10187/gas-chromatography-gc-with-flame-ionization-detection> [Accessed 16 July 2022].

Kampars, V., Abelnieve, Z., Lazdovica, K. and Kampare, R., 2020. Interesterification of rapeseed oil with methyl acetate in the presence of potassium tert-butoxide solution in tetrahydrofuran. *Renewable Energy*, 158, pp. 668-674.

Kashyap, S. S., Gogate, P. R. and Joshi, S. M., 2018. Ultrasound assisted intensified production of biodiesel from sustainable source as karanja oil using interesterification based on heterogeneous catalyst (γ-alumina). *Chemical Engineering & Processing: Process Intensification*, 136, pp. 11-16.

Khan, I. W., Naeem, A., Farooq, M., Ghazi, Z. A., Saeed, T., Perveen, F. and Malik, T., 2022. Biodiesel production by valorizing waste non-edible wild olive

oil using heterogeneous base catalyst: Process optimization and cost estimation. *Fuel*, 320.

Kirubakaran, M. and Selvan, V. A. M., 2018. A comprehensive review of low cost biodiesel production from waste chicken fat. *Renewable and Sustainable Energy Reviews*, 82, pp. 390-401.

Kumar, N. and Raheman, H., 2022. Production, characterization and utilization of second generation biodiesel blend in diesel engine using water and nanoparticles as additives. *Fuel¸* 308.

Lamba, N., Modak, J. M. and Madras, G., 2017. Fatty acid methyl esters synthesis from non-edible vegetable oils using supercritical methanol and methyl tert-butyl ether. *Energy Conversion and Management*, 138, pp. 77-83.

Lei, Q. and Li, T., 2014. Functional monoesters of jojoba oil can be produced by enzymatic interesterification: Reaction analysis and structural characterization. *European Journal of Lipid Science and Technology*, 117(5), pp. 630-636.

Lim, J., 2021. Malaysia's energy consumption, primary energy supply both grew 2.8% in 2019 – commission. *The Edge Markets*. [online] 13 December. Available at: < https://www.theedgemarkets.com/article/malaysias-energy-consumption-primary-energy-supply-both-grew-28-2019-%E2%80%94-commission> [Accessed 4 June 2022].

Lima, A. C., Hachemane, K., Ribeiro, A. E., Queiroz, A., Gomes, M. C. S. and Brito, P., 2022. Evaluation and kinetic study of alkaline ionic liquid for biodiesel production through transesterification of sunflower oil. *Fuel*, 324.

Lin, L., Cunshan, Z., Vittayapadung, S., Xiangqian, S. and Mingdong, D., 2011. Opportunities and challenges for biodiesel fuel. *Applied Energy*, 88, pp. 1020-1031.

Lin, C. Y. and Ma, L., 2020. Influences of Water Content in Feedstock Oil on Burning Characteristics of Fatty Acid Methyl Esters. *Process*, 8.

Lin, T., Meng, F., Zhang, M. and Liu, Q., 2022. Effect of different low temperature pretreatments on properties of corn stover biochar for precursors of sulfonated solid acid catalysts. *Bioresource Technology*, 357.

Lucideon, n.d. *Testing & Characterization*. [online] Available at: < https://www.lucideon.com/testing-characterization/techniques/sem-edx#:~:text=SEM%20provides%20detailed%20high%20resolution,identification%20and%20quantitative%20compositional%20information.> [Accessed 15 July 2022].

Maleki, B., Ashraf Talesh, S. S. and Mansouri, M., 2022. Comparison of catalysts types performance in the generation of sustainable biodiesel via

transesterification of various oil sources: a review study. *Materials Today Sustainability*, 18.

Mandari, V. and Devarai, S. K., 2021. Biodiesel Production Using Homogeneous, Heterogeneous, and Enzyme Catalysts via Transesterification and Esterification Reactions: a Critical Review. *BioEnergy Research*, 15, pp. 935-961.

Mani Rathnam, V. and Madras, G., 2019. Conversion of Shizochitrium limainum microalgae to biodiesel by non-catalytic transesterification using various supercritical fluids. *Bioresource Technology*, 288.

Mansir, N., Taufiq-Yap, Y. H., Rashid, U. and Lokman, I. M., 2017. Investigation of heterogeneous solid acid catalyst performance on low grade feedstocks for biodiesel production: A review. *Energy Conversion and Management*, 141, pp. 171-182.

Martinez, A., Mijangos, G. E., Romero-Ibarra, I. C., Hernandez-Altamirano, R., Mena-ervantes, V. Y. and Gutierrez, S., 2018. A novel green one-pot synthesis of biodiesel from Ricinus communis seeds by heterogeneous catalysts. *Journal of Cleaner Production*, 196, pp. 340-349.

McCarthy, P., Rasul, M. G. and Moazzem, S., 2011. Comparison of the performance and emissions of different biodiesel blends against petroleum diesel. *International Journal of Low-Carbon Technologies*, 6(4), pp. 255-260.

Miceli, M., Frontera, P., Macario, A. and Malara, A., 2021. Recovery/Reuse of Heterogeneous Supported Spent Catalysts. *Catalysts*, 11.

Miladinovic, M. R., Krstic, J. B., Zdujic, M. V., Veselinovic, L. M., Velijovic, D. N., Banjovic-Ilic, I. B., Stamenkovic, O. S., and Veljkovic, V. B., 2022 Transesterification of used cooking sunflower oil catalyzed by hazelnut shell ash. *Renewable Energy*, 183, pp. 103-113.

Moradi, P., Saidi, M. and Taheri Najafabdi, A., 2021. Biodiesel production via esterification of oleic acid as a representative of free fatty acid using electrolysis technique as a novel approach: Non-catalytic and catalytic conversion. *Process Safety and Environmental Protection*, 147, pp. 684-692.

Mostafa Marzouk, N., Abo El Naga, A.O., Younis, S.A., Shaban, S.A., el Torgoman, A.M. and el Kady, F.Y., 2021. Process optimization of biodiesel production via esterification of oleic acid using sulfonated hierarchical mesoporous ZSM-5 as an efficient heterogeneous catalyst. *Journal of Environmental Chemical Engineering*, 9(2).

Murguia-Ortiz, D., Cordova, I., Manriquez, M. E., Ortiz-Islas, E., Cabrera-Sierra, R., Contreras, J. L., Alcantar-Vazquez, B., Trejo-Rubio, M., Vazquez-Rodriguez, J. T. and Castro, L. V., 2021. Na-CaO/MgO dolomites used as heterogeneous catalysts in canola oil transesterification for biodiesel production. *Materials Letters*, 291.

Mutreja, V., Singh, S. and Ali. A., 2011. Biodiesel from mutton fat using KOH impregnated MgO as heterogeneous catalysts. *Renewable Energy*, 36, pp. 2253-2258.

Naji, S. Z. and Tye, C. T., 2022. A review of the synthesis of activated carbon for biodiesel production: Precursor, preparation, and modification. *Energy Conversion and Management: X¸*13.

Nazir, M. H., Ayoub, M., Zahid, I., Shamsuddin, R. B., Yusup, S., Ameen, M., Zulqarnain, Qadeer, M. U., 2021. Development of lignin based heterogeneous solid acid catalyst derived from sugarcane bagasse for microwave assisted-transesterification of waste cooking oil. *Biomass and Bioenergy*, 146.

Ngamprasertsith, S. and Sawangkeaw, R., n.d. *2 Transesterification in Supercritical Conditions*. [online] Available at: <www.intechopen.com>.

Ngaosuwan, K., Goofwin, J. G. and Praserdham, P., 2016. A green sulfonated carbon-based catalyst derived from coffee residue for esterification. *Renewable Energy*, 86, pp. 262-269.

Nguyen, H. C., Liang, S. H., Chen, S. S., Su, C. H., Lin, J. H. and Chien, C. C., 2018. Enzymatic production of biodiesel from insect fat using methyl acetate as an acyl accepter: Optimization by using response surface methodology. *Energy Conversion and Management*, 158, pp. 168-175.

Nunes, A. L. B. and Castilhos, F., 2020. Chemical interesterification of soybean oil and methyl acetate to FAME using CaO as catalyst. *Fuel*, 267.

Pagalan, J. E., Sebron, M., Gomez, S., Salva, S. J., Ampusta, R., Macarayo, S. J., Joyno, C., Ido A. and Arazo, R., 2020. Activated carbon from spent coffee grounds as an adsorbent for treatment of water contaminated by aniline yellow dye. *Industrial Crops & Products*, 145.

Pallarés, J., González-Cencerrado, A. and Arauzo, I., 2018. Production and characterization of activated carbon from barley straw by physical activation with carbon dioxide and steam. *Biomass and Bioenergy*, 115, pp. 64-73.

Rizwanul Fattah, I. M., Ong, H. C., Mahlia, T. M. I., Mofijur, M., Silitonga, A. S., Ashrafur Rahman, S. M. and Ahman, A., 2020. State of the Art of Catalysts for Biodiesel Production. *Frontiers in Energy Research.*

Saka, S. and Kusdiana, D., 2000. *Biodiesel fuel from rapeseed oil as prepared in supercritical method*. [online] Available at: < http://www.elsevier.com/locate/fuel> [Accessed 25 June 2022].

Sandouqa, A., Al-Hamamre, Z. and Asfar, J., 2019. Preparation and performance investigation of a lignin-based solid acid catalyst manufactured from olive cake for biodiesel production. *Renewable Energy*, 132, pp. 667-682.

Sangsiri, P., Laosiripojana, N. and Daorattanachai, P., 2022. Synthesis of sulfonated carbon-based catalysts from organosolv lignin and methanesulfonic acid: Its activity toward esterification of strearic acid. *Renewable Energy*, 193, pp. 113-127.

Sani, Y. M., Raji, A. O., Alaba, P. A., Abdul Aziz, A. R. and Wan Daud, W. M. A., n.d. Palm Frond and Spikelet as Environmentally Benign Alternative Solid Acid Catalysts for Biodiesel Production. *BioResources*, 10(2), pp. 3393-3408.

Shahidul Islam, M., Robin Hart, C. and Casadonte, D., 2022. Ultrasound-assisted solid Lewis acid-catalyzed transesterification of Lesquerella fendleri oil for biodiesel synthesis. *Ultrasonics Sonochemistry*, [online] 88.

Simões, S.S., Ribeiro, J.S., Celante, D., Brondani, L.N. and Castilhos, F., 2020. Heterogeneous catalyst screening for fatty acid methyl esters production through interesterification reaction. *Renewable Energy*, 146, pp. 719–726.

Singh, D., Sharma, D., Soni, S. L., Sharma, S., Sharma, P. K. and Jhalani, A., 2020. A review on feedstocks, production processes, and yield for different generations of biodiesel. *Fuel*.

Singh, N. K., Singh, Y. and Sharma, A., 2022. Optimization of biodiesel synthesis from Jojoba oil via supercritical methanol: A response surface methodology approach coupled with genetic algorithm. *Biomass and Bioenergy*, 156.

Soltani, S., Khanian, N., Shean, Y. C. T., Asim, N. and Zhao, Y., 2021. Microwave-assisted hydrothermal synthesis of sulfonated TiO_2-GO core-shell solid spheres as heterogeneous esterification mesoporous catalyst for biodiesel production. *Energy Conversion and Management*, 238.

Supang, W., Ngamprasertsith, S., Sakdasri, W. and Sawangkeaw, R., 2022. Ethyl acetate as extracting solvent and reactant for producing biodiesel from spent coffee grounds: A catalyst- and glycerol-free process. *The Journal of Supercritical Fluids*, 186.

Thommes, M., Kaneko, K., Neimark, A. V., Olivier, J. P., Rodriguez-Reinoso, F., Rouquerol, J. and Sing, K. S. W., 2015. Physisorption of gases, with special reference to the evaluation of surface are and pore size distribution (IUPAC Technical Report). *Pure Applied Chemistry*, 87, pp. 1051-1069.

Tian, H., Zhou, T., Huang, Z., Wang, J., Cheng, H. and Yang, Y., 2021. Integration of spent coffee grounds valorization for co-production of biodiesel and activated carbon: An energy and techno-economic case assessment in China. *Journal of Cleaner Production*, 324.

Tyson, S. and McCormick, R., 2006. *Biodiesel Handling and Use Guidelines (Third Edition)*. [online] Available at: < http://www.osti.gov/bridge> [Accessed 13 June 2022].

United Nations, n.d. *Population*. [online] Available at: <https://www.un.org/en/global-issues/population> [Accessed 4 June 2022].

U.S EIA, 2021. *Internal Energy Outlook 2021*. [pdf] Washington. Available at: <https://www.eia.gov/outlooks/ieo/pdf/IEO2021_ReleasePresentation.pdf> [Accessed 3 June 2022].

U.S EIA, 2020. *Biomass-based diesel and the environment*. [online] Available at: <https://www.eia.gov/energyexplained/biofuels/biodiesel-and-the-environment.php> [Accessed 13 June 2022].

U.S. EPA, n.d. *Local Renewable Energy Benefits and Resources*. [online] Available at: <https://www.epa.gov/statelocalenergy/local-renewable-energy-benefits-and-resources#:~:text=Benefits%20of%20Renewable%20Energy,-Environmental%20and%20economic&text=Generating%20energy%20that%20produces%20no,in%20manufacturing%2C%20installation%2C%20and%20more [Accessed 5 June 2022].

Wang, S., Xue, Y., Zhao, X. and Yuan, H., 2021. Preparation of a carbon microsphere-based solid acid application to waste frying oil transesterification. *Diamond & Related Materials*, 116.

Wong, W.Y., Lim, S., Pang, Y.L., Chen, W.H., Lam, M.K. and Tan, I.S., 2022. Synthesis of glycerol-free fatty acid methyl ester using interesterification reaction based on solid acid carbon catalyst derived from low-cost biomass wastes. *International Journal of Energy Research*, 46(1), pp.147–162.

Wong, W. Y., Lim, S., Pang, Y. L., Shuit, S. H., Chen, W. H. and Lee, K. T., 2020. Synthesis of renewable heterogeneous acid catalyst from oil palm empty fruit bunch for glycerol-free biodiesel production. *Science of the Total Environment*, 727.

Xiao, Y. and Hill, J. M., 2020. Solid acid catalysts produced by sulfonation of petroleum coke: Dominant role of aromatic hydrogen. *Chemosphere*, 248.

Yuliana, M., Santoso, S. P., Soetaredji, F. E., Ismadji, S., Ayucitra, A., Angkawijaya, A. E., Ju, Y. H. and Tran-Nguyen, P. L., 2020. A one-pot synthesis of biodiesel from leather tanning waste using supercritical ethanol: Process optimization. *Biomass and Bioenergy*, 142.

Zailan, Z., Tahir, M., Jusoh, M. and Zakaria, Z. Y., 2021. A review of sulfonic group bearing porous carbon catalyst for biodiesel production. *Renewable Energy*, 175, pp. 430-452.

Zhang, B., Gao, M., Geng, J., Cheng, Y., Wang, X., Wu, C., Wang, Q., Liu, S. and Cheung, S. M., 2021. Catalytis performance and deactivation mechanism of a one-step sulfonated carbon-based solid-acid catalyst in an esterification reaction. *Renewable Energy*, 164, pp. 824-832.

Zhang, B., Gao, M., Tang, W., Wang, X., Wu, C., Wang, Q., Cheung, S. M. and Chen, X., 2023. Esterification efficiency improvement of carbon-based solid acid catalysts induced by biomass pretreatments: Intrinsic mechanism. *Energy*, 263.

Zhou, C. and Wang, Y., 2020. Recent progress in the conversion of biomass wastes into function materials for value-added applications. *Science and Technology of Advanced Materials*, 21(1), pp. 787-804.

Zięzio, M., Charmas, B., Jedynak, K., Hawryluk, M. and Kucio, K., 2020. Preparation and characterization of activated carbons obtained from the waste materials impregnated with phosphoric acid (V). *Applied Nanoscience*, 10, pp. 4703-4716.

APPENDICES

Appendix A: Catalyst Characterisation – Acid Density

Table A-1: Acid Density of Sample Catalyst via Titration.

Sample	Weight of Sample (g)		Volume of HCl Used (mL)		Acid Density (mmol NaOH/g)		
	1	**2**	**1**	**2**	**1**	**2**	**Average**
SCSCG$_{80}$	0.142	0.146	20.0	20.9	2.113	1.993	2.053
SCSCG$_{120}$	0.142	0.118	18.6	22.1	2.211	2.364	2.288
SCSCG$_{160}$	0.128	0.124	14.9	19.0	2.742	2.500	2.621
SCSCG$_{200}$	0.117	0.107	14.2	0.18	3.060	2.991	3.025
SCSCG$_{240}$	0.114	0.112	15.9	16.8	2.991	2.964	2.978

<u>SAMPLE CALCULATION</u>

Given that 0.01M NaOH and 0.01M HCl are used,

Taking SCSCG$_{80}$ as an example, the weight of the sample used (W_{CAT}) is 0.142 g.

$$Acid\ Density = \{[NaOH]V_{NaOH} - [HCl]V_{HCl}\} \times \frac{1}{W_{CAT}}$$

$$Acid\ Density = \left\{\left[0.01\frac{mmol}{mL}\right]50\ mL - \left[0.01\frac{mmol}{mL}\right]20\ mL\right\} \times \frac{1}{0.142g}$$

$$Acid\ Density = 2.113\frac{mmol}{g}$$

Appendix B: Catalyst Characterisation – SEM & Surface Analysis

Table B-1: SEM Images of CSCG and $SCSCG_{80}$ with Different Magnification.
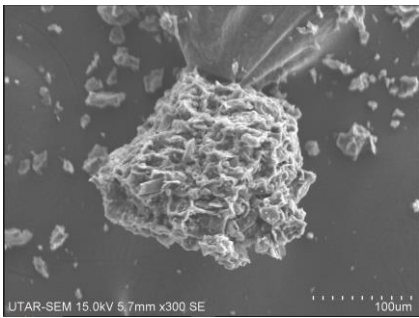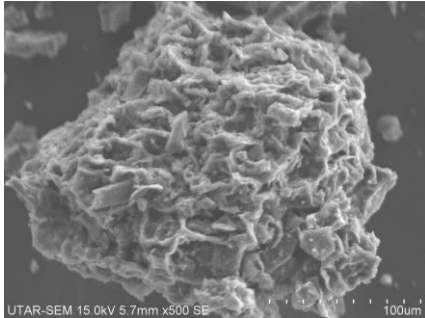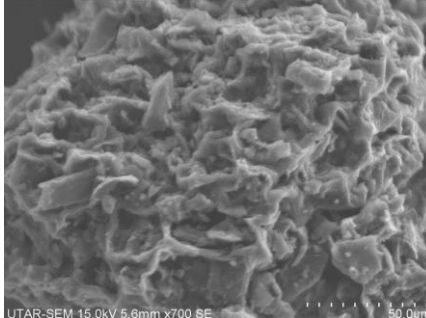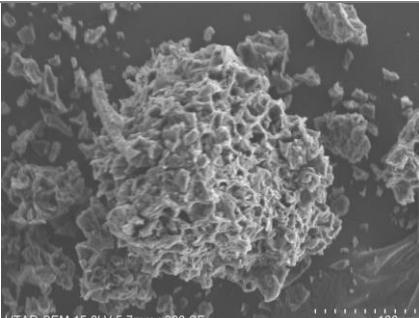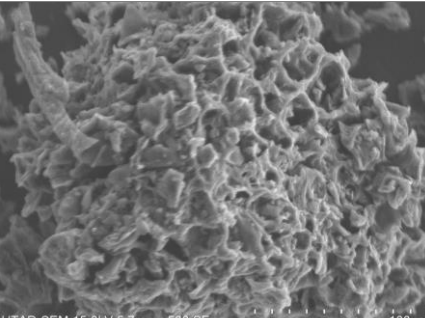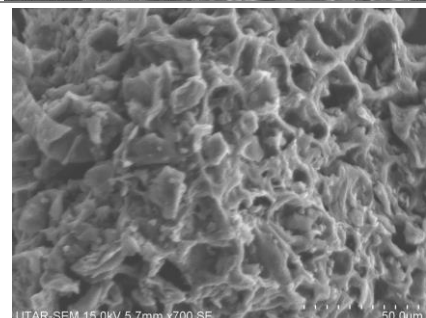
Sample	Magnification		
Catalyst	300X	500X	700X
CSCG			
$SCSCG_{80}$			

Table B-2: SEM Images of SCSCG$_{120}$ and SCSCG$_{160}$ with Different Magnification.
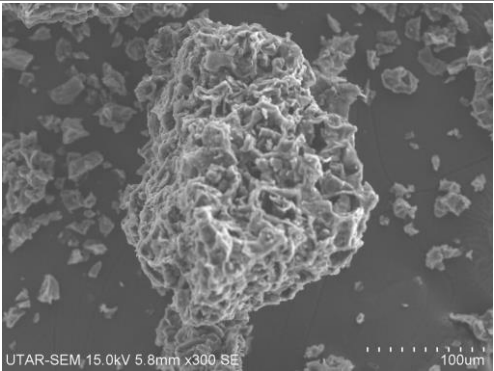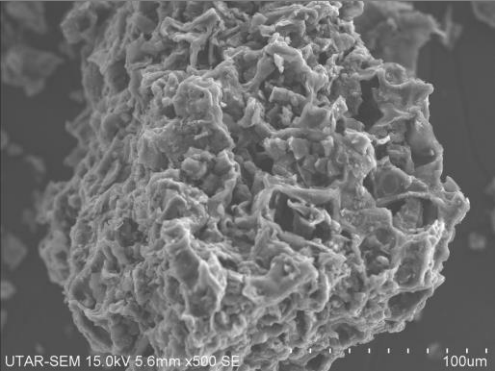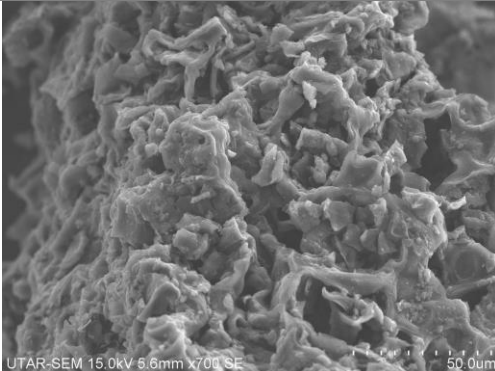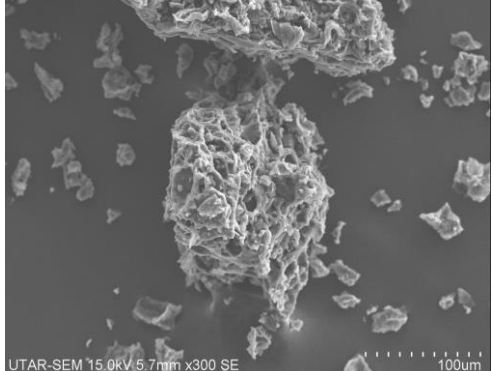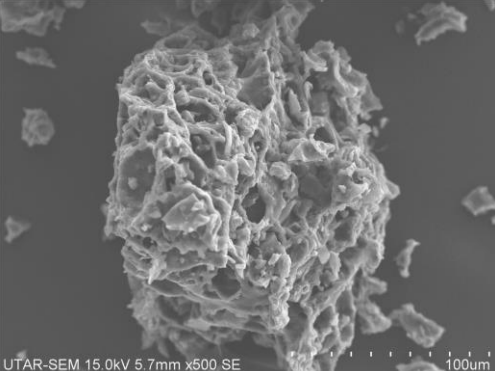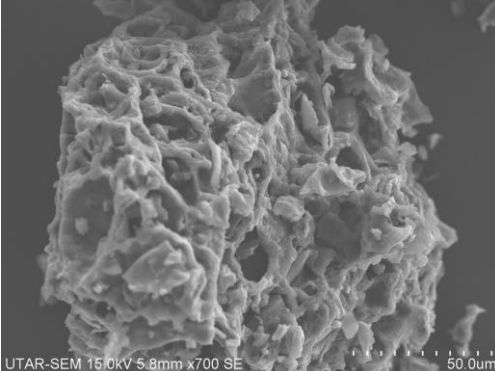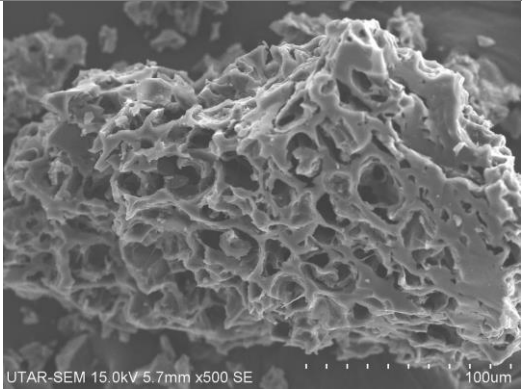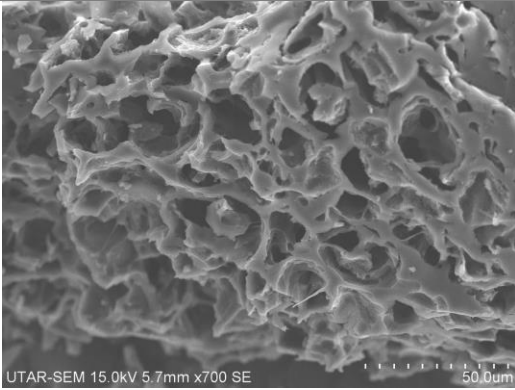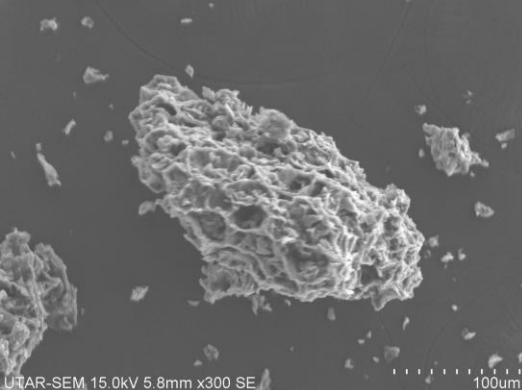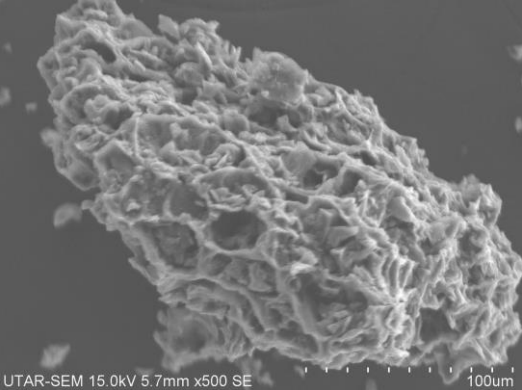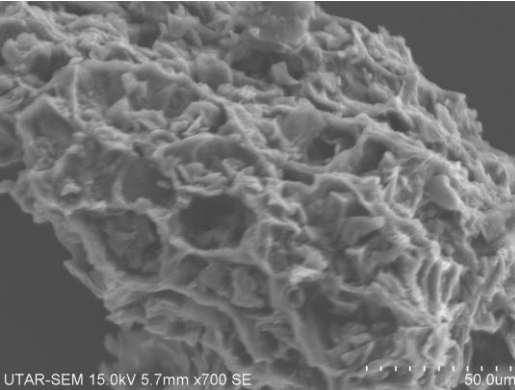
Sample	Magnification		
Catalyst	300X	500X	700X
SCSCG$_{120}$			
SCSCG$_{160}$			

Table B-3: SEM Images of SCSCG$_{200}$ and SCSCG$_{240}$ with Different Magnification.

Sample	Magnification		
Catalyst	300X	500X	700X
SCSCG$_{200}$			
SCSCG$_{240}$			
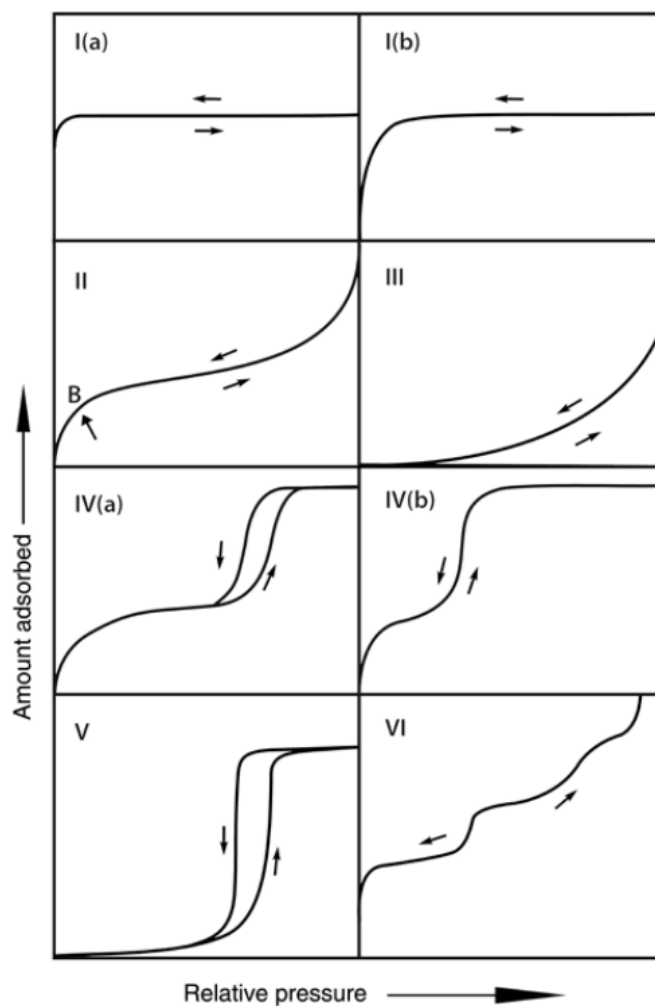
Figure B-1:   IUPAC Classification of Isotherms.
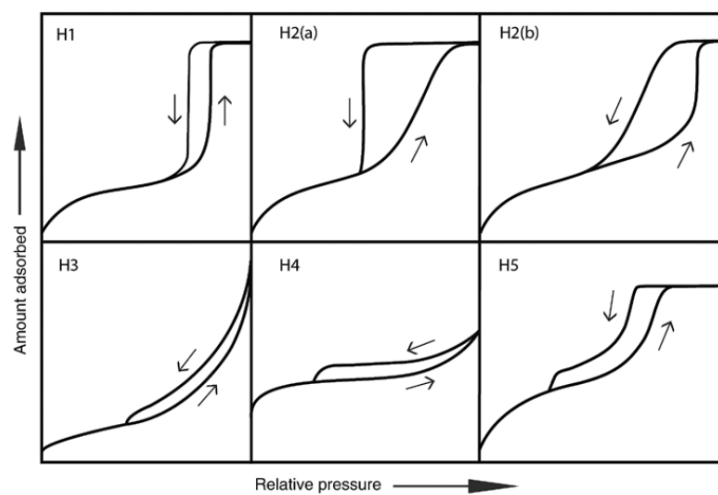
Figure B-2:   IUPAC Classification of Hysteresis Loops.

Appendix C: Catalyst Characterisation – EDAX

Element	Wt%	At%
CK	61.02	67.48
NK	03.40	03.23
OK	35.00	29.05
SK	00.58	00.24
Matrix	Correction	ZAF

Element	Wt%	At%
CK	62.61	68.95
NK	03.25	03.07
OK	33.55	27.74
SK	00.59	00.24
Matrix	Correction	ZAF

Element	Wt%	At%
CK	61.56	67.99
NK	02.45	02.32
OK	35.61	29.53
SK	00.38	00.16
Matrix	Correction	ZAF

Element	Wt%	At%
CK	58.65	65.15
NK	03.95	03.76
OK	37.16	30.99
SK	00.25	00.10
Matrix	Correction	ZAF
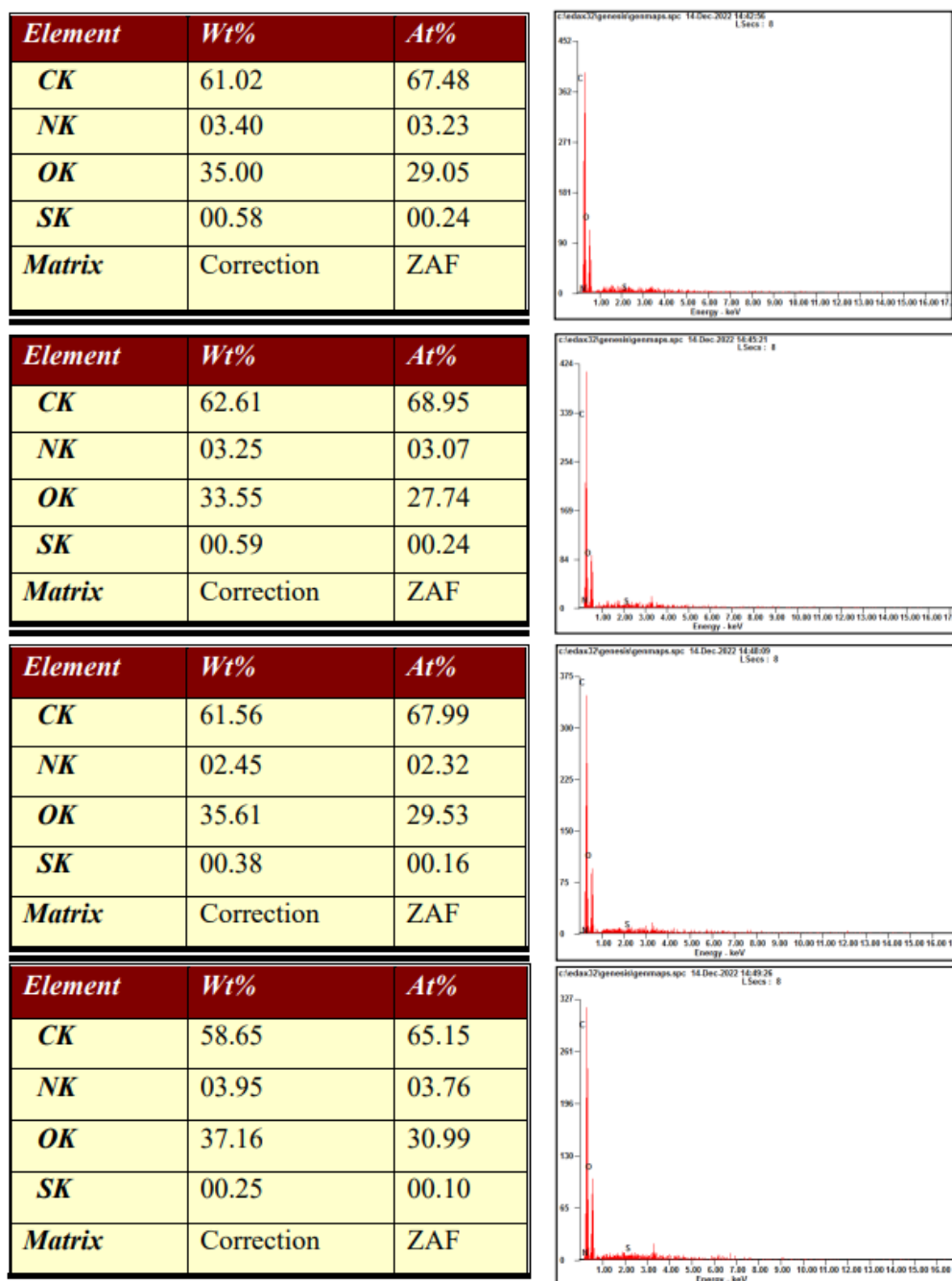
Figure C-1:   EDX Result of Raw Spent Coffee Ground at Different Locations.

Element	Wt%	At%
CK	81.20	85.58
NK	05.20	04.70
OK	10.91	08.63
PK	02.33	00.95
SK	00.37	00.15
Matrix	Correction	ZAF

Element	Wt%	At%
CK	79.56	84.34
NK	07.05	06.41
OK	09.76	07.77
PK	03.01	01.24
SK	00.62	00.25
Matrix	Correction	ZAF

Element	Wt%	At%
CK	79.03	83.85
NK	06.36	05.79
OK	11.33	09.03
PK	02.63	01.08
SK	00.64	00.26
Matrix	Correction	ZAF

Element	Wt%	At%
CK	79.72	84.38
NK	05.05	04.58
OK	12.47	09.91
PK	02.62	01.08
SK	00.14	00.06
Matrix	Correction	ZAF

Figure C-2:   EDX Results of CSCG at Different Locations.

Element	Wt%	At%
CK	79.25	84.33
NK	04.06	03.70
OK	13.23	10.57
PK	00.90	00.37
SK	02.57	01.02
Matrix	Correction	ZAF
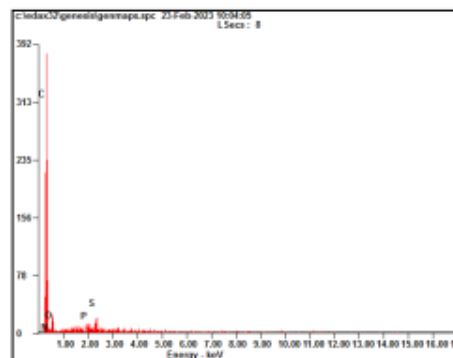
Element	Wt%	At%
CK	81.52	86.56
NK	02.31	02.10
OK	12.23	09.75
PK	01.18	00.49
SK	02.76	01.10
Matrix	Correction	ZAF
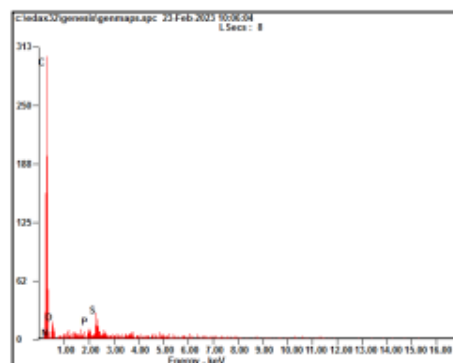
Element	Wt%	At%
CK	78.65	83.96
NK	04.46	04.09
OK	12.91	10.34
PK	01.41	00.58
SK	02.57	01.03
Matrix	Correction	ZAF
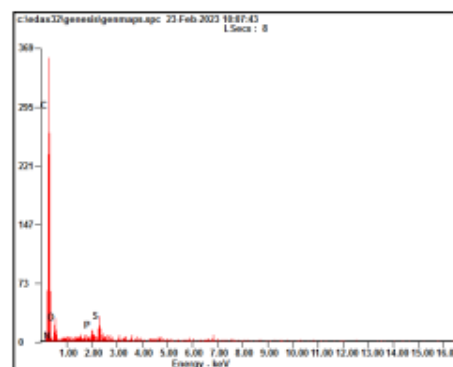
Element	Wt%	At%
CK	82.22	87.13
NK	02.57	02.34
OK	11.23	08.94
PK	01.23	00.51
SK	02.74	01.09
Matrix	Correction	ZAF
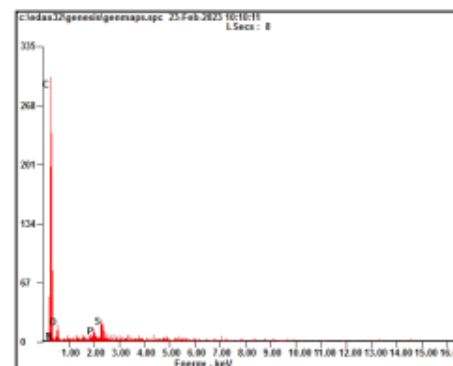
Figure C-3:EDX Results of $SCSCG_{80}$ at Different Locations.

Element	Wt%	At%
CK	77.15	82.76
NK	05.08	04.67
OK	13.42	10.81
PK	00.62	00.26
SK	03.74	01.50
Matrix	Correction	ZAF

Element	Wt%	At%
CK	80.00	85.13
NK	05.38	04.90
OK	10.32	08.25
PK	00.63	00.26
SK	03.67	01.46
Matrix	Correction	ZAF

Element	Wt%	At%
CK	77.29	82.71
NK	06.10	05.60
OK	12.47	10.02
PK	00.71	00.29
SK	03.43	01.38
Matrix	Correction	ZAF

Element	Wt%	At%
CK	76.09	81.76
NK	07.35	06.77
OK	11.85	09.56
PK	01.07	00.44
SK	03.63	01.46
Matrix	Correction	ZAF

Figure C-4:   EDX Results of $SCSCG_{120}$ at Different Locations.

Element	Wt%	At%
CK	78.04	84.03
NK	02.51	02.32
OK	14.33	11.58
PK	00.54	00.23
SK	04.58	01.85
Matrix	Correction	ZAF
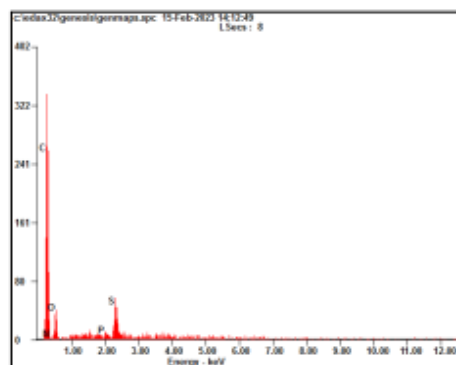
Element	Wt%	At%
CK	78.98	84.64
NK	01.92	01.77
OK	14.71	11.83
PK	00.32	00.13
SK	04.06	01.63
Matrix	Correction	ZAF
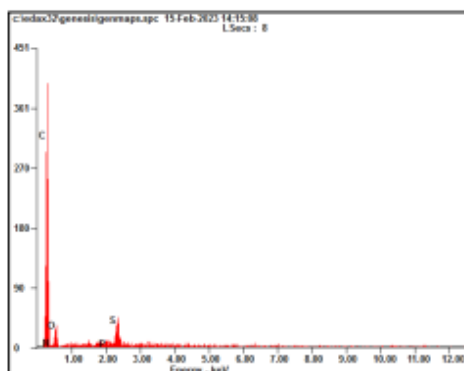
Element	Wt%	At%
CK	76.76	82.69
NK	04.82	04.45
OK	13.38	10.82
PK	00.63	00.26
SK	04.42	01.78
Matrix	Correction	ZAF
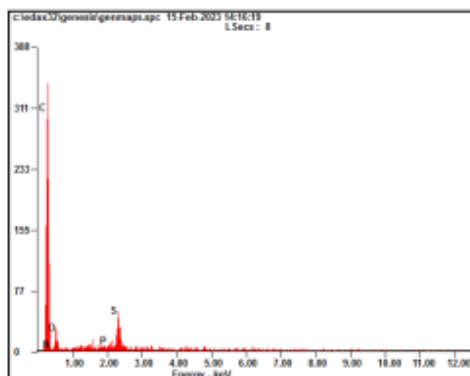
Element	Wt%	At%
CK	79.35	84.99
NK	03.74	03.44
OK	11.87	09.54
PK	00.71	00.29
SK	04.32	01.73
Matrix	Correction	ZAF
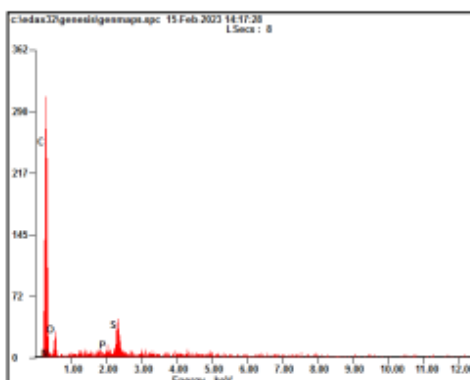
Figure C-5:　　　EDX Results of $SCSCG_{160}$ at Different Locations.

Element	Wt%	At%
CK	76.67	82.80
NK	03.62	03.35
OK	14.44	11.71
PK	00.50	00.21
SK	04.76	01.93
Matrix	Correction	ZAF

Element	Wt%	At%
CK	77.06	83.09
NK	03.37	03.12
OK	14.52	11.75
PK	00.35	00.15
SK	04.70	01.90
Matrix	Correction	ZAF

Element	Wt%	At%
CK	76.89	82.86
NK	03.45	03.18
OK	14.85	12.01
PK	00.20	00.08
SK	04.61	01.86
Matrix	Correction	ZAF

Element	Wt%	At%
CK	76.51	82.75
NK	02.65	02.46
OK	15.61	12.67
PK	00.40	00.17
SK	04.82	01.95
Matrix	Correction	ZAF

Figure C-6:   EDX Results of SCSCG$_{200}$ at Different Locations.

Element	Wt%	At%
CK	80.10	85.87
NK	00.00	00.00
OK	15.21	12.24
PK	00.50	00.21
SK	04.18	01.68
Matrix	Correction	ZAF

Element	Wt%	At%
CK	74.72	81.19
NK	01.90	01.77
OK	18.39	15.00
PK	00.44	00.19
SK	04.54	01.85
Matrix	Correction	ZAF

Element	Wt%	At%
CK	74.76	80.96
NK	04.16	03.86
OK	16.23	13.20
PK	00.52	00.22
SK	04.33	01.76
Matrix	Correction	ZAF

Element	Wt%	At%
CK	75.26	81.39
NK	03.08	02.86
OK	17.14	13.91
PK	00.34	00.14
SK	04.17	01.69
Matrix	Correction	ZAF

Figure C-7: EDX Results of SCSCG$_{240}$ at Different Locations.

Appendix D: GC Reports – Methyl Oleate Calibration Curve

```
Peak RetTime Type  Width     Area       Height      Area
  #   [min]        [min]    [pA*s]       [pA]        %
----|-------|----|-------|----------|----------|--------|
  1   2.018 BB S  0.0186 5.35760e5  4.61121e5  99.49957
  2  13.198 BB    0.0479 1336.41638  433.98987  0.24819
  3  14.866 BB    0.0626 1358.17334  339.96143  0.25224

Totals :                   5.38455e5  4.61895e5
```

Figure D-1:   GC Results of 5 g/L Methyl Oleate.

```
Peak RetTime Type  Width     Area       Height      Area
  #   [min]        [min]    [pA*s]       [pA]        %
----|-------|----|-------|----------|----------|--------|
  1   2.017 BB S  0.0186 5.40421e5  4.62985e5  99.25668
  2  13.184 BB    0.0475 1401.66833  460.33984  0.25744
  3  14.859 BB    0.0624 2645.46802  650.48853  0.48588

Totals :                   5.44468e5  4.64096e5
```

Figure D-2:   GC Results of 10 g/L Methyl Oleate.

```
Peak RetTime Type  Width     Area       Height      Area
  #   [min]        [min]    [pA*s]       [pA]        %
----|-------|----|-------|----------|----------|--------|
  1   2.016 BB S  0.0185 5.32752e5  4.61903e5  98.62782
  2  13.183 BB    0.0476 1286.24072  422.04321  0.23812
  3  14.887 BB    0.0673 6125.75439 1392.11780  1.13405

Totals :                   5.40164e5  4.63718e5
```

Figure D-3:   GC Results of 20 g/L Methyl Oleate.

```
Peak RetTime Type  Width     Area       Height      Area
  #   [min]        [min]    [pA*s]       [pA]        %
----|-------|----|-------|----------|----------|--------|
  1   2.016 BB S  0.0170 5.32064e5  4.76421e5  98.19110
  2  13.183 BB    0.0488 1393.83777  454.60965  0.25723
  3  14.901 BB    0.0690 8407.95703 1815.15674  1.55167

Totals :                   5.41866e5  4.78691e5
```

Figure D-4:   GC Results of 30 g/L Methyl Oleate.

```
Peak RetTime Type  Width     Area      Height     Area
  #   [min]        [min]    [pA*s]      [pA]       %
----|-------|----|-------|----------|----------|--------|
   1   2.016 BB S  0.0186 5.33032e5  4.55724e5  97.70355
   2  13.182 BB    0.0480 1393.61084  451.93967  0.25545
   3  14.916 BB    0.0749 1.11349e4  2244.70435  2.04101

Totals :                  5.45561e5  4.58420e5
```

Figure D-5:   GC Results of 40 g/L Methyl Oleate.

```
Peak RetTime Type  Width     Area      Height     Area
  #   [min]        [min]    [pA*s]      [pA]       %
----|-------|----|-------|----------|----------|--------|
   1   2.015 BB S  0.0180 5.32505e5  4.76434e5  97.14196
   2  13.181 BB    0.0478 1306.08484  425.49332  0.23826
   3  14.932 BB    0.0782 1.43609e4  2694.05151  2.61978

Totals :                  5.48172e5  4.79553e5
```

Figure D-6:   GC Results of 50 g/L Methyl Oleate.

Table D-1: Data Needed for Calibration Curve of Methyl Oleate.

| Concentration of Methyl Oleate (g/L) | Peak Area | | MO/IS |
	Methyl Oleate (MO)	Internal Standard (IS)	
5	1358.17334	1336.41638	1.01628
10	2645.46802	1401.66833	1.88737
20	6125.75439	1286.24072	4.76253
30	8407.95703	1393.83777	6.03224
40	1.11349e+04	1391.61084	7.98996
50	1.43609e+04	1306.08484	10.99538
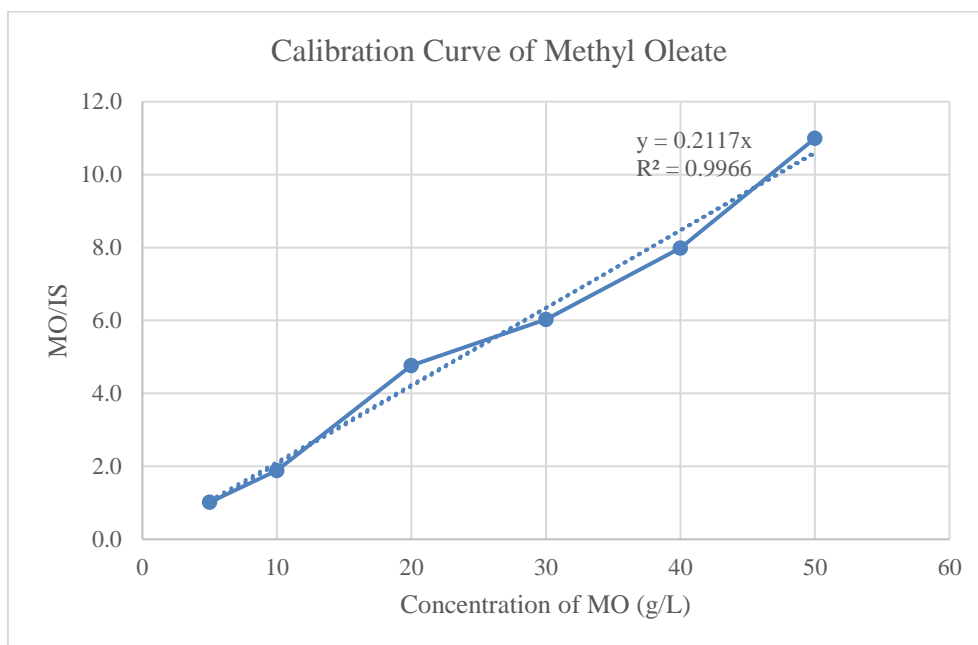
Figure D-7: Calibration Curve of Methyl Oleate for GC Analysis.

From the calibration curve, the response factor of methyl oleate is **0.2117.**

Appendix E: Characterisation of Catalyst Activated by $ZnCl_2$

Element	Wt%	At%
CK	82.08	86.17
NK	03.47	03.13
OK	12.71	10.02
SK	01.73	00.68
Matrix	Correction	ZAF

Element	Wt%	At%
CK	81.62	85.55
NK	04.05	03.64
OK	13.16	10.35
SK	01.18	00.46
Matrix	Correction	ZAF

Element	Wt%	At%
CK	80.90	85.03
NK	04.24	03.82
OK	13.40	10.57
SK	01.46	00.58
Matrix	Correction	ZAF

Element	Wt%	At%
CK	78.99	83.31
NK	04.22	03.82
OK	15.73	12.46
SK	01.05	00.42
Matrix	Correction	ZAF
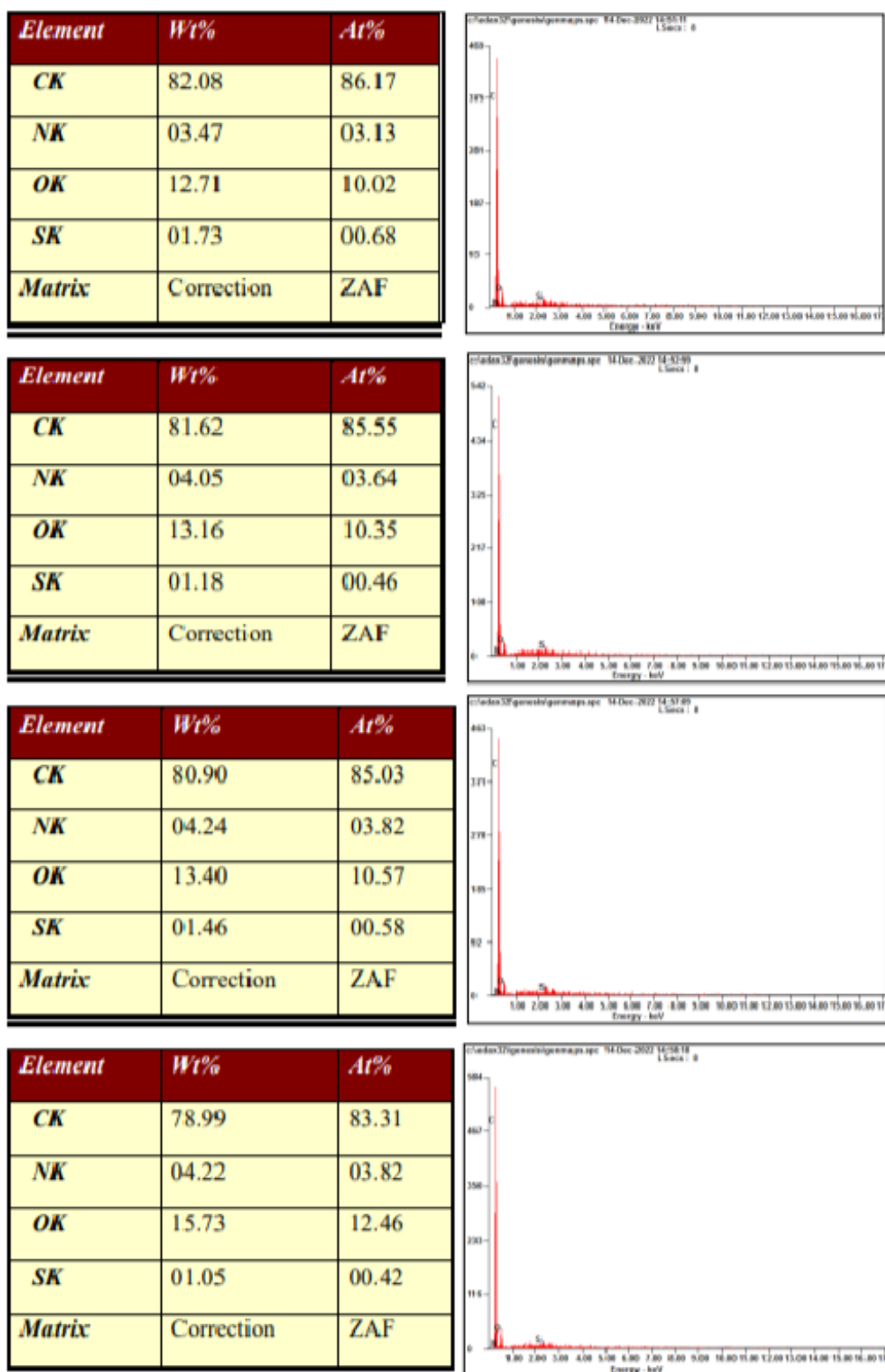
Figure E-1: EDX Results of Catalyst Activated by $ZnCl_2$ and Sulfonated at 160 ℃.

Surface Area

Single point surface area at P/Po = 0.252967727: 718.0726 m²/g

BET Surface Area: 697.5835 m²/g

Langmuir Surface Area: 1,013.3918 m²/g

t-Plot Micropore Area: 571.8685 m²/g

t-Plot external surface area: 125.7150 m²/g

Figure E-2: Summary of BET Report of Carbonised Carbon, which was Impregnated in $ZnCl_2$.

Surface Area

Single point surface area at P/Po = 0.256621816: 1,188.6883 m²/g

BET Surface Area: 1,191.8602 m²/g

Langmuir Surface Area: 1,797.0932 m²/g

t-Plot Micropore Area: 545.0118 m²/g

t-Plot external surface area: 646.8484 m²/g

Figure E-3: Summary of BET Report of Catalyst, which was Impregnated in $ZnCl_2$ and Sulfonated at 160 °C.

Appendix F: GC Reports – Effect of Catalyst Loading on Biodiesel Yield

```
Peak RetTime Type  Width     Area       Height     Area
  #   [min]        [min]    [pA*s]      [pA]        %
----|-------|----|-------|----------|----------|--------|
  1    2.015 BB S  0.0185 5.34655e5  4.61292e5  96.14418
  2    2.199 BB T  0.0235  575.24518  384.07779  0.10344
  3   12.109 BB    0.0422   62.09467   23.25008  0.01117
  4   13.211 BB    0.0514 1352.95825  411.25092  0.24330
  5   14.539 BB    0.0685  286.41122   64.90076  0.05150
  6   14.947 BB    0.0742 1.12162e4  2247.68896  2.01694
  7   15.660 BV    0.0765  739.35089  147.54816  0.13295
  8   27.350 BB    0.1989  124.44364    9.56009  0.02238
  9   43.480 BB    0.3211 7085.44238  261.52554  1.27414
 Totals :                 5.56097e5  4.64841e5
```

Figure F-1: GC Reports of Product from Esterification with 4 wt.% Catalyst.

```
Peak RetTime Type  Width     Area       Height     Area
  #   [min]        [min]    [pA*s]      [pA]        %
----|-------|----|-------|----------|----------|--------|
  1    2.014 BB S  0.0189 5.33324e5  4.48936e5  94.92551
  2    2.198 BB T  0.0235  274.91779  183.55701  0.04893
  3   12.101 BB    0.0428  109.28869   40.03671  0.01945
  4   13.203 BB    0.0521 1377.33691  410.46600  0.24515
  5   14.540 BB    0.0753  474.73663   98.44991  0.08450
  6   14.969 BB    0.0810 1.82736e4  3181.10132  3.25249
  7   15.654 BB    0.0757 1190.40955  240.84650  0.21188
  8   27.313 BB    0.2073  162.46854   11.90043  0.02892
  9   43.404 BB    0.3287 6647.47070  244.90669  1.18317
 Totals :                 5.61834e5  4.53347e5
```

Figure F-2: GC Reports of Product from Esterification with 8 wt.% Catalyst.

```
Peak RetTime Type  Width     Area       Height     Area
  #   [min]        [min]    [pA*s]      [pA]        %
----|-------|----|-------|----------|----------|--------|
  1    2.011 BB S  0.0187 5.21294e5  4.44042e5  95.14338
  2    2.195 BB T  0.0234  278.96271  187.09256  0.05091
  3   12.095 BB    0.0411  102.57552   38.43164  0.01872
  4   13.195 BB    0.0521 1326.41260  396.06955  0.24209
  5   14.530 BB    0.0748  479.77481  100.38750  0.08757
  6   14.962 BB    0.0780 1.86878e4  3252.45483  3.41078
  7   15.644 BV R  0.0771 1404.78967  249.75627  0.25639
  8   27.288 BB    0.2150  117.25293    8.18934  0.02140
  9   43.277 BB    0.3351 4212.03955  154.94724  0.76876
 Totals :                 5.47904e5  4.48429e5
```

Figure F-3: GC Reports of Product from Esterification with 12 wt.% Catalyst.

```
Peak RetTime Type  Width     Area      Height     Area
  #    [min]        [min]    [pA*s]      [pA]       %
----|-------|----|-------|----------|----------|--------|
  1   2.025 BB S  0.0187 5.16162e5  4.38123e5  95.52080
  2   2.210 BB T  0.0236  193.59756 128.44293   0.03583
  3  12.129 BB    0.0411  101.10635  37.97914   0.01871
  4  13.235 BB    0.0523 1339.98462 397.29111   0.24798
  5  14.581 BB    0.0759  475.59769  99.23182   0.08801
  6  15.017 BB    0.0822 1.86904e4  3195.12061  3.45883
  7  15.703 BB    0.0748 1209.53772 243.97520   0.22384
  8  27.438 BB    0.2249  143.12599   9.49163   0.02649
  9  43.406 BB    0.3209 2050.73975  76.95325   0.37951
Totals :                 5.40366e5  4.42312e5
```

Figure F-4: GC Reports of Product from Esterification with 16 wt.% Catalyst.

```
Peak RetTime Type  Width     Area      Height     Area
  #    [min]        [min]    [pA*s]      [pA]       %
----|-------|----|-------|----------|----------|--------|
  1   2.016 BB S  0.0186 5.26996e5  4.52066e5  95.78094
  2   2.199 BB T  0.0236  400.52844 265.41736   0.07280
  3  12.102 BB    0.0426   87.91733  32.45371   0.01598
  4  13.203 BB    0.0522 1343.04468 400.02991   0.24410
  5  14.535 BB    0.0744  409.02344  86.08440   0.07434
  6  14.958 BB    0.0758 1.55175e4  2836.22070  2.82028
  7  15.651 BB    0.0760  994.75183 200.08072   0.18079
  8  27.317 BB    0.2052  176.49158  12.77133   0.03208
  9  43.333 BB    0.3128 4284.45117 161.84377   0.77869
Totals :                 5.50210e5  4.56061e5
```

Figure F-5: GC Reports of Product from Esterification with 20 wt.% Catalyst.

Table F-1: Data Needed for Calculation of Methyl Oleate Concentration and Yield.

| Catalyst Loading (wt.%) | Peak Area | | MO/IS | Concentration of MO (g/L) | Yield (%) |
	Methyl Oleate (MO)	Internal Standard (IS)			
4	11216.2	1352.9583	8.2901	39.1598	73.33
8	18273.6	1377.3369	13.2673	62.6705	78.24
12	18687.8	1326.4126	14.0890	66.5516	83.09
16	18690.4	1339.9846	13.9482	65.8867	82.25
20	15517.5	1343.0447	11.5540	54.5771	68.14

<u>SAMPLE CALCULATION</u>

Taking esterification with 12 wt.% as an example,

From the calibration curve, the line equation derived is $y = 0.2117x$, where y is the MO/IS while x is the concentration of methyl oleate. Therefore, by substituting the y value,

$$14.0890 = 0.2117x$$

$$x = \frac{14.0890}{0.2117} = 66.5516$$

$$Concentration\ of\ methyl\ oleate = 66.5516\ g/L$$

Then, the yield can be calculated accordingly. While preparing the sample for GC analysis, the sample was evaporated until 20 mL was left. Besides, the density and purity of the oleic acid used are 0.89 g/mL and 90 %, respectively.

$$DF = \frac{Sample\ volume\ after\ dilution}{Sample\ volume\ before\ dilution}$$

$$DF = \frac{1000\ \mu L}{100\ \mu L} = 10$$

$$Yield\ (\%) = \frac{C_{MO} \times DF \times V_S}{V_{OC} \times D_{OC}} \times 100\%$$

$$Yield\ (\%) = \frac{66.5516\frac{g}{L} \times 10 \times 0.02\ L}{20\ mL \times 0.89\frac{g}{mL} \times 0.9} \times 100\%$$

$$Yield\ (\%) = 83.09\%$$

Appendix G: GC Reports – Effect of Methanol-to-Oleic Acid Molar Ratio
(MOAMR) on Biodiesel Yield

```
Peak RetTime Type  Width     Area       Height      Area
  #    [min]        [min]   [pA*s]       [pA]         %
----|-------|----|-------|----------|----------|--------|
   1    2.025 BB S  0.0188 5.34673e5  4.51373e5  92.93764
   2    2.210 BB T  0.0236  253.17493  167.60905   0.04401
   3   12.137 BB     0.0426   27.61863   10.20489   0.00480
   4   12.903 BB     0.0529 1368.11890  399.64001   0.23781
   5   13.243 BB     0.0516 1227.42529  371.10840   0.21335
   6   14.699 BV     0.0735 6407.67480 1347.47815   1.11379
   7   14.942 VB     0.0691 4471.73828 1020.19489   0.77728
   8   15.468 BV     0.0771  399.56540   78.85494   0.06945
   9   15.694 VB     0.0760  286.00668   56.60057   0.04971
  10   27.411 BB     0.2250  382.81146   24.67931   0.06654
  11   40.928 BB     0.3493  595.44885   22.68176   0.10350
  12   43.981 BB     0.4417 2.39931e4   691.65808   4.17052
  13   48.598 BB     0.3437 1217.22888   43.07502   0.21158

Totals :                    5.75303e5  4.55606e5
```

Figure G-1: GC Reports of Product from Esterification with 4:1 MOAMR.

```
Peak RetTime Type  Width     Area       Height      Area
  #    [min]        [min]   [pA*s]       [pA]         %
----|-------|----|-------|----------|----------|--------|
   1    2.018 BB S  0.0187 5.35849e5  4.56556e5  94.89240
   2    2.202 BB T  0.0236  103.24010   68.53602   0.01828
   3   12.109 BB     0.0422   88.15296   32.98273   0.01561
   4   13.212 VB     0.0518 1380.52209  414.78070   0.24447
   5   14.548 BB     0.0732  404.20731   86.98270   0.07158
   6   14.970 BB     0.0772 1.58491e4  2879.39771   2.80668
   7   15.663 BB     0.0761 1022.98749  205.30074   0.18116
   8   27.333 BB     0.2084  174.28604   12.59910   0.03086
   9   43.540 BB     0.3611 9819.67383  346.01349   1.73895
 Totals :                   5.64691e5  4.60603e5
```

Figure G-2: GC Reports of Product from Esterification with 8:1 MOAMR.

```
Peak RetTime Type  Width     Area       Height      Area
  #    [min]        [min]   [pA*s]       [pA]         %
----|-------|----|-------|----------|----------|--------|
   1    2.011 BB S  0.0187 5.21294e5  4.44042e5  95.14338
   2    2.195 BB T  0.0234  278.96271  187.09256   0.05091
   3   12.095 BB     0.0411  102.57552   38.43164   0.01872
   4   13.195 BB     0.0521 1326.41260  396.06955   0.24209
   5   14.530 BB     0.0748  479.77481  100.38750   0.08757
   6   14.962 BB     0.0780 1.86878e4  3252.45483   3.41078
   7   15.644 BV R  0.0771 1404.78967  249.75627   0.25639
   8   27.288 BB     0.2150  117.25293    8.18934   0.02140
   9   43.277 BB     0.3351 4212.03955  154.94724   0.76876
 Totals :                   5.47904e5  4.48429e5
```

Figure G-3: GC Reports of Product from Esterification with 12:1 MOAMR.

```
Peak RetTime Type  Width     Area       Height      Area
  #   [min]        [min]    [pA*s]       [pA]         %
----|-------|----|-------|----------|----------|--------|
   1   2.024 BB S  0.0188 5.18254e5  4.38607e5  94.41185
   2   2.208 BB T  0.0236  388.20795  257.35587  0.07072
   3  12.135 BB    0.0416  120.19754   44.42429  0.02190
   4  13.243 VB    0.0538 1315.69238  385.24350  0.23968
   5  14.594 BB    0.0770  545.66858  109.80233  0.09941
   6  15.032 BB    0.0831 2.15531e4  3537.80029  3.92639
   7  15.711 BV R  0.0752 1407.13684  279.10376  0.25634
   8  27.426 BB    0.2195  271.44717   19.02099  0.04945
   9  43.538 BB    0.3575 5073.56055  188.22185  0.92427
 Totals :                  5.48929e5  4.43428e5
```

Figure G-4: GC Reports of Product from Esterification with 16:1 MOAMR.

```
Peak RetTime Type  Width     Area       Height      Area
  #   [min]        [min]    [pA*s]       [pA]         %
----|-------|----|-------|----------|----------|--------|
   1   2.025 BB S  0.0186 5.21559e5  4.48647e5  94.95052
   2   2.210 BB T  0.0237  204.49986  135.05241  0.03723
   3  12.135 BB    0.0424  110.88103   41.25202  0.02019
   4  13.244 BB    0.0536 1377.16663  405.50195  0.25072
   5  14.593 BB    0.0752  505.58066  103.19761  0.09204
   6  15.029 BB    0.0815 1.99774e4  3353.39966  3.63691
   7  15.712 BV R  0.0759 1303.42078  260.06348  0.23729
   8  27.417 BB    0.2257  294.39191   19.54527  0.05359
   9  43.495 BB    0.3022 3963.24023  154.54260  0.72151
 Totals :                  5.49295e5  4.53120e5
```

Figure G-5: GC Reports of Product from Esterification with 20:1 MOAMR.

Table G-1: Data Needed for Calculation of Methyl Oleate Concentration and Yield.

| Methanol-to-Oleic Acid Molar Ratio | Peak Area | | MO/IS | Concentration of MO (g/L) | Yield (%) |
	Methyl Oleate (MO)	Internal Standard (IS)			
4:1	4471.74	1227.4253	3.6432	17.2092	21.48
8:1	15849.1	1380.5221	11.4805	54.2301	67.70
12:1	18687.8	1326.4126	14.0890	66.5516	83.09
16:1	21553.1	1315.6924	16.3816	77.3810	96.61
20:1	19977.4	1377.1666	14.5062	68.5223	85.55

<u>SAMPLE CALCULATION</u>

Taking esterification with 16:1 as an example,

From the calibration curve, the line equation derived is $y = 0.2117x$, where y is the MO/IS while x is the concentration of methyl oleate. Therefore, by substituting the y value,

$$16.3816 = 0.2117x$$

$$x = \frac{16.3816}{0.2117} = 77.3810$$

$$Concentration\ of\ methyl\ oleate = 77.3810\ g/L$$

Then, the yield can be calculated accordingly. While preparing the sample for GC analysis, the sample was evaporated until 20 mL was left. Besides, the density and purity of the oleic acid used are 0.89 g/mL and 90 %, respectively.

$$DF = \frac{Sample\ volume\ after\ dilution}{Sample\ volume\ before\ dilution}$$

$$DF = \frac{1000\ \mu L}{100\ \mu L} = 10$$

$$Yield\ (\%) = \frac{C_{MO} \times DF \times V_S}{V_{OC} \times D_{OC}} \times 100\%$$

$$Yield\ (\%) = \frac{77.38106\frac{g}{L} \times 10 \times 0.02\ L}{20\ mL \times 0.89\frac{g}{mL} \times 0.9} \times 100\%$$

$$Yield\ (\%) = 96.61\ \%$$

Appendix H: Acid Value & Conversion of Oleic Acid and Product

Table H-1: Acid Value and Conversion of Esterification Product with Different Catalyst Loading.

Catalyst Loading (wt.%)	Weight of Sample (g)		Volume of KOH Used (mL)		Acid Value (g KOH/g)		Conversion (%)		
	1	2	1	2	1	2	1	2	Average
4	1.020	1.196	15.2	17.6	0.0836	0.0826	59.12	59.61	59.27
8	1.133	1.013	12.3	11.4	0.0609	0.0631	70.22	69.14	69.68
12	1.199	1.283	4.8	5.2	0.0225	0.0227	89.00	88.90	88.95
16	1.004	1.105	7.5	8.3	0.0419	0.0421	79.51	79.41	79.46
20	1.113	1.033	9.9	9.2	0.0499	0.0499	75.59	75.59	75.59

Table H-2: Acid Value and Conversion of Esterification Product with Different Methanol-to-Oleic Acid Molar Ratio.

Methanol-to-Oleic Acid Molar Ratio	Weight of Sample (g)		Volume of KOH Used (mL)		Acid Value (g KOH/g)		Conversion (%)		
	1	2	1	2	1	2	1	2	Average
4:1	1.023	1.064	26	28	0.1426	0.1476	30.27	27.80	29.04
8:1	1.032	1.130	16.2	18.3	0.0881	0.0909	56.92	55.55	56.24
12:1	1.199	1.283	4.8	5.2	0.0225	0.0227	89.00	88.90	88.95
16:1	1.185	1.175	4.1	3.8	0.0194	0.0181	90.51	91.15	90.83
20:1	1.022	1.128	7.8	8.7	0.0428	0.0433	79.07	78.83	78.95

<u>SAMPLE CALCULATION</u>

Taking esterification with 16:1 as an example,

$$AV_{bd} = \frac{MW_{KOH} \times C_{KOH} \times (V_1 - V_0)}{m_{bd}}$$

$$AV_{OC} = \frac{56.1056 \frac{g\ KOH}{mol} \times 0.1 \frac{mol}{L} \times 0.0041\ L}{1.185\ g} = 0.0194\ g\ KOH/g$$

Given that the acid value of oleic acid, 0.2045 g KOH/g, is determined via the same method,

$$FFA\ conversion\ (\%) = \frac{AV_{OC} - AV_{bd}}{AV_{OC}} \times 100\%$$

$$FFA\ conversion\ (\%) = \frac{0.2045 - 0.0194}{0.2045} \times 100\% = 90.51\%$$

Appendix I: Reusability Study

```
Peak RetTime Type  Width     Area      Height    Area
  #   [min]        [min]    [pA*s]      [pA]       %
----|-------|----|-------|----------|----------|--------|
   1   2.023 BB S  0.0190 5.28654e5  4.41081e5  94.18896
   2   2.207 BB T  0.0240  248.87267  160.89314  0.04434
   3  12.131 BB     0.0437  125.40790   44.69426  0.02234
   4  13.240 BB     0.0553 1348.32605  380.64832  0.24023
   5  14.590 BB     0.0812  580.88397  112.48337  0.10349
   6  15.026 BB     0.0870 2.27883e4  3691.88501  4.06013
   7  15.700 BV R   0.0763 1502.11621  297.40790  0.26763
   8  27.387 BB     0.2173  159.97704   11.02411  0.02850
   9  43.509 BB     0.3521 5861.76367  213.65100  1.04437
Totals :                   5.61270e5  4.45994e5
```

Figure I-1: GC Reports of Product from Esterification at Identified Optimum

Conditions (1st Run).

```
Peak RetTime Type  Width     Area      Height    Area
  #   [min]        [min]    [pA*s]      [pA]       %
----|-------|----|-------|----------|----------|--------|
   1   2.031 BB S  0.0186 5.19906e5  4.45988e5  94.87644
   2   2.217 BB T  0.0234   50.74324   33.94378  0.00926
   3  12.152 BB     0.0445   89.46233   31.17531  0.01633
   4  13.264 BB     0.0552 1436.00195  406.50626  0.26205
   5  14.607 BB     0.0761  409.13718   85.05658  0.07466
   6  15.030 BB     0.0810 1.59229e4  2856.29712  2.90573
   7  15.729 BV R   0.0761 1049.21252  204.87506  0.19147
   8  27.480 BB     0.2225  216.52240   14.64252  0.03951
   9  43.741 BB     0.3371 8902.18359  313.71790  1.62454
Totals :                   5.47982e5  4.49934e5
```

Figure I-2: GC Reports of Product from Esterification using Catalysts from the

1st Run at Identified Optimum Conditions (2nd Run).

```
Peak RetTime Type   Width     Area       Height      Area
  #    [min]         [min]    [pA*s]       [pA]        %
----|-------|----|-------|----------|----------|--------|
   1    2.021 BB  S  0.0186 5.24060e5  4.50127e5  95.10083
   2    2.206 BB  T  0.0235  216.95499  144.27650   0.03937
   3   12.138 BB     0.0449   47.46606   16.81519   0.00861
   4   13.245 BB     0.0540 1298.94922  378.56458   0.23572
   5   14.576 BB     0.0692  217.23524   48.55663   0.03942
   6   14.969 BB     0.0682 8319.77441 1759.95337   1.50978
   7   15.700 BB     0.0761  540.35095  106.69738   0.09806
   8   27.427 BB     0.2154  261.80264   18.24906   0.04751
   9   40.933 BB     0.3818  406.46701   15.76288   0.07376
  10   43.851 BBA    0.3950 1.56882e4   502.87012   2.84694
Totals :                    5.51057e5  4.53118e5
```

Figure I-3: GC Reports of Product from Esterification using Catalysts from the 2nd Run at Identified Optimum Conditions (3rd Run).

Table I-1: Data Needed for Calculation of Methyl Oleate Concentration and Yield.

Run	Peak Area		MO/IS	Concentration of MO (g/L)	Yield (%)
	Methyl Oleate (MO)	Internal Standard (IS)			
1st Run	22788.3	1348.3261	16.9012	79.8355	99.67
2nd Run	15922.9	1436.0020	11.0884	52.3777	65.39
3rd Run	8319.7744	1298.9492	6.4050	30.2551	26.82

SAMPLE CALCULATION

Taking esterification with 1st run as an example,

From the calibration curve, the line equation derived is $y = 0.2117x$, where y is the MO/IS while x is the concentration of methyl oleate. Therefore, by substituting the y value,

$$16.9012 = 0.2117x$$

$$x = \frac{16.9012}{0.2117} = 79.8355$$

$$Concentration\ of\ methyl\ oleate = 79.8355\ g/L$$

Then, the yield can be calculated accordingly. While preparing the sample for GC analysis, the sample was evaporated until 20 mL was left. Besides, the density and purity of the oleic acid used are 0.89 g/mL and 90 %, respectively.

$$DF = \frac{Sample\ volume\ after\ dilution}{Sample\ volume\ before\ dilution}$$

$$DF = \frac{1000\ \mu L}{100\ \mu L} = 10$$

$$Yield\ (\%) = \frac{C_{MO} \times DF \times V_S}{V_{OC} \times D_{OC}} \times 100\%$$

$$Yield\ (\%) = \frac{79.8355 \frac{g}{L} \times 10 \times 0.02\ L}{20\ mL \times 0.89 \frac{g}{mL} \times 0.9} \times 100\%$$

$$Yield\ (\%) = 99.67\ \%$$

Appendix J: Gallery

Figure J-1: Spent Coffee Ground Collected from the Coffee Shop Before Drying.

Figure J-2: Dry the Spent Coffee Ground after Washing it with Water.

Figure J-3: Sieve the Spent Coffe Ground using Sieve with 600 μm Mesh Size.

Figure J-4: Impregnation of Spent Coffee Ground in H_3PO_4.

Figure J-5: Filtration using Vacuum Pump.

Figure J-6: Oven-Drying.

Figure J-7: Carbonisation in a Programmable Furnace.

Figure J-8: Further Grinding of Activated Carbon using Sieve with 300 μm
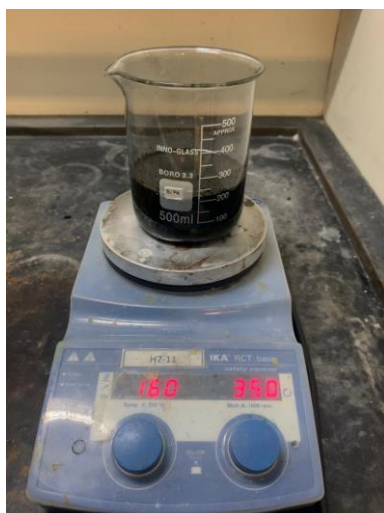
Mesh Size.

Figure J-9: Sulfonation of Activated Carbon in Concentrated Sulfuric Acid.

Figure J-10: Apparatus Set-up for Esterification.

Figure J-11: Apparatus Set-up for Titration to Determine Acid Density of

Synthesised Catalyst and Acid Value of Esterification Product.

Figure J-12: Synthesised Catalyst at Different Sulfonation Temperatures.

Figure J-13: Sample of Biodiesel Production from Esterification of Oleic Acid and Methanol.